# Molecular studies on the interaction of leptin with its receptor

A dissertation submitted to the University of Glasgow for the degree of Doctor of Philosophy

Pavel Mistrík

Institute of Biomedical and Life Sciences
Department of Chemistry

September, 2000



ProQuest LLC.
789 East Eisenhower Parkway
P.O. Box 1346
Ann Arbor, MI 48106 – 1346

# Preface

The research reported within this thesis is my own work, except where otherwise stated, and has not been submitted for any other degree.

Pavel Mistrík

September, 2000

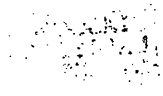

# Abstract

Leptin is a hormonal protein involved in energy homeostasis, acting to inhibit food intake, stimulate energy expenditure and influence insulin secretion, lipolysis and sugar transport. Its action is mediated by a specific receptor whose activation is highly controversial. As a member of the cytokine receptor superfamily, it has been predicted to be activated by ligand-induced dimerization. However, recent evidence has suggested that this receptor exists as a dimer in both ligand-free and ligand-bound states.

The aim of this project was to determine the kinetics and stoichiometry of leptin receptor interaction with its ligand, using a variety of biophysical techniques, namely BiaCore and microcalorimetry. To achieve this, it was necessary to express the leptin receptor. Because the receptor cDNA was not available at the start of this project, the initial goal was to obtain the cDNA encoding the extracellular domain of the receptor by RT-PCR. The open reading frame consisting of 839 a.a. encoded by 2517 nucleotides was generated by several molecular approaches, as the mRNA is a rare species.

To generate large amounts of the receptor required for microcalorimetry, Baculovirus expression system for the leptin receptor production was developed. At the same time BiaCore analysis of the interaction was performed since it requires small amounts of protein, and commercially available protein could be used.

BiaCore was used to measure the thermodynamics of the interaction. Human or mouse receptor chimeras comprising two receptor extracellular domains fused to the Fc region of $IgG_1$ were captured on to the sensor via Protein G. The kinetics and stoichiometry of interactions with human, mouse or rat leptin were measured. This data demonstrated a high affinity interaction. The $K_D$ was $0.2 \pm 0.1$ nM, with $k_a = (1.9 \pm 0.4) \times 10^6$ $M^{-1}s^{-1}$ and $k_d = (4.6 \pm 0.9) \times 10^{-4}$ $s^{-1}$ for human leptin with its cognate receptor. The observed stoichiometry was 1:1. Little difference was observed for different species of leptin. Thus, leptin forms a very stable 1:1 complex with its receptor. This observation indicates that the leptin receptor oligomerization state is not altered during its interaction with a ligand. This contradicts the common paradigm of cytokine receptor activation.

A truncated version of the leptin molecule with deleted glutamine at position 28 was also expressed in *E. coli*. Its affinity for human and mouse leptin receptor chimeras was analysed by BiaCore, which revealed a 10-fold decrease in affinity, indicating a possible involvement of $Q^{28}$ in binding.

# Acknowledgements

I would like to thank first of all my supervisors, Professor Janet M. Allen and Professor Alan Cooper for advice and support over the years. I also wish to thank Dr Patrick T. Harrison for day-to-day supervision in the second half of my project as well as all people from the Institute, who were very helpful with their advice and suggestions, mainly Professor Malcolm Kennedy and Ms Margaret Nutley and all other colleagues from the laboratory. Finally, I would like to thank Dr Francois Moreau from Parke-Davis, France, for training me to use the BiaCore instrument and Ms Sue Chinnick for kindly checking the English.

# Contents

# List of Figures

# List of Tables

# Abbreviations

**3V** third ventricle

**$\alpha$-MSH** $\alpha$-melanocyte-stimulating hormone

**$\Delta$Q28** human leptin with deleted $Q^{28}$

$\chi^2$ the mean square of signal noise

**AcNPV** *Autographa californica* nuclear polyhedrosis virus

**AGRP** Agouti gene related peptide

**ARC** arcuate nucleus

**ADP** adenosine diphosphate

**AM** amygdala

**ATP** adenosine triphosphate

**BAT** brown adipose tissue

**BIA** Biomolecular Interaction Analysis

**BMI** body mass index

**BV** baculovirus

**CART** cocaine- and amphetamine-regulated transcript

**CC** corpus callosum

**CCX** cerebral cortex

**CHR** cytokine-binding homology region

**CNS** central nervous system

**CNTF** ciliary neurotropic factor

**CRH** corticotropin-releasing hormone

**DEPC** diethylpyrocarbonate

**DMEM** Dulbecco's modified Eagles medium

**DMN** dorsomedial nucleus

**dATP** deoxyadenosine 5'-triphosphate

**dCTP** deoxycytidine 5'-triphosphate

**dGTP** deoxyguanosine 5'-triphosphate

**dTTP** deoxythymidine 5'-triphosphate

**dNTP** deoxynucleoside 5'-triphosphate

**EPOR** erythropoietin receptor

**$FADH_2$** flavin adenine dinucleotide (reduced form)

**Fc** fragment crystallisable

**FFA** free fatty acid

**FX** fornix

**G-CSF** granulocyte-colony stimulating factor

**GH** growth hormone

**GHR** growth hormone receptor

**GTC** guanidinium isothiocyanate

**HBM** honeybee melittin

**HI** hippocampus

**HRP** horseradish peroxidase

**HPLC** high performance liquid chromatography

**IFN** interferon

**i.c.v.** intracerebroventricular

**IgG** immunoglobulin G

**IL** interleukin

**IPTG** isopropyl-$\beta$-D-thiogalactopyranoside

**JAK** Janus kinase

$k_a$ association rate constant

**kb** kilobase pairs

$k_d$ dissociation rate constant

$K_D$ dissociation constant

**kDa** kilodalton

**LB** Luria-Bertani (broth)

**LHA** lateral hypothalamic area

**LIF** leukemia inhibitory factor

**MC** melanocortin

**ME** median eminence

**Met** Methionine

**NADH** nicotinamide adenine dinucleotide (reduced form)

**NPY** neuropeptide Y

**NTA** nitrilo-tri-acetic acid

**Ob** leptin

**Ob-R** leptin receptor

**ObR-Fc** leptin receptor chimera

**OC** optic chiasm

**OD** optical density

**ORF** open reading frame

**OXY** oxytocin

**PAGE** polyacrylamide gel electrophoresis

**PBS** phosphate buffered saline

**PBS-T** PBS-Tween

**PCR** polymerase chain reaction

**pfu** plague-forming unit(s) = virus

**PFA** perifornicular area

**PIPAR$\gamma$** peroxisome proliferator-activated receptor

**POMC** pro-opiomelanocortin

**PRLR** prolactin receptor

**PVN** paraventricular nucleus

**RT** reverse transcriptase

**RU** resonance units

**SAP** Shrimp alkaline phosphatase

**SDS** sodium dodecyl sulfate

**SE** septum

***Sf*** *Spodoptera frugiperda*

**SH2** Src homology domain

**SNA** sympathetic nerve activation

**TAE** Tris-acetate/EDTA (electrophoresis buffer)

**STAT** signal transducer and activator of transcription

**TBS** Tris-buffered saline

**TBS-T** TBS-Tween

**TE** Tris-EDTA

**TH** thalamus

**TNF** tumour necrosis factor

**TRH** thyrotropin-releasing hormone

**UCP** uncoupling protein

**VMN** ventromedial nucleus

**WAT** white adipose tissue

**X-Gal** 5-bromo-4-chloro-3-indoyl-$\beta$-D-galactopyranoside

# Chapter 1

# Introduction

## 1.1 Leptin and slimness

Leptin is derived from the Greek word *lepton* which means thin. The choice of name indicates why this protein attracted such a high level of attention in 1994 when it was isolated [1]. Obesity is a severe problem in developed societies where heart disease, hypertension and diabetes are the most common causes of death. In some countries, this problem has attained alarming proportions. In the USA, 30% of the inhabitants are obese, with the highest occurrence among black American women, of whom 50 % have a body mass index (BMI, weight kg/height $m^2$) exceeding 30 (a criteria for obesity) [2]. Such a large group represents a very attractive market for the pharmaceutical industry in the search for suitable molecular candidates for treatment of obesity.

The existence of a molecule such as leptin that controls feeding behaviour was forecast in 1953, when the lipostasis theory was formulated [3]. According to this theory, body weight is controlled by a peripheral signal produced in proportion to the amount of adipose tissue in the body. This signal molecule informs the brain about energy stored in adipose tissue. High levels lead to a suppression of appetite. This phenomenon forms a basis for intervention in the treatment of obesity. An appropriate drug could decrease brain demands for energy stored in the body and thereby suppress appetite.

The lipostasis theory as a concept is difficult to resist. The only problem was that no molecule had been identified. Thus, in 1994 the isolation of a new protein, leptin, generated great enthusiasm; in particular as it was reported to be expressed exclusively in adipose tissue and to interact with brain centres involved in the control of feeding behaviour [1].

Since 1994, leptin has attracted a large number of investigators who have

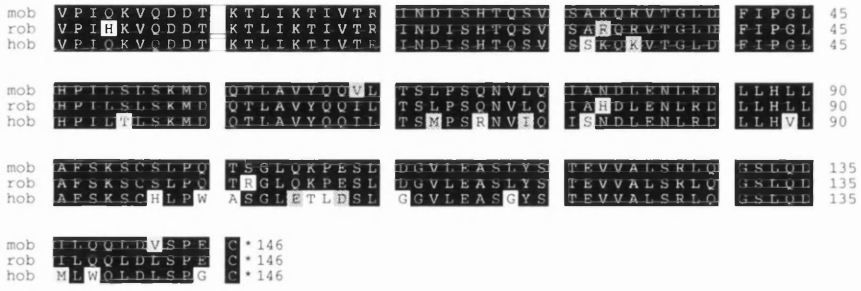

Figure 1.1: Sequence alignment of human, mouse and rat leptin (ob) proteins.

explored its many features. Human, mouse and rat leptin have been characterised, and the protein from these three species is highly conserved in primary sequence (Fig. 1.1). This concentrated effort has resulted in a very rapid accumulation of a huge body of knowledge. However, many parts of it are still very controversial.

## 1.2 Leptin - the cytokine

The interest in leptin has been fuelled from the beginning by the fact that it met the two conditions required by the lipostasis theory. Leptin was thought to be expressed in the adipose tissue in proportion to the amount of tissue [4, 5] and to activate the feeding control centres in the brain [6]. However, it has been shown more recently that leptin is expressed not only in the adipose tissue but also in the stomach [7] and placenta [8]. This suggests that the physiological role of leptin is not fully described in terms of a negative feedback for control of body weight and body composition. It rather indicates that leptin is involved in a much more complex network of interactions, including genetic, environmental, behavioural and social factors.

This suspicion has been further confirmed by solving the crystal structure of a leptin homologue, leptin-E100 [10], which represents wild-type human leptin with a single amino-acid substitution of Glu for Trp at position 100 to enhance crystallisation.

The leptin-E100 crystal structure (Fig. 1.2) consists of four antiparallel $\alpha$-helices (A, B, C and D), connected by two long crossover links (AB and CD ) and one short loop (BC), arranged in a left-hand twisted helical bundle (Fig. 1.2). The CD loop contains a short distorted helical segment E, which is packed almost perpendicularly (87°) against the four helical bundle. The first part of the AB loop, residues Thr27 to Gly38, is not visible in the structure

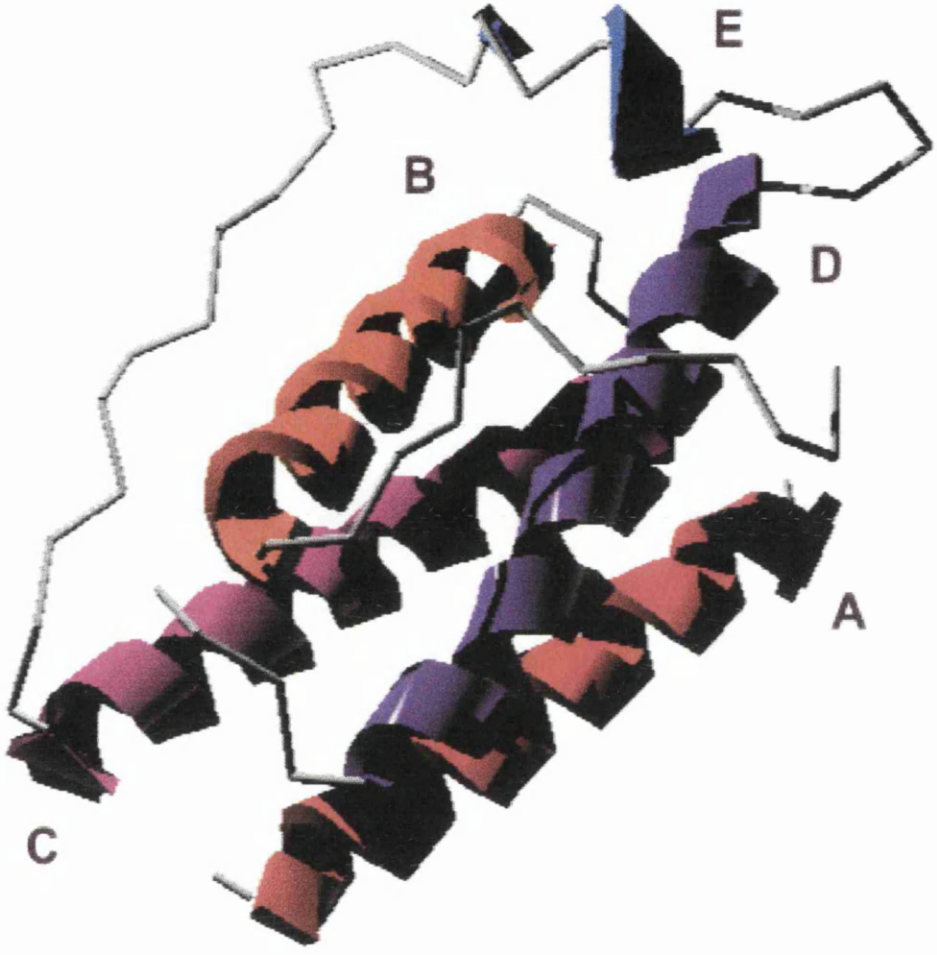


Figure 1.2: The crystal structure of leptin-E100. Leptin-E100 consists of four antiparallel $\alpha$-helices (A, B, C and D), connected by two long crossover links (AB and CD) and one short loop (BC), arranged in a left-hand twisted helical bundle. The CD loop contains a short distorted helical segment E, which is packed almost perpendicularly against the four helical bundle (87°). The first part of the AB loop, residues Thr27 to Gly38, is not visible in the structure because of high flexibility in this region.Derived from PDB file using Swiss-PdbViewer [9] and Pov-Ray software.

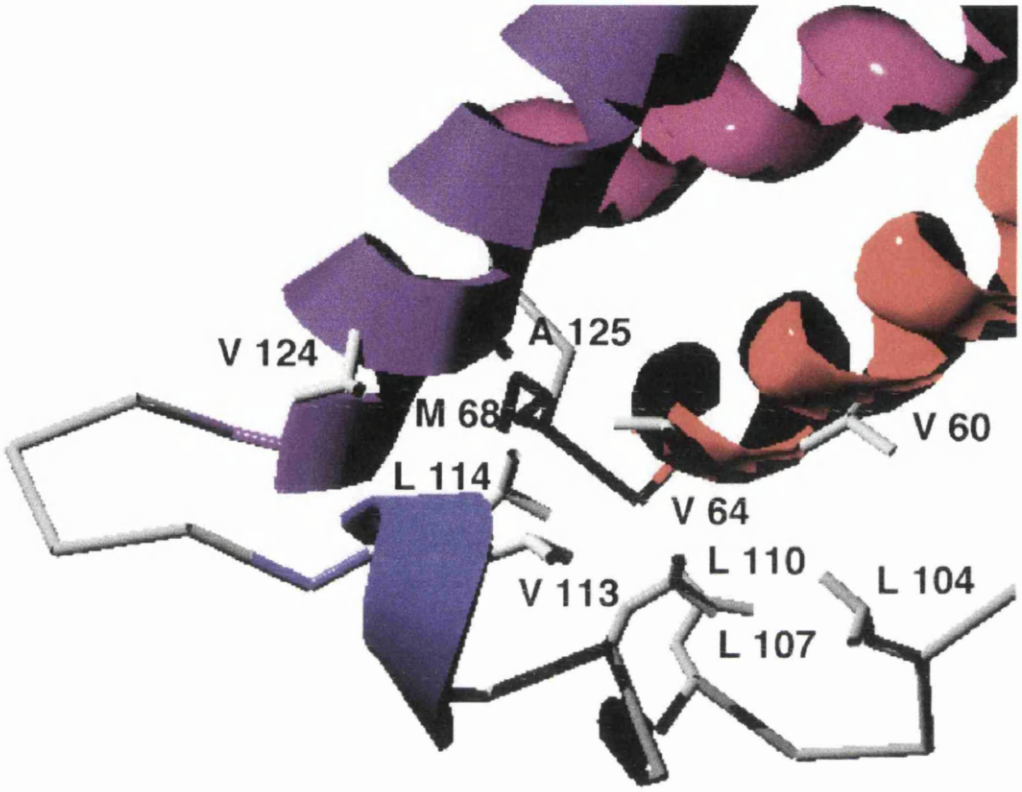


Figure 1.3: A hydrophobic cylindrical core of leptin-100. It is formed by the most conserved residues of the four $\alpha$ helices that face each other (in black). They are residues Val 60 and Ile 64 in the BD bundle, Met 63 in the C-terminal end of helix B and Val 124 and Ala 125 in the N terminus of helix D. This lipophilic surface is buried by Leu 104, Leu 107, Leu 110, Leu 114 and Val 113 of helix E in the CD loop, which serves as a hydrophobic cap. The hydrophobic core is parallel to the helical bundle axis. Derived from PDB file using Swiss-PdbViewer [9] and Pov-Ray software.

because of high flexibility in this region. The hGH and hGH/hGHR complex structures show extensive conformational changes upon receptor binding in this region: from a coil in the free-ligand structure to a helix in the receptor complex. It is possible that leptin, in the receptor-bound form, may also assume an ordered conformation in this region.

A significant feature of the structure is a large hydrophobic cylindrical core parallel to the helical bundle axis (Fig 1.3). This is formed by the most conserved residues of the four $\alpha$ helices that face each other comprising residues Val 60, Ile 64 in the BD bundle, Met 63 in the C-terminal end of helix B and Val 124 and Ala 125 in the N terminus of helix D. This lipophilic surface is buried by Leu 104, Leu 107, Leu 110, Leu 114 and Val 113 of helix E in the CD loop. The E helix serves as a hydrophobic cap.

The intrahelical angles and features of the long crossover loops in the leptin-E100 structure are similar to those found in the crystal structures of the long-chain helical cytokines , which include Granulocyte Colony-Stimulating Factor (G-CSF) [11], Leukemia Inhibitory factor (LIF) [12], Ciliary Neurotropic Factor (CNTF) [13] and human Growth hormone (hGH) [14]. Despite the absence of any sequence similarity between leptin-E100 and these molecules, the solved structures have striking structural similarities. The four-helical bundle of leptin-E100 superimposes on LIF (85 C$\alpha$ atoms) with an r.m.s. deviation of 2.50 Å, on G-CSF (101 C$\alpha$ atoms) (2.37 Å), and on hGH (85 C$\alpha$ atoms) (1.95 Å).

The fact that leptin-E100 protein bears structural similarity to the long-chain helical cytokine family is very surprising. Cytokines are a group of soluble secreted factors which are involved in communication between cells of the immune system. In particular, they control *haematopoiesis*, the process of blood-cell production. Haematopoiesis comprises a complex sequence of events including blood-cell proliferation, differentiation and maturation. Functions of molecules structurally most closely related to leptin are summarised in Table 1.1. They have nothing in common with the control of appetite.

The characterisation of leptin as a cytokine has been strengthened by the finding that leptin activates the JAK-STAT signalling pathway, which is viewed as an integral and widespread mediator of cytokine signal transduction within the immune system [15].

The cytokine-related structure of leptin raised the possibility of a cytokine role for this molecule. There is some evidence to support this. It has been shown in mice that leptin possesses an endogenous protective activity against

Table 1.1: Molecules structurally related to leptin and their function

| | |
|---|---|
| G-CSF | released from activated monocytes, macrophages, and neutrophils as well as from stromal cells, fibroblast and endothelial cells; primarily involved in the proliferation and differentiation of haematopoietic progenitor cells of the neutrophil/granulocyte linage |
| LIF | inhibits many myeloid leukaemia cells, inhibits migration of PMN leucocytes, regulates early haematopoietic cells, activates acute phase protein synthesis, inhibits proliferation and adipogenesis of endothelial cells |
| CNTF | a neurotrophin located predominantly in peripheral nerve tissue; it might be involved in the maintenance and regulation of neurons |
| GH | synthesised in the pituitary gland; it acts upon every tissue of the body, exerting powerful effects on growth and metabolism |

the toxicity of Tumour Necrosis Factor (TNF) [16]. TNF is a cytokine with potent antitumour activity. Its effects are largely mediated by a complex network of cytokines, hormones, and low-molecular weight mediators induced by TNF. The finding that leptin, which is also induced by TNF [17, 18], possesses endogenous protective activity against TNF may mean that leptin has immunomodulatory and anti-inflammatory effects.

It has also been demonstrated that leptin has a stimulatory effect on the proliferation of cells of tracheal (lung) epithelial tissue [19]. This raises the possibility that leptin may be involved in the peripheral regulation of respiratory functions in humans.

These structural and functional observations together create a picture of leptin acting as a cytokine. However, the precise details are unclear. It is therefore surprising that leptin was originally isolated as a molecule acting inside the brain. Leptin must cross the blood-brain barrier to access the central nervous system. A receptor for leptin was identified from the choroid plexus and it is thought that this receptor may play a role in transporting leptin into the central nervous system.

| Factor | Treatment | |
|---|---|---|
| | acute | chronic |
| Caloric intake | rodents | humans |
| Energy expenditure | rodents | humans |

Table 1.2: Behaviour factors regulating the concentration of circulating leptin in humans and animals.

## 1.3 Regulation of circulating leptin

Leptin was originally cloned as a molecule whose plasma level in circulation is proportional to the amount of adipose tissue [1]. However, there are several other factors that regulate leptin levels in plasma. First of all is gender. Second, and more interesting one, is caloric intake (references in [20]). It was observed that both caloric restriction and excess caloric intake affect the level of circulating leptin. Thus, leptin is controlled by both adipose tissue mass and caloric intake.

An important aspect of this regulation is a fundamental difference between humans and rodents. The increase in leptin observed in humans occurs only after chronic increase in caloric intake (references in [20]). In humans, unlike rodents, leptin levels do not change acutely following normal meal consumption. This may indicate that leptin does not act as a satiety signal in humans, its proposed role in rodents.

An additional factor which alters the circulating level of leptin is energy expenditure. Here again significant differences between humans and rodents were observed (references in [20]). In rats, a significant reduction in leptin mRNA levels was observed immediately after acute exercise. In contrast, there was no effect on leptin levels immediately following exercise in man, Table 1.2.

As discussed above, serum leptin concentrations can change with alterations in the amount of adipose tissue, caloric intake and energy expenditure. Changes in serum leptin concentration can result from alteration in production, hormone clearance or both. Leptin has been shown to have a half life of approximately 1.6 h in the circulation of both normal lean and obese humans and lean rats and is primarily removed by the kidney [20]. Nothing is known about clearance in dynamic states such as fasting.

Circulating leptin concentrations appear to be directly proportional to the amount of leptin mRNA in the adipose tissue. The amount of leptin mRNA in adipocytes from obese individuals is greater than that in adipocytes from lean subjects (references in [20]). The size of the adipocyte appears to be a major

determinant of leptin mRNA expression, Table 1.3. However, it is not known whether it is stretching of the cell wall, the increase in stored triglyceride or the presence of a particular intracellular metabolite that determines the amounts of leptin mRNA.

Several hormones that interfere with leptin action have been identified. The most extensively studied is insulin. In humans, a significant correlation between fasting insulin, leptin and leptin mRNA is observed, Table 1.4 However, the leptin response to insulin is much slower than that observed in rodents. In humans, insulin does not have an acute effect but a chronic effect exists.

Thiazolidinediones are a new class of anti-diabetic drugs that improve insulin sensitivity in both humans and animals. Treatment of rodents with thiazolidinediones results in significant reduction in leptin mRNA and circulating leptin which is associated with weight gain [20]. In humans, treatment with these compounds did not have any measurable effect, Table 1.5 Thiazolidinediones seem to mediate their effect on leptin mRNA via the adipose tissue-specific transcription factor PIPAR$\gamma$ (peroxisome proliferator-activated receptor), although the specific consensus sequence for PIPAR$\gamma$ has not yet been identified on the leptin gene promoter.

Glucocorticoids have the opposite effect, Table 1.6. Their administration results in a significant increase in leptin mRNA in rodents [20].

Various other factors have been tested for effects on leptin mRNA in isolated rodent adipocytes, Table 1.7 17$\beta$-estradiol stimulated leptin mRNA, but testosterone was without effect (references in [20]). In vivo administration of endotoxin (LPS), tumor necrosis factor, or interleukin-1 resulted in an increase in epididymal fat leptin mRNA in hamsters (references in [20]). Both leptin mRNA and leptin were reduced by exposure to cold, an effect believed to be mediated by the sympathetic system (references in [20]).

| Factor | | Species |
|---|---|---|
| adipocytes size ↓/↑ | ⇓/⇑ | both |
| weight loss/gain | ↓/↑ | both/r |
| fasting | ⇓ | both |
| refeeding | ⇑ | both |
| overfeeding (no weight gain) | ↑ | rats |

Table 1.3: The size of the adipocyte is a major determinant of leptin mRNA expression. Leptin mRNA decreases with weight loss in both humans and rodents and increases with weight gain in rodents. In humans and animals fasting results in a substantial fall in leptin mRNA that can be reversed upon refeeding. Overfeeding has been demonstrated to increase leptin mRNA in the absence of a significant weight gain in rats (references in [20]).

| Insulin | |
|---|---|
| **Rodents** | |
| single injection | ↑ |
| 2-day infusion | ↑ |
| hyperinsulinemia | ↑ |
| | |
| **Humans** | |
| 5-hr hyperinsul. euglycemia | – |
| 6-hr | 37-88% ↑ |
| 3-day hyperinsul./hyperglyc. | ↑ |
| | |
| **In Vitro** | |
| rat adipocytes | ↑ |
| human adipocytes | ↑ after 48-72 hr |

Table 1.4: Regulatory effects of insulin on leptin mRNA expression.

| Thiazolidinediones | | |
|---|---|---|
| **Rodents** | | |
| AD-5075 | 67% ↓ (weight gain) | Zucker fatty rats |
| | ↓ (weight gain) | *db/db* mice |
| **Humans** | | |
| troglitazone | no effect ( 40-50% ↓ insulin, no weight gain) | |
| | | |
| **In Vitro** | | |
| troglitazone | 40% ↓ (no weight gain, insulin effect blocked) | human adipocytes |
| BRL49653 | ↓ (weight gain) | rat adipocytes |

Table 1.5: Regulatory effects of thiazolidinediones on leptin mRNA expression.

| Glucocorticoids | |
|---|---|
| **Rats** | |
| hydrocortisone 1 - 100 $\mu$g/g body wt | $\Uparrow$ (no weight gain) |
| dexamethasone 3.7 $\mu$g/g body wt | 2.2-fold $\uparrow$ after 24 hr |
| **Isolated adipocytes** | |
| dexamethasone ($10^{-7}M$) | 4$\sim$8-fold $\uparrow$ after 10 hr |
| hydrocortisone | 350% $\uparrow$ after 24 hr |
| dexamethasone | 350% $\uparrow$ after 24 hr |

Table 1.6: Regulatory effects of glucocorticoids on leptin mRNA expression.

| Other factors | | |
|---|---|---|
| **Rodent adipocytes** | | |
| 17$\beta$-estradiol | $\uparrow$ | |
| testosteron | – | |
| h(m) leptin (100$\mu$g/ml) | – | after 24 hr |
| **Hamsters** | | |
| endotoxin (LPS; 1-100 $\mu$g/g body wt) | | $\uparrow$ |
| TNF (17 $\mu$g/g body wt) | | $\uparrow$ |
| IL-1 (1 $\mu$g/g body wt) | | $\uparrow$ |
| **Exposure to cold** | | $\downarrow$ |

Table 1.7: Several other factors were found to modulate leptin mRNA expression.

## 1.4 Leptin and energy balance

The ability of organisms to maintain the stability of their internal environment is a challenging area for understanding. An interesting aspect of homeostasis is the subconscious nature of the regulation of these processes.

### 1.4.1 Adaptive thermogenesis

In this approach, internalised energy (food) is either stored or consumed in physical activity or transformed to heat. This applied version of the first law of thermodynamic provides a useful clue for our examination of energy balance. A component of this balance is heat production, also referred to as *adaptive thermogenesis*, and represents heat produced in response to environmental temperature or diet. It serves the purpose of protecting us from cold exposure or regulating energy balance after changes in diet. The other two components, food intake and amount of physical activity, can be regulated by conscious processes.

#### Factor influencing adaptive thermogenesis

Adaptive thermogenesis can be induced in two ways. These are either cold or diet. Cold-induced adaptive thermogenesis protects us from stress following exposure to environmental temperatures that differ substantially from the physiological temperature. Humans, as opposed to rodents, have a broad thermo-neutral zone with relatively small changes in metabolic rate occurring over relatively wide temperature changes. This should raise concerns over the use of rodents as models for obesity because it suggests that we react to temperature challenge in differently from rodents.

Diet is also a potent regulator of adaptive thermogenesis. Starvation can decrease the resting metabolic rate by as much as 40 % (references at [21]). Similarly, food restriction sufficient to maintain a 10 % reduction in body weight is associated with decreased energy expenditure. The adaptive value of decreasing energy expenditure when food intake is limited is obvious. However, this response is counter-productive for weight control by dieting and contributes to the poor long-term efficacy of this treatment for obesity. Feeding, on the other hand, increases energy expenditure, having both acute and chronic effects on metabolic rate. Feeding acutely increases metabolic rate by 25 - 40 % in humans and rodents; a phenomenon referred to as the thermic effect of food. Long-term overfeeding also increases energy expenditure.

The consequence of increased energy expenditure with overfeeding is relative protection against the development of obesity. Of interest, this protective adaptation is influenced by genetic background, and abnormal responses could contribute to the development of obesity.

Diet-induced thermogenesis is particularly apparent during ingestion of diets that are low in protein. Food serves two important functions: provision of calories to meet energy demands and provision of amino acids to maintain protein synthesis. If the diet is low in protein, then the food intake must be increased to sustain protein biosynthesis. This would lead to obesity if the organism lacked the capacity to waste excess calories. Indeed, metabolic efficiency, or the ability to store ingested calories, is decreased by as much as 40 % when rodents are fed low-protein diets.

### Role of mitochondria

A major site of adaptive thermogenesis in rodents is brown adipose tissue. The role of brown adipose tissue in man is controversial. Humans may represent an exception as we do not have large, distinct depots of brown adipose tissue. Thus, results obtained from mouse or rat experiments may not be that relevant to humans. The tissue responsible for adaptive thermogenesis may not be clear in man, but the cellular compartment has been defined as mitochondria. In mitochondria, metabolism is part of a complex reaction chain, Fig. 1.4.

Metabolism leads to the production of NADH and $FADH_2$, which in turn donate electrons to the electron-transport chain. As electrons move down through the electron-transport chain, protons are pumped out of the mitochondrial inner membrane, thereby creating an electrochemical potential gradient. Protons re-enter the mitochondrial matrix through $F_0/F_1$ – ATP synthase; a reaction that is linked tightly to the synthesis of ATP from ADP. This synthesised ATP is the intracellular energy source.

The pathway is normally tightly coupled. The only way to generate more heat is through the conversion of energy normally used in cellular work. This can be achieved by uncoupling the reaction chain. One established site of uncoupling is the leakage of protons back across the mitochondrial inner membrane; thus, bypassing ATP synthase and converting energy stored within the proton motive force directly to heat. Mitochondrial proton leaks are a biophysical property of proteolipid bilayers juxtaposed between a strong proton motive force. They are also catalysed by specific inner-membrane proteins such as the uncoupling proteins UCP-1, UCP-2 and UCP-3. This is an inter-

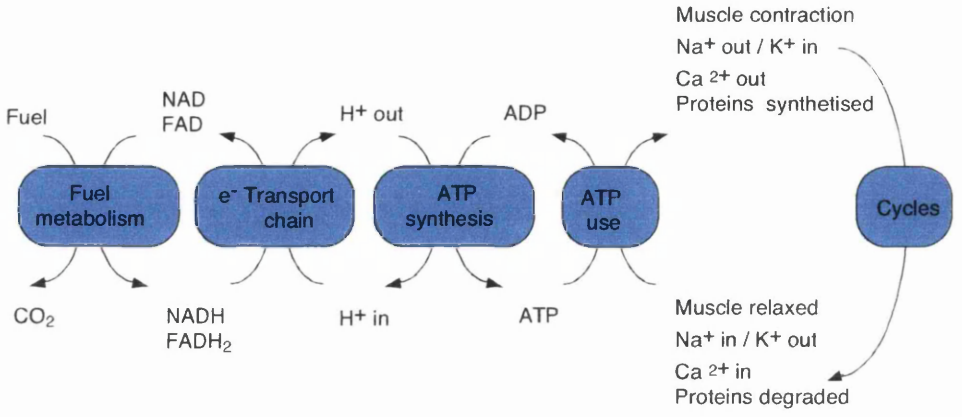


Figure 1.4: Energy production in mitochondria.Metabolism leads to the production of NADH and $FADH_2$, which in turn donate electrons to the electron transport chain. As electrons move down through the electron transport chain, protons are pumped out of the mitochondrial inner membrane, thereby creating an electrochemical potential gradient. Protons re-enter the mitochondrial matrix through $F_0/F_1$ – ATP synthase; a reaction that is linked tightly to the synthesis of ATP from ADP. Synthesised ATP is the intracellular energy source.

esting way in which thermogenesis can be adapted to environmental or diet demands.

Leptin is involved in the control of energy balance in mammals. Energy balance comprises the maintenance of a constant inner environment (temperature), the processing of internalised energy to forms more suitable for storage and finally the expenditure of redundant energy, mainly by thermogenesis. Energy balance has this interesting aspect that we are conscious of some aspects, while unaware of others. The most striking example of a conscious aspect of energy balance is appetite. Thermogenesis and fat metabolism, on the other hand, are examples of subconscious processes contributing to energy balance.

Energy balance is a complex task which can be described only in terms of the whole organism. Therefore, when studying the role of leptin in energy balance, one can not focus on leptin action in a single region in our body but must consider all organs as a possible target for leptin action.

### 1.4.2 Leptin interactions with CNS

Functional analysis of the brain performed some six decades ago [22] first demonstrated that the hypothalamus is the major centre controlling food intake and body weight, Fig. 1.5. The 'satiety' and 'hunger' centres were defined in the ventromedial hypothalamic nucleus (VMN) and the lateral hypothala-

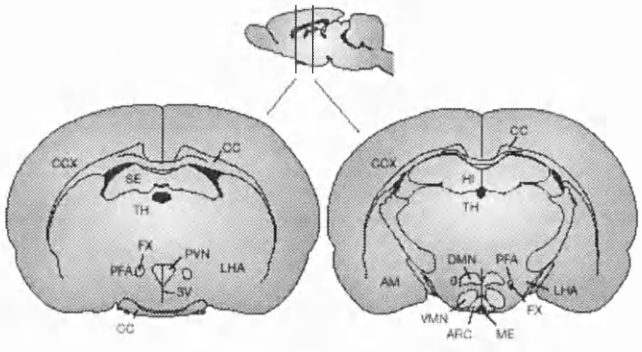


Figure 1.5: Diagrams of rat brain, showing major hypothalamic regions implicated in adiposity signalling and regulation of food intake. The small figure at the top is a longitudinal view of a rat brain, with olfactory bulb at the anterior end on the left and the caudal hindbrain on the right. Cross-sections of the brain at two levels (indicated by vertical lines) are shown at the left and right. First-order neurons responding to adiposity signals are located in the arcuate nucleus (ARC) and project anteriorly to the paraventricular nucleus (PVN) as well as the perifornicular area (PFA) adjacent to the fornix (FX) and the lateral hypothalamic area (LHA). Other regions implicated in regulating food intake include the ventromedial nucleus (VMN) and dorsomedial nucleus (DMN). The figure taken from [23].

mic area (LHA), respectively. These areas were identified by experiments in which electrical stimulation of the VMN suppressed food intake and bilateral lesions of the VMN induced hyperphagia and obesity. Conversely, stimulation or lesioning of the LHA induced the opposite set of responses.

From the physiological perspective, the 'satiety centre' monitors the status of stored energy. It initiates actions aimed to limit stored energy. It suppresses food intake, stimulates heat production (thermogenesis), alters hormone (especially insulin) secretion and partitions energy stores away from fat. The 'hunger centre' evokes a distinct set of adaptive responses, including diminished reproductive capacity and lower thyroid hormone levels, to conserve energy for survival.

An investigation of specific neuronal subpopulations which could be involved in energy homeostasis revealed a more subtle nature of these hypothalamic 'centres'. Visualised by immunocytochemical studies and *in situ* hybridisation, these 'centres' were found to form not compact centres but rather discrete neuronal pathways that generate integrated responses.

Leptin seems to interact with both of these centres by acting on specific

molecules resident in the hypothalamus. These leptin molecular targets have attracted great attention in the recent past. As a result, several distinct hypothalamic pathways were identified as candidate mediators of leptin action in the CNS. The molecules can be divided into two groups according to their effect on energy intake. Energy intake is promoted by orexigenic molecules while anorexigenic ones do the opposite, Table 1.8.

### Neuropeptide Y

A prominent appetite-stimulating molecule is Neuropeptide Y (NPY). NPY is expressed in the arcuate nucleus of the lateral hypothalamus and is downregulated by leptin (reviewed in [24]). Furthermore, injection of NPY centrally evokes virtually all of the features of leptin deficiency, including hyperphagia, decreased thermogenesis by brown adipose tissue (BAT), and hyperinsulinemic insulin resistance. Repetitive injection results in obesity. However, NPY knocked out through targeted gene disruption did not alter the satiety effects of leptin. Thus, other targets of leptin must exist within the brain.

### Melanocortins

Attractive candidates for suppression of food intake are melanocortins (reviewed in [23]). Corticotropin-releasing hormone (CRH), $\alpha$-melanocyte-stimulating hormone ($\alpha$-MSH), thyrotropin-releasing hormone (TRH), cocaine- and amphetamine-regulated transcript (CART) and interleukin-1$\beta$ are among a growing list of peptides that promote negative energy balance. Neuronal synthesis of these peptides increases in response to increased adiposity. Among these, the melanocortin system stands out as being remarkable both for its complexity and its importance to energy homeostasis.

Melanocortins are peptides that are cleaved from the pro-opiomelanocortin (POMC) precursor molecule. They act by binding to members of a family of melanocortin receptors. Of particular importance are the MC3- and MC4-receptors which are expressed primarily in the brain. A possible involvement of these receptors in the control of energy homeostasis emerged after the discovery that a synthetic agonist of these receptors suppresses food intake, whereas a synthetic antagonist has the opposite effect. Mice lacking the MC4 receptor (owing to gene targeting) are hyperphagic and very obese indicating that tonic signalling by MC4 receptors limits food intake and body fat mass. Mice heterozygous for the deleted MC4 allele also become obese, although less so than homozygous knockouts. Lack of a full complement of central MC4 recep-

| Molecule | Regulation by adiposity signals |
|---|---|
| **Orexigenic** | |
| NPY* | ↓ |
| AGRP* | ↓ |
| MCH | ↓ |
| Hypocretin 1 and 2/orexin A and B | ↓ |
| Galanin | ? |
| Noradrenaline | ? |
| **Anorexigenic** | |
| $\alpha$-MSH* | ↑ |
| CRH* | ↑ |
| TRH* | ↑ |
| CART* | ↑ |
| IL-1$\beta$* | ↑ |
| Urocortin* | ? |
| Glucagon-like peptide 1 | ? |
| Oxytocin | ? |
| Neurotensin | ? |
| Serotonin | ? |

Table 1.8: Neuropeptides implicated in the control of energy homeostasis. An asterisk designates documented, coordinated effects on both food intake and energy expenditure that promote a change in energy stores; arrows designate direction of effect exerted by one or both of the adiposity signals, leptin and insulin.

tors, therefore, predisposes to hyperphagia and pathological weight gain. This finding has since been extended to humans with MC4-receptor mutations.

Another antagonist of MC3 and MC4 receptors is a product of the *Agrp* gene. Agouti Gene Related Peptide (AGRP) is expressed in the hypothalamus. Its production, like that of NPY and POMC, is localised to the arcuate nucleus, and is upregulated by fasting and by leptin deficiency. Data with AGRP indicates that antagonism of CNS melanocortin receptors is important in body-weight regulation. Consistent with its role as an anabolic signalling molecule, AGRP causes hyperphagia when administered intracerebroventricularly (i.c.v.) or expressed transgenically, and the increase of food intake following a single i.c.v. injection of AGRP is sustained for up to a week.

Further evidence for the involvement of the melanocortin receptors in the control of energy balance came from studies of Agouti ($A^y/a$) mice, an autosomal dominant model of genetic obesity characterised by a yellow coat colour and an obese phenotype. Cloning of the Agouti gene identified the Agouti function as an antagonist of cutaneous MC1 receptors that are normally expressed by hair follicles. Increased cutaneous agouti protein reduces MC1 signalling and thereby lightens the coat colour. Agouti mice, however, express agouti in tissues throughout the body and consequently develop both a yellow coat colour and obesity. Therefore, Agouti mice obesity is a result of ectopic agouti production in the brain, which blocks the MC4 receptors.

Although NPY is described as the most potent orexigenic molecule (that is, a molecule that stimulates increased energy intake) when the feeding response is measured over a few hours, its effects are short-lived in comparison to those of AGRP. AGRP must therefore be considered as the most robust orexigenic molecule if potency is measured as the cumulative increment of energy intake after a single i.c.v. injection. The mechanism underlying the extraordinary duration of action of AGRP remains a fascinating area for further investigation.

### Transduction of adiposity signals into a neuronal response

The primary site of action of leptin in the hypothalamus is the *arcuate nucleus* (reviewed in [23]). The arcuate nucleus is an elongate ('arc-like') collection of neuronal cell bodies occupying approximately one half of the length of the hypothalamus. It is situated adjacent to the floor of the third ventricle. NPY and AGRP are co-localised in arcuate nucleus neurons while POMC and CART are co-localised in a distinct, but adjacent, subset of arcuate nucleus neurons, Fig. 1.6. This suggests that the arcuate nucleus transduces information related

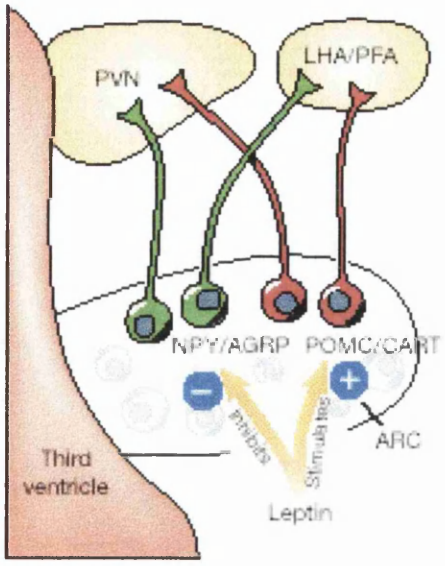


Figure 1.6: NPY/AGRP and POMC/CART neurons in the arcuate nucleus. Populations of first-order NPY/AGRP and POMC/CART neurons in the arcuate nucleus (ARC) are regulated by leptin and project to the paraventricular nucleus (PVN) and to the lateral hypothalamic area (LHA) and perifornicular area (PFA), which are locations of second-order hypothalamic neuropeptide neurons involved in the regulation of food intake and energy homeostasis. The figure taken from [23].

to signalling by leptin into a neuronal response.

This hypothesis is supported by the anorexic response to local microinjection of leptin into this area, and the inability of i.c.v. leptin to reduce food intake after the arcuate nucleus has been destroyed. The majority of both NPY/AGRP and POMC/CART neurons have been found to co-express leptin receptors and both types of neurons are regulated by leptin, but in an opposing manner, as judged by changes in neuropeptide gene expression. Thus, NPY/AGRP neurons are inhibited by leptin, and consequently are activated in conditions where leptin levels are low, Fig. 1.7. Although less well studied, a deficiency of insulin also seems to activate these neurons, and insulin receptors are also highly concentrated in the arcuate nucleus.

Conversely, conditions characterised by reduced insulin or leptin inhibit POMC and CART expression in the arcuate nucleus, and administration of these hormones can prevent or attenuate these neuropeptide responses. Moreover, involuntary overfeeding in rats, which potently inhibits spontaneous food intake once body weight has increased by more than 5 %, elicits a threefold

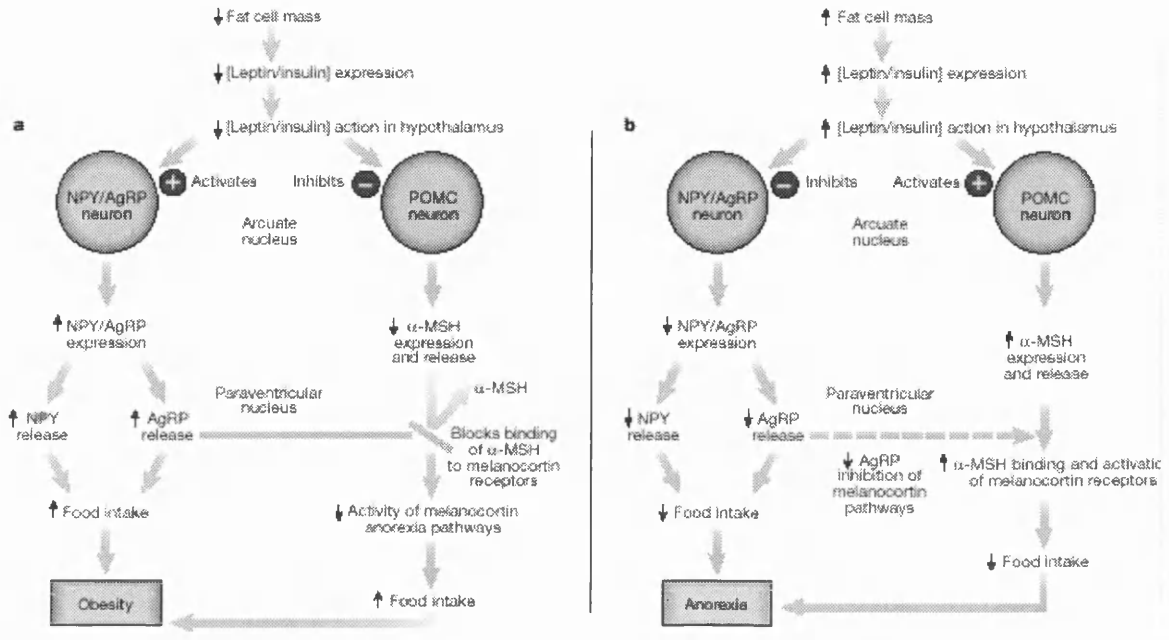


Figure 1.7: Role of arcuate nucleus neurons in adiposity signalling. a, Activity of leptin/insulin-sensitive adiposity signalling pathways in hypothalamus under conditions of leptin/insulin deficiency. b, Increased action of leptin/insulin in arcuate nucleus inhibits the NPY/AGRP anabolic pathway and stimulates the POMC catabolic pathway, resulting in reduced food intake and anorexia. The figure taken from [23].

increase of POMC messenger RNA levels in the arcuate nucleus. The demonstration that anorexia induced either by leptin or by involuntary overfeeding is reversed by central administration of a melanocortin-receptor antagonist (at a low dose that has no effect on food intake in control animals) indicates that melanocortin signalling is a mediator of the anorexic response induced by increased adiposity signalling to the brain.

Taken together, these findings indicate that the arcuate nucleus is a major site for transducing afferent input from circulating leptin and insulin into a neuronal response.

### Model for second-order neuronal signalling pathways

Leptin activity is transduced from the arcuate nucleus to the 'hunger' centre through second-order neurons (reviewed in [23]). These are neurons innervated by the arcuate nucleus that form an integrated signalling system with an element of redundancy in which variety neurotransmitters appear to mediate the same response, Fig. 1.8. It includes the paraventricular nucleus (PVN), zona

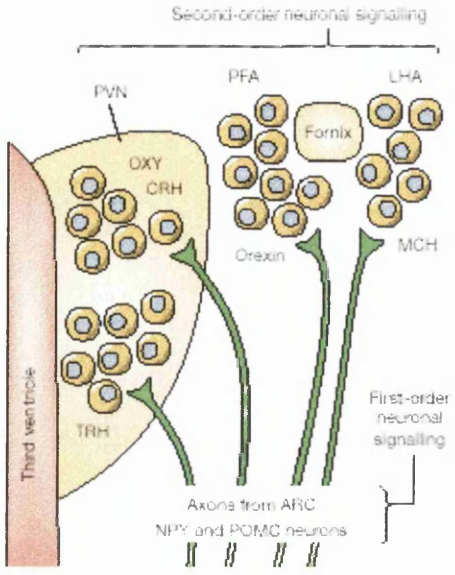


Figure 1.8: Diagram showing locations of candidate second-order neurons involved in the hypothalamic response to leptin adiposity signalling. Neuronal axons containing NPY and $\alpha$-MSH from the arcuate nucleus (ARC) innervates the PVN, LHA and PFA (adjacent to the fornix). Candidate second-order neurons include those that express TRH, CRH and oxytocin (OXY) in the PVN (which cause anorexia), and neurons that express orexins and MCH in the PFA and LHA (which increase feeding). The figure taken from [23].

incerta, perifornical area (PFA) and lateral hypothalamic area (LHA).

Signalling in these regions is conducted through a network of intrinsic neurons. For PVN several candidates are known, which reduce food intake and body weight when administered centrally. These include corticotropin-releasing hormone (CRH), which causes anorexia and also activates the sympathetic nervous system in addition to its role as a major regulator of the hypothalamic-pituitary-adrenal axis; thyrotropin-releasing hormone (TRH), which reduces food intake in addition to stimulating the thyroid axis; and oxytocin (OXY), which reduces food intake in addition to regulating uterine function. The engagement of these molecules in the control of energy balance is in good agreement with observations that stimulation of the PVN inhibits food intake and bilateral PVN lesions cause a hyperphagic obesity syndrome.

The involvement of neurones of LHA/PFA as the second-order mediators is based on physiological properties of another neuropeptide, Melanin-Concentrating Hormone (MCH), which is expressed in this brain area. MCH synthesis is elevated by both energy restriction and leptin deficiency and MCH-

knockout mice have reduced food intake and are excessively lean. MCH exerts its effect through its specific receptor, a G-protein-coupled receptor which is coupled to the $G_i$ subunit of the plasma membrane G-protein assembly. By activating $G_i$, binding of MCH to its receptor inhibits formation of cyclic AMP and consequently reduces signalling by protein kinase A (PKA). This effect is opposite to that mediated by activation of receptors that exert anorexic effects, such as MC4 or CRH receptors, which are coupled to $G_s$ and consequently increase cAMP and PKA signalling.

Two additional peptides are expressed exclusively in the LHA, zona incerta and PFA. These peptides, termed 'hypocretins 1 and 2' or 'orexins A and B' by the two groups [25, 26] that simultaneously discovered them, increase food intake and cause generalised behavioural arousal when administered centrally. Targeted deletion of the hypocretin/orexin gene in mice induces narcolepsy, a disorder characterised by the sudden onset of sleep at times when it would not ordinarily occur. This finding indicates that reduced hypocretin/orexin signalling may contribute to the onset and maintenance of sleep, in addition to its potential role in the control of food intake. Integration of MCH and hypocretin/orexin neurons into a model of the hypothalamic pathways controlling energy homeostasis predicts that they should be inhibited by melanocortin or CART input, and stimulated by NPY signalling, from neurons of the arcuate nucleus.

#### Leptin and potassium channels

Although the exact manner of leptin effectors in the hypothalamus is still to be clarified, the end-point of this pathway has already been identified. The final target of leptin signalling in the hypothalamus appears to be the ATP-sensitive potassium ($K_{ATP}$) channel [27]. This hypothesis is based on the finding that leptin hyperpolarises glucose-receptive hypothalamic neurons of lean Sprague-Dawley and Zucker rats, model system for functional leptin signalling, but is ineffective on neurons of obese Zucker (*fa/fa*) rats, a system with nonfunctional leptin signalling. This hyperpolarisation is due to the activation of a potassium current, and single-channel recordings have directly demonstrated that leptin activates the $K_{ATP}$ channel.

### 1.4.3 Peripheral actions of leptin

Recent studies have demonstrated important peripheral actions of leptin in humans, including modulation of insulin action on liver cells [28], suppression

of insulin secretion by pancreatic $\beta$-cells [29], stimulation of hematopoietic stem cells [30, 31], and inhibition of estradiol secretion by the ovaries [32]. Leptin also increases sympathetic nerve activity (SNA) to the kidney and hindlimb in lean Sprague-Dawley rats [33].

### Leptin and Sympathetic Nerve Activation

Leptin also affects energy expenditure as it increases thermogenesis in brown adipose tissue. Thermogenesis activity of the brown adipose tissue is controlled by the autonomic nervous system.

The autonomic nerve system (ANS) represents the efferent (motor) pathway that links specific effectors such as blood vessels, the heart, the gut etc. with specific areas of the brain concerned with the regulation of these internal organs. The ANS coordinates the operation of the internal organs to support the activity of the body as a whole. The autonomic nervous system is divided into the sympathetic division, which broadly acts to prepare the body for activity (increases heart rate, metabolism etc.) and to the parasympathetic division, which tends to promote restorative functions (digestion, slowing heart rate).

The efferent fibres of the autonomic nerve system do not directly link the CNS with target organs. The sympathetic ANS fibres pass from the CNS to *autonomic ganglia* which are located outside the CNS. These efferents are known as *preganglionic fibres.* The ganglia are connected with the effector organs by *postganglionic fibres.*

Recent experiments in lean Sprague-Dawley rats [33] indicated that leptin increases activity of the sympathetic nervous system. Because the ANS is under control of the CNS (the hypothalamus), it is possible that leptin performs this effect through its action in the CNS. On the other hand, leptin receptors were recently identified in many peripheral tissues and it could be possible that leptin increases activity of the ANS directly via specific receptors expressed in autonomic ganglia in addition to the CNS.

This hypothesis was recently supported by the detection of leptin receptor immunoreactivity in human sympathetic prevertebral ganglia [34]. Prevertebral ganglia regulate gastrointestinal function by affecting motility, absorption and secretion of the gastrointestinal tract. Leptin receptor immunoreactivity was also localised to the celiac and superior mesenteric ganglia (mouse and rat origin). All these findings suggest that leptin may modulate gastrointestinal function and responses to food ingestion and digestion through receptors

present in prevertebral ganglia in addition to the effect of leptin at the level of the central nervous system.

One puzzling feature of these studies is the cellular localisation of the receptor, which was identified in the cytoplasm and not on the cell surface [34]. This raises the question of the nature and role of this receptor. Does it represent a population of recycled receptors or a pool of receptors waiting to be exported to the plasma membrane? Can the leptin receptor possess a functional intracellular role? How could leptin activate it?

Leptin increases the activity of the ANS fibres innervating the brown adipose tissue (BAT). Because BAT is the thermogenic organ, leptin enhances energy expenditure. This leptin effect is likely to be mediated via a central nervous system receptor because BAT sympatho-activation was not clearly related to plasma concentrations of leptin [33]. However, sympathetic nerve activation of BAT is also increased in *obese* Zucker rats, though non-significantly [33]. Zucker rats lack intact leptin receptor in the hypothalamus. This may suggest that the effect of leptin on the sympathetic innervation to BAT is partially independent of CNS and that leptin could act directly through receptors in the autonomic nervous system.

### Auto-Mode of Leptin Action

Findings that the leptin receptor (Ob-R) is expressed in white and brown adipocytes (WAT, BAT) [35] as well as in many other tissues, opened a possibility that leptin may exert its weight-reducing action not only through an endocrine, hypothalamic mode of action, but also through an auto- or paracrine pathway.

This possibility has been investigated recently [36] and results from this study demonstrated that leptin has direct effects on BAT and WAT at a metabolic and molecular level. This conclusion was supported by several independent lines of evidence: (a) peripheral, but not central, administration of leptin increased the insulin-stimulated utilisation of glucose in BAT when compared with pair-fed control rats; (b) leptin at concentrations as low as 0.1 nM stimulated basal lipolysis in white fat pads *ex vivo* in a time- and dose-dependent manner, and this effect was absent in fat pads from obese fa/fa rats which are known to be deficient in functional OB-R; (c) leptin induced the expression of malic enzyme and lipoprotein lipase in primary cultures of brown adipocytes; (d) BAT, WAT, and primary adipocyte cultures all express OB-Rb mRNA (section 1.5); and (e) treatment of brown and white adipocytes

with leptin *in vivo* or *in vitro* induced the nuclear translocation of STATs, compatible with the currently known mechanism of action of leptin through the OB-R.

Taken together, these results suggested that physiological levels of leptin had a direct and specific effect on the metabolism and gene expression of brown and white adipocytes which is likely to be mediated through an auto- or paracrine pathway.

### Leptin and Adrenal Gland

Leptin also increases sympathetic nerve activity (SNA) to the adrenal gland, as demonstrated in lean Sprague-Dawley rats [33]. The adrenal glands are paired organs, each one lying above the kidney, enclosed in a fibrous capsule and surrounded by fat. Each adrenal gland is, in effect, structurally and functionally divided into two endocrine glands. The inner *adrenal medulla* derives from ectodermal cells of the embryonic neural crest and secretes the catecholamines, *epinephrine* and *norepinephrine*, in response to activation of its sympathetic nerve supply. It thereby acts as an autonomic ganglion of the sympathetic nervous system. The outer *adrenal cortex*, which encapsulates the medulla and forms the bulk of the gland, is derived from embryonic mesoderm and secretes a number of steroid hormones. Unlike the adrenal medulla, the secretions of the adrenal cortex are controlled hormonally. The adrenal medulla is involved in energy metabolism through epinephrine regulation. The adrenal cortex affects many other body functions through cortisol and aldosterone production.

The effect of leptin on sympatho-activation of the adrenal gland raises again a question of a direct action of leptin on the ANS through a specific receptor. Leptin receptor expression in the human adrenal gland has been demonstrated [37]. At the mRNA level, the long form of the leptin receptor (section 1.5) was detected in both adrenocortical and adrenomedullary tissues. Furthermore, isoforms, previously characterised in human fetal liver, were observed in normal human adrenal cell cultures and adrenal tissues. At the protein level, the full length Ob-R (section 1.5) was detected by immunostaining in all three zones of the cortex but only a weak signal was detected in the adrenal medulla [37].

Leptin acts on adrenal cortex functions. Leptin administered in concentrations that are equivalent to the *in vivo* range led to a mild, but significant, inhibition of adrenal steroidogenesis [37]. This effect was most significant on

aldosterone. A strong inhibition required concentrations higher than those normally found in plasma. However, the adrenal gland is naturally embodied in the adipose tissue and thus, high local leptin concentrations may be innate in this organ.

The inhibition effect of leptin has been proposed to act through this hormone, modulating the expression of steroid hormones. This was proposed following the finding that leptin administration led to a 50 % decrease in ACTH-stimulated cytochrome P450 mRNA expression [37]. This suggested that the inhibitory effect may be through action on the expression of steroid enzymes.

These data suggest that leptin decreases glucocorticoid production. This may have an indirect connection to energy control because glucocorticoids produce the biochemical features of visceral fat syndrome, including obesity, insulin resistance, dyslipidemia, and hypertension.

A decrease in mineralocorticoid (aldosterone) secretion also leads to a fall in blood pressure, indicating that leptin may have a counter-regulatory function in hypertension.

On the other hand, leptin does not have any direct effect on human adrenal catecholamine production. This diminishes a potential direct effect of leptin in energy metabolism through *epinephrine* regulation. This is in contrast to other mammals (rat and mice) where the adrenal medulla expresses abundant leptin receptor [37]. This difference can contribute to different leptin effects observed in these species.

| Splice Variant | Intracellular Domain | |
|---|---|---|
| Ob-Ra | SHQRMKKL**FWDDVPNP**KNCSWAQGLNFQK | RTDTL* |
| Ob-Rb | SHQRMKKL**FWDDVPNP**KNCSWAQGLNFQK | PETFEHLFIKHTASVTCGPLLLEPETIS |
| | | EDISVDTSWKNKDEMMPTTVVSLLST |
| | | TDLEKGSVCISDQFNSVNFSEAEGTEV |
| | | TYEAESQRQPFVKYATLISNSKPSETG |
| | | EEQGLINSSVTKCFSSKNSPLKDSFSNS |
| | | SWEIEAQAFFILSDQHPNIISPHLTFSE |
| | | GLDELLKLEGNFPEENNDKKSIYYLG |
| | | VTSIKKRESGVLLTDKSRVSCPFPAPC |
| | | LFTDIRVLQDSCSHFVENNINLGTSSK |
| | | KTFAS**YMPQ**FQTCSTQTHKIMENKM |
| | | CDLTV* |
| Ob-Rc | SHQRMKKL**FWDDVPNP**KNCSWAQGLNFQK | VTV* |
| Ob-Rd | SHQRMKKL**FWDDVPNP**KNCSWAQGLNFQK | DISFHEVFIFR* |
| Ob-Re | FYIH | GMCTVLFMD* |

Table 1.9: The intracellular domain of the mouse leptin receptor splicing variants. The consensus box 1 and box 2 motifs are indicated. * stands for the terminal codon.

## 1.5 Leptin receptor

### 1.5.1 Receptor splicing variants

The leptin receptor (Ob-R) was originally cloned from the mouse choroid plexus [38]. Its DNA sequence suggests that Ob-R is a single membrane-spanning receptor consisting of extracellular, transmembrane and intracellular domains, Fig. 1.9.

Further investigation in the mouse hypothalamus [39] revealed multiple splice variants of the leptin receptor gene [39]. Four variants are identical until the lysine residue at position 889, which is within the predicted cytoplasmic tail. Thus, they have identical extracellular and transmembrane domains but different cytoplasmic portions, Table 1.9. These four variants are designed: Ob-Ra, Ob-Rb, Ob-Rc and Ob-Rd. A fifth splice variant, Ob-Re, predicts a different amino-acid sequence after His 796, and may encode a soluble receptor, Fig. 1.9.

Ob-Ra corresponds to the Ob-R cloned originally from mouse choroid plexus cDNA library [38]. Ob-Rb is the "long" form of the receptor and has been classified as a mouse homologue for human Ob-R, because the C terminus of Ob-Rb is 78% identical to the human receptor[1]. Ob-Rc and Ob-Rd

[1]The human sequence was cloned from the fetal total cDNA library [38].

| Tissue | Ob-Ra | Ob-Rb |
|---|---|---|
| Heart | low | very low |
| Hypothalamus | low | high |
| Choroid Plexus | low | very low |
| Spleen | low | very low |
| Lung | high | very low |
| Liver | low | very low |
| Sk. Muscle | low | very low |
| Kidney | high | very low |
| Testes | low | very low |
| White Fat | not tested | very low |
| Brown Fat | not tested | very low |
| Pancreas Islet | not tested | none |
| Pancreas | not tested | none |

Table 1.10: An expression level of the leptin receptor splicing variants in different mouse tissues.

are suspected to represent nonfunctional variants [40].

The Ob-Ra and Ob-Rb splice variants differ in the nature of their cytoplasmic tails. The Ob-Rb variant is able to signal through the activation of the JAK/STAT signalling pathway whereas Ob-Ra is not.

A functional difference between Ob-Ra and Ob-Ra became obvious when a single point mutation in the Ob-R gene was identified in the *db/db* mice (C57BL/KsJ strain) [39, 41]. This mutation leads to a replacement of Ob-Rb by Ob-Ra. This can account for the *db/db* phenotype which is characterised by a resistance to leptin.

The leptin receptor has been localised not only in the mouse hypothalamus [38, 42] and choroid plexus but also in several other tissues, Table 1.10. High levels of Ob-R expression were detected in lung and kidney. Lower levels were detected in heart, spleen, liver, skeletal muscle and testes [35, 38, 40]. The majority of Ob-R in these tissues is the short form, Ob-Ra. Ob-Rb is present in these tissues but in much smaller amounts. Ob-Rc, Ob-Rd and Ob-Re were not identified. Ob-Rb has also been detected at low levels in white and brown fat, but not in pancreatic islets or whole pancreas [40]. The significance of the Ob-R tissue distribution is not clear and a role of individual receptor splice variants is still speculative.

It is useful to introduce an alternative classification of the receptor splice variants according to their cytoplasmic tail. The splice variants Ob-Ra, Ob-Rc and Ob-Rd then represent different versions of the short form of the receptor

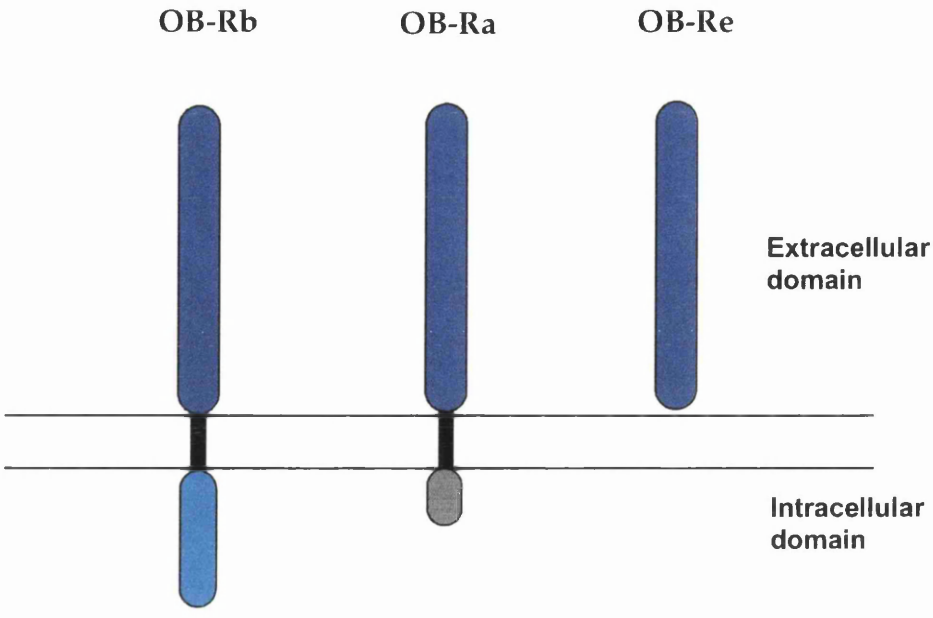


Figure 1.9: The leptin receptor splicing variants: OB-Rb and OB-Ra are the long and short forms of the leptin receptor, while Ob-Re is likely to represent the soluble form of the receptor.

(Ob-Rs) while the Ob-Rb is receptor long form (Ob-Rl)[2]. The cytoplasmic region of the short forms (Ob-Rs) only comprises about 30 aa. The long form (Ob-Rl) has a cytoplasmic tail of 336 amino acids. Table 1.9. This difference has been predicted to account for the distinct signaling capability of the splice variants. The intracellular domain of the Ob-Rl contains a consensus box 1 motif, JAK tyrosine kinase binding site [43] as well as the box 2 motif which is the binding sequence for the STAT3 transcription factor, a JAK substrate [44, 45]. Therefore, Ob-Rl can activate the JAK-STAT intracellular signalling pathway. Ob-Rs with just the box 1 motif lack this activity.

### 1.5.2 Cytokine receptor superfamily

Sequence analysis of the shared extracellular region of all Ob-R forms revealed several motifs that are common for the cytokine receptor superfamily. These are the Trp-Ser-X-Trp-Ser motif (where X is a nonconserved amino acid) and four conserved Cys residues in its extracellular domain [46]. Together with the presence of a typical "Box 1; Box 2" motif in Ob-Rl, this suggests that the Ob-R may be a member of the cytokine receptor superfamily.

This proposal has been supported by the solution of the crystal structure

[2]The splice variant Ob-Rb is from now on referred to also as Ob-Rl.

of leptin, the receptor ligand [1]. It has revealed that leptin shares structural features common for cytokines (molecules which ensure the communication between different organs in our body). Thus, the classification of leptin as a cytokine supports the concept that the leptin receptor is a cytokine receptor.

Although Ob-R is now accepted as a cytokine receptor family member, the homology between its primary sequence and other family members is relatively low. The most closely related protein: the gp130 protein (the signal-transducing component of the interleukin-6 (IL-6) receptor) has only 21% homology with the Ob-R. The other "closely" related proteins are: the granulocyte colony-stimulating factor (G-CSF) receptor, the leukaemia inhibitory factor (LIF) receptor ($\alpha$ chain) and the growth hormone (GH) receptor.

### 1.5.3 Canonical extracellular domain

The extracellular domain of cytokine receptors, which plays a crucial role in the interaction with the ligand, is relatively well characterised. Sequence analysis [47] has revealed several conserved motifs and the canonical extracellular domain has been formulated (Fig. 1.10). According to this analysis the extracellular region of many cytokine receptors consists of an immunoglobulin-like domain in its N terminus followed by a cytokine-binding homology region (CHR) which contains the ligand binding site and two or three copies of fibronectin III-like domains. However, a small number of the cytokine receptors contain not one but two copies of the CHR. This is the case for the LIFR $\alpha$ chain, the IL-5R $\beta$ chain and also the Ob-R. The cytokine receptor extracellular domain subdivision predicted from the sequence analysis [47] has been confirmed by the solution of the crystal structure of several members of this family: namely, the growth hormone receptor (GHR; [14]), the prolactin receptor (PRLR; [48]), the erythropoietin receptor (EPOR; [49]), and the interferon-$\gamma$ receptor (IFN$\gamma$-R; [50]). These studies have also shown that the CHR alone contains two fibronectin III-like domains (N and C). Its amino-terminal domain (N) is characterised by four conserved cysteine residues while the carboxy-terminal domain (C) contains the signature motif Trp-Ser-X-Ser motif, which is now recognised as the distinguishing feature for this family of receptors.

### 1.5.4 Canonical intracellular domain

The first of the cytokine receptor conserved motifs localised in their intracellular domain is a Box 1 motif. Both the short and long forms of the leptin

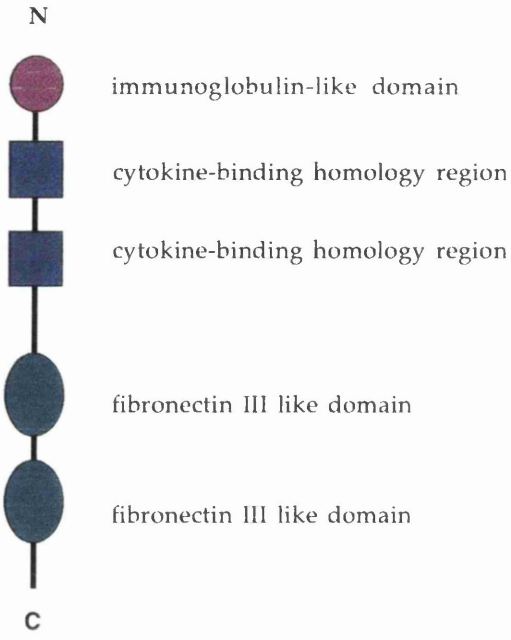


Figure 1.10: Canonical motifs in the Ob-R extracellular domain. An immunoglobulin like domain is followed by two copies of the cytokine-binding homology region (CHR) and two copies of fibronectin III-like domains.

receptor possess the Box 1 motif, which is usually located within the first 20 cytoplasmic residues. The Box 2 motif, a less conservative motif, is usually found in the first 50-60 amino acids of the cytoplasmic domain. This Box 2 motif is only present in Ob-Rl, the long form of the receptor. Mutational analysis of these conserved regions in several receptors suggests that these two domains are both required for the activation of JAK-STAT signalling pathway [51, 52, 44]. The absence of the Box 2 motif in the cytoplasmic domain of the Ob-Rs suggests that the short form of receptor activates a different pathway (if any).

## 1.6 Receptor activation

The topic of my project is the activation of the leptin receptor by interaction with its ligand. Cytokine receptors have been shown to function as dimers and this dimerisation is induced by the ligand [53]. The sequence similarities of leptin/leptin receptor with the cytokine/cytokine receptor family presupposes that a similar activation process may hold for leptin activation. However, this presumption may be misleading and inaccurate.

The current model of the common cytokine receptor activation [53] sup-

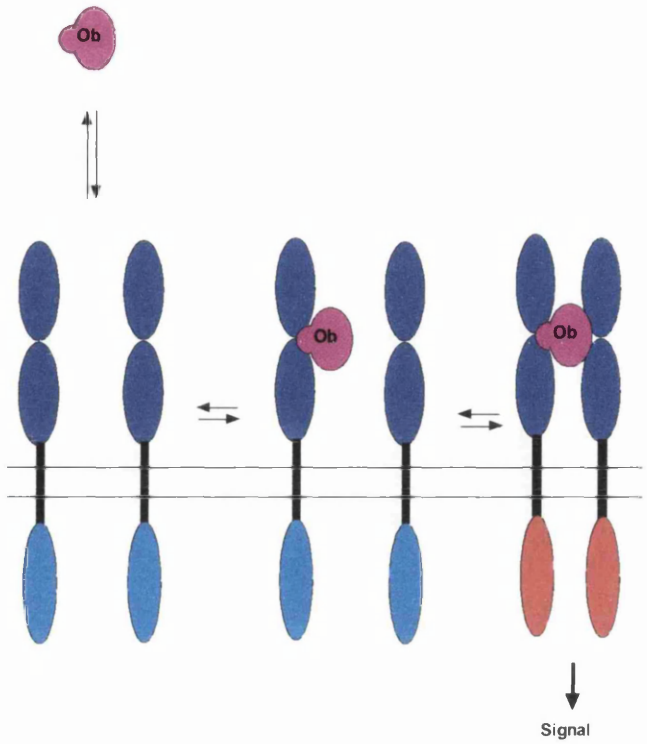


Figure 1.11: The proposed mechanism of leptin receptor activation based on GH-GHR interactions. A ligand free receptor exists in a monomeric form. The ligand binding induces its dimerization.

poses that the ligand-free receptor is expressed on the cell surface in a monomeric form and that the ligand induces the receptor di/oligomerisation, Fig. 1.11. The number and character of molecules involved in receptor activation differ between the family members. For example, the growth hormone receptor (GHR) undergoes a simple homodimerisation in the presence of the ligand [14], while the activated interleukin-6 receptor (IL-6R) complex contains (apart from IL-6) the monomeric IL-6R together with two gp130 molecules [54].

A weak point of the model presented is that it is based mainly on theoretical analysis and is backed only by a weak experimental confirmation. The main piece of evidence is the crystal structure of a complex of growth hormone and its receptor [14], which indicates that the receptor is dimerised in the presence of the ligand, but there is no evidence that ligand-free receptor is expressed on the cell surface as monomer.

### 1.6.1 JAK/STAT signalling pathway

An activated cytokine receptor is able to initiate the intracellular signalling cascade. The membrane receptors signal normally via the phosphorylation of spe-

cific tyrosine residues of the target molecules. However, cytokine receptors lack intrinsic tyrosine kinase activity. These receptors engage receptor-associated JAK kinases [38]. JAKs are rapidly activated and tyrosine phosphorylated, after ligand binding to a particular receptor. JAK activation is followed by tyrosine phosphorylation of receptor subunits and additional signaling intermediates, including cytosolic proteins known as STATs. Phosphorylation of STATs results in their homo- or hetero-dimerization via reciprocal phosphotyrosine SH2 domain interactions [55]. These transcription factors then translocate to the nucleus using the importing $\alpha/\beta$ localisation pathway [56]; in the nucleus, they bind to cognate response elements adjacent to target genes and activate downstream gene transcription [57]. This general scheme, Fig 1.12, is now recognised to serve as a high-speed connection between many cytokine receptors and their downstream biological responses.

One can try to deduce the potential effects of leptin receptor activation by determining the JAK and STAT molecules engaged by leptin receptor. The leptin receptor *in vitro* employs Jak2, STAT-1, STAT-3 and STAT-5b components [59]. The *in vivo* role of these molecules has been investigated using gene disruption studies.

Targeted disruption of Jak2 gene results in an embryonic lethal phenotype [58]. This implies that leptin receptor signalling through Jak2 could be critical in early developmental processes. Disruption of STAT-1 gene leads to marked unresponsiveness to interferon (INF)-$\alpha$ or $\gamma$ and increased sensitivity to microbial pathogens [60, 61]. Thus, leptin may play a role in antimicrobial defence. A nonfunctional STAT-3 gene results in the same phenotype observed when Jak2 was disrupted: i.e. it is embryonic lethal [62]. This phenotype is likely to be attributed to the pleiotropic action of STAT-3 in early development. Targeted disruption of STAT-5 results in very limited immunological defects.

From these disruption studies, one would conclude that leptin receptor signalling is important for the early development of an organism and antimicrobial defence. However, this is a very different role from the one originally proposed for leptin: control of feeding behaviour through an interaction with the central nervous system. This discrepancy raises several questions. Does leptin in neuronal cells utilise the JAK/STAT signalling pathway previously characterised for cells of the immune system? If not, does leptin activate other signalling pathways in the CNS? What role would leptin signalling via the JAK/STAT pathway have in that case?

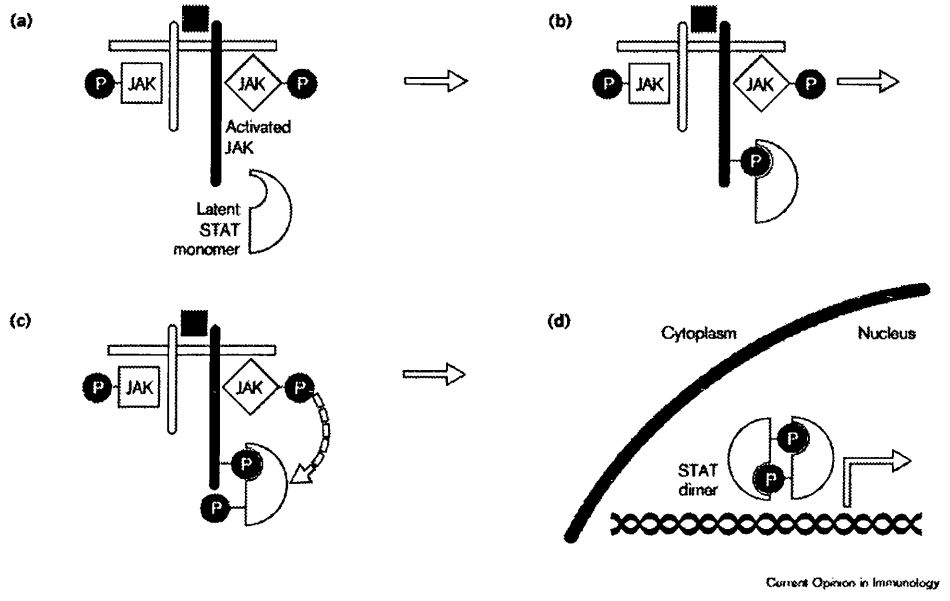


Figure 1.12: The basic JAK/STAT signal transduction paradigm. Receptor-associated JAKs remain quiescent until (a) ligand-induced receptor multimerisation promotes their activation, apparently through a trans-autophosphorylation mechanism. (b) Subsequent phosphorylation of select tyrosines within one or both receptor cytoplasmic tails provides attachment sites for latent cytoplasmic STAT factors via specific SH2 phosphotyrosine interactions. (c) It is believed that the juxtaposition of STAT factors in a specific configuration adjacent to activated JAKs within the receptor complex facilitates their tyrosine phosphorylation. (d) Phosphorylated STAT monomers subsequently associate as dimers via reciprocal SH2 phosphotyrosine interactions, and are then able to translocate into the nucleus to bind sequence-specific DNA response elements and promote transcription of target genes. Reprinted from [58]

The hypothesis that the leptin receptor uses the JAK/STAT pathway in neuronal cells *in vivo* was investigated in rats [63]. The STAT-3 protein was found to be localised in the Ob-R-containing neurons in rat hypothalamus by means of indirect immunofluorescence histochemistry. STAT-3 protein was also identified in the paraventricular nucleus (parvocellular part), periventricular nucleus, arcuate nucleus and in the lateral hypothalamic area.

In this same study, direct double-labelling showed the presence of STAT-3 immunoreactivity in Neuropeptide Y (NPY)-containing neurons of the ventromedial part of the arcuate nucleus and in pro-opiomelanocortin (POMC)-containing neurons of the ventrolateral part of the arcuate nucleus.

These results provide an anatomical basis for leptin action mediated by STAT3 in Ob-R containing NPY and POMC neurons of the arcuate nucleus, as well as by Ob-R containing neurons of the parvocellular, paraventricular nucleus and lateral hypothalamic area.

The ability of leptin to activate STAT-3 in the hypothalamus of rats *in vivo* was confirmed by immunoblotting analysis of STAT-3 phosphorylation [64], when STAT-3 was found to be phosphorylated after leptin injection.

By contrast, leptin did not increase the phosphorylation of Jak2, or STAT-1 and -5 despite abundant expression of these signaling molecules in the hypothalamus. It remains unclear how signaling is propagated downstream from the leptin receptor to STAT-3, but this may involve novel signaling intermediates.

### 1.6.2 Construction of receptor chimeras

The first attempts to determine the order of multimerisation of the Ob-R aggregation have already been undertaken. It has been shown so far that the Ob-R activation does not require gp130 protein [59], IL-2 R$\gamma$ or IL-3 R$\beta$ signal transduction components [65] because it can signal in hepatoma cells (which do not express Il-2 R $\gamma$ or IL-3 R$\beta$ components) in the presence of the neutralising antibodies to the gp130. These results suggested that the Ob-R may undergo homodimerisation during its activation.

This hypothesis has been investigated through several experimental approaches. In one of them, the chimeras between the leptin receptor and the granulocyte-colony stimulating factor receptor (G-CSFR) have been constructed [66]. The G-CSFR is a member of the cytokine receptor superfamily predicted to undergo homodimerisation [67]. Thus, the replacement of one of the G-CSFR domains (intracellular or extracellular ones) with the Ob-R analogue should demonstrate whether the Ob-R undergoes the same process,

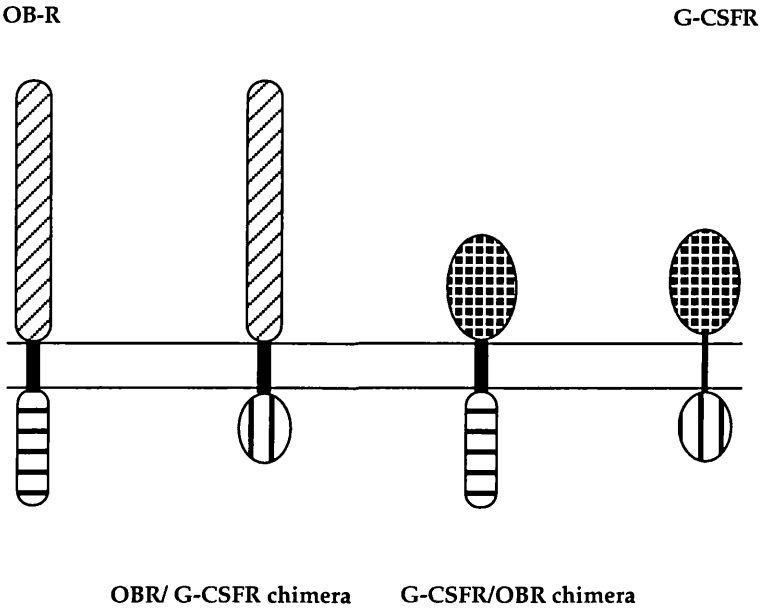


Figure 1.13: The OBR/G-CSFR and the G-CSFR/OBR chimeras. The OBR/G-CSFR chimera consists of the extracellular and transmembrane domains of the mouse Ob-R and the intracellular domain of the human G-CSFR. The G-CSFR/OBR chimera consists of the human G-CSFR extracellular domain and the human Ob-R transmembrane and intracellular domains.

(Fig. 1.13.)

To verify the ability of leptin to activate the leptin receptor via homodimerisation, the chimera (OBR/G-CSFR) consisting of the extracellular and transmembrane domains of the mouse Ob-R and the intracellular domain of the human G-CSFR, has been constructed, (Fig. 1.13) If leptin binding to the Ob-R extracellular domain causes dimerization the chimera will activate signalling because the intracellular domain of G-CSFR is only active in dimeric form. The results showed that incubation of the chimera with leptin resulted in the signal activation. This finding suggested that leptin induces dimerization of the chimera.

The role of dimerization of the Ob-R intracellular domain in mediating receptor activation has been investigated through the construction of the converse chimera, namely G-CSFR/OBR chimera, which consists of the human G-CSFR extracellular domain and the human Ob-R transmembrane and intracellular domains. Incubation of the chimera with G-CSF resulted again in the signal activation, implying that the Ob-R intracellular domain mimics the G-CSFR one (i.e. that it is dimerised in an activated receptor).

A combination of these results leads to the conclusion that leptin is able to

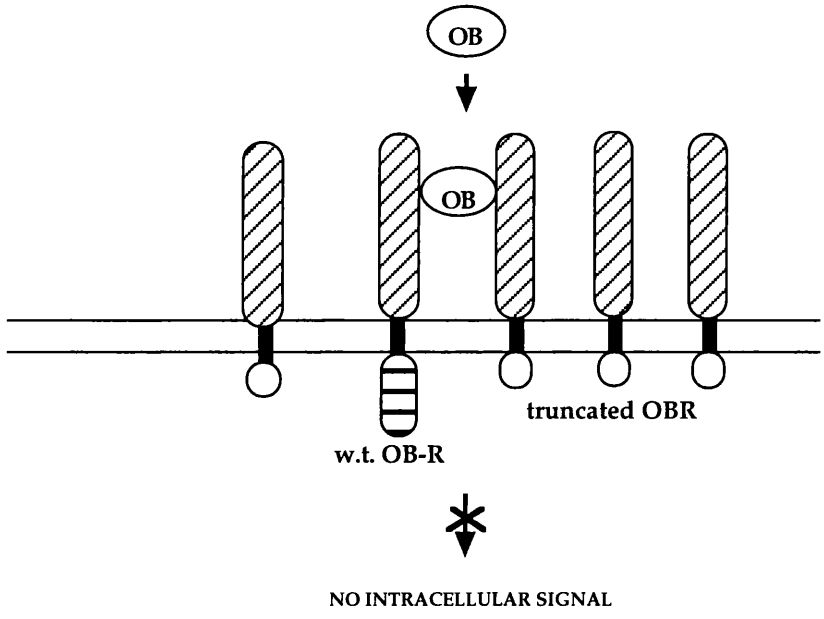


Figure 1.14: The Ob-R signalling is cancelled by the overexpression of a signal-deficient homodimerising partner.

induce the receptor dimerization and that its dimerised intracellular domain activates the signalling pathway.

### 1.6.3 Order of oligomerisation

The possibility that the order of the receptor oligomerisation is higher than 2 (the Ob-R acts as a trimer or tetramer etc.) has been further investigated [66]. This experiment was based on a presumption that if the Ob-R only undergoes dimerization, then signalling should be negated by the overexpression of a homodimerising partner that is signalling deficient (Fig. 1.14). This effect has been observed for the receptor tyrosine kinase family [68, 69].

A truncated form of the Ob-R containing only 6 a.a. of the intracellular domain (OBRD868) was employed as the signalling-defective component. It was used in increasing amounts (relative to the full-length OBR) to investigate whether overexpression of OBRD868 was able to cancel wild-type receptor signalling. However, the results have shown that even a large excess of the truncated receptor is unable to diminish the signalling. The conclusion (based on the above presumption) is that the Ob-R does not act as a dimer but in a higher order oligomerisation form.

Similar effects have been observed for the interleukin-10 (IL-10) receptor [70]. The model of the IL-10R activation suggests that more than two

IL-10R molecules are involved in the receptor activation but that the juxtaposition of only two intracellular domains is sufficient for a signal activation. This mechanism would also fit the data obtained for the Ob-R.

However, the observed failure of truncated Ob-R to diminish the activity of signalling cascade can be explained in a different way. Wild-type leptin receptor may be unable to form homodimer when co-expressed with the truncated receptor because the truncated receptor would prevent physical contact between wild-type leptin receptor molecules.

Nevertheless, the method employed, co-expression of wild-type and truncated Ob-R forms on the cell surface, with subsequent measurement of the response to the ligand binding, is not able to distinguish between these two possibilities.

### 1.6.4 Receptor dimerization

The problem of receptor oligomerisation has been investigated further with the employment of another technique: namely, chemical cross-linking [71]. This has been used to compare the efficiency of ligand binding between the receptor long form (the wild-type version) and its short form (the truncated one).

Chemical cross-linking of leptin to the Ob-Rl has identified a homodimer and homo-oligomer complexes of the Ob-R. In contrast, chemical crosslinking of leptin to the short form of receptor has not revealed any complex formation. No interaction between leptin and the Ob-Rs has been proved even in the presence of the Ob-Rl form [71]. These results indicated that the incapability of the Ob-Rs form to diminish the signalling of Ob-Rl form discussed above is not due to the formation of a oligomeric complex between Ob-Rs and Ob-Rl [66], but rather that the overexpression of the Ob-Rs form does not come into physical contact with the Ob-Rl molecules.

The role of the Ob-R extracellular domain alone in the formation of the receptor oligomeric complex has also been studied. An aggregation state of the soluble Ob-R extracellular domain has been studied using leptin affinity and gel filtration chromatography [71]. Surprisingly, it has revealed that the Ob-R extracellular domain is present in a dimerised form even in the absence of leptin. Thus, the wild-type Ob-R may also be present on a cell surface as a dimer even before leptin binding. This observation makes the hypothesis that leptin activates the receptor through its dimerization rather problematic.

### 1.6.5 Experimental design

The cross-linking experiments together with the ligand binding studies represent very indirect methods for characterisation of the interaction of the leptin receptor with its ligand. In the ligand binding experiments, the strength of the leptin binding has been deduced from the level of the transcription of a specific reporter gene. However, this gene (Luciferase assay) does not represent the *in vivo* leptin signalling target. Therefore, leptin action in its authentic environment may be significantly different. Chemical cross-linking on the other hand represents quite a harmful technique. It covalently links proteins which are close to each other. The short distance between proteins however does not necessarily mean that these proteins interact.

Data obtained using these techniques must therefore be treated with caution and conclusions made about the receptor activation mechanism should be kept open for further modification. The design of less harmful and more accurate experimental configuration is therefore highly desirable. The optimal technique should use methods more strictly based on the physical phenomena. Attractive candidates for the determination of the number of the involved receptor and ligand molecules are analytical techniques, such as BiaCore, microcalorimetry and analytical centrifugation.

Parallel use of these techniques should provide another useful piece of information. BiaCore represents a powerful new technique used mainly for studying of reaction kinetics, but it is expected to be useful also for the determination of reaction stoichiometry. Data obtained by BiaCore analysis can be directly compared with results obtained by microcalorimetry or analytical centrifugation. Such data comparison would provide a very valuable justification of BiaCore for the use in the stoichiometrical experiments.

Until recently, the application of these techniques, with the exception of BiaCore, has been restricted only to the study of synthetic components because natural ones have not been available in sufficient amounts. This problem has now been overcome by the development of new highly efficient expression systems which today generate adequate quantities of proteins.

The employment of BiaCore, microcalorimetry or analytical centrifugation in the analysis of the interaction between leptin receptor and its ligand should provide much more accurate results than those from classical biological techniques. A parallel use of more then one technique would furthermore minimise biases which accompany every single experimental method. Ideally, BiaCore would be accompanied by microcalorimetry or analytical centrifugation in the

characterisation of the leptin-leptin receptor interaction.

### 1.6.6 Aim of the project

The aim of the project was to determine the thermodynamics of the leptin–leptin receptor interaction using a variety of biophysical techniques. To achieve this, it was necessary to express the leptin receptor, as the cDNA was not available at the start of this project. The initial goal was to obtain the cDNA encoding the extracellular domain of the receptor by RT-PCR. The open reading frame comprising 839 a.a. encoded by 2517 nucleotides was generated by several molecular approaches as the mRNA was a rare species.

Because biophysical techniques require large amounts of protein, different expression systems were attempted. However, BiaCore analysis requires small amounts of protein and this method was used to evaluate the leptin–leptin receptor interaction.

# Chapter 2

# Materials and Methods

## 2.1 Molecular biology

### 2.1.1 General laboratory supplies and procedures

General stock chemicals and equipment were obtained from Sigma Chemical Co., Fisons Scientific Equipment or BDH Merck and, when necessary, were of analytical, molecular biological, or HPLC grade. Compositions of all solutions used are listed in Appendix II when not specified in the text. Water for general laboratory use was single-distilled. Equipment and solutions were sterilised by heating to high temperature (121°C) with high pressure (1.05 bar) for 20 minutes in an autoclave (Labclave II, Dent and Hellyer).

In addition, general precautions and procedures [72] were followed to minimise RNase contamination in the laboratory. When working with solutions and equipment used for RNA analysis, gloves were worn at all times to prevent "finger nucleases" contamination. Sterile, disposable plasticware was used wherever possible and plastic disposable pipette tips and microcentrifuge tubes were autoclaved prior to use. All glassware and other bakeable equipment, such as steel tweezers and foil, were baked at 270°C for at least eight hours to inactivate nucleases. Where possible, separate chemical stocks were designated for RNA use only. Solutions for RNA use (with the exception of Tris-containing solutions) were treated overnight with 0.05% diethylpyrocarbonate (DEPC), a non-specific inhibitor of ribonuclease, and then autoclaved to destroy any remaining DEPC. Dilutions of stock chemicals and enzyme reaction buffers were made with DEPC-treated water. Electrophoresis gel rigs, combs and baffles dedicated for RNA use were well rinsed with DEPC-treated water, covered and stored away from other general laboratory equipment.

## 2.1.2 Cell culture

### Mammalian cell culture

Cell culture was performed in laminar-flow tissue-culture hoods (Microflow Biological Safety Cabinet, Airflow ServiceCare). Solutions, materials and reagents used for cell culture were sterilised either by autoclaving or by filtration through 0.22 $\mu$m filter units (Millex-GV, Millipore).

**COS and HEK cell cultures** Both cell lines were grown on plastic tissue culture plates. COS cells [73] were grown in Dulbecco's Modified Eagles Medium (DMEM, Gibco BRL) supplemented with 10% calf serum, 2mM glutamine, 1000 i.u. penicillin and 0.1 mg/ml streptomycin. Human embryo kidney (HEK) cells [74] were grown in Dulbecco's Modified Eagles Medium (RPMI, Gibco BRL) supplemented with 10% foetal calf serum, 2mM glutamine, 1000 i.u. penicillin and 0.1 mg/ml streptomycin. Cells were routinely maintained on 100 mm diameter plates and subcultured every third day. Typically, 2 - 8 $\cdot 10^5$ cells were plated. Cells were routinely passaged up to a maximum of twenty times. Adherent cells were dislodged by a 10 min treatment with Trypsin (1:250, Gibco BLR) at 37°C. Cultures were maintained at 37°C in a water-saturated atmosphere of 95% air and 5% carbon dioxide in tissue culture designated incubators (Napco 5410).

**Cell quantification** Total cell counts were determined using a haemocytometer (Sigma). The cell sample was prepared as follows. 0.5 ml of 0.4% Trypan Blue solution (w/v) (SIGMA) was added to a test tube with 0.5 ml of cell suspended in phosphate-buffered saline (PBS) and mix thoroughly. The solution was allowed to stand for 5 to 15 min With the cover-slip in place, 15 $\mu$l of cell solution was transferred to the haemocytometer. Cells in four corner squares as well those touching top and left middle line of the perimeter of each square were counted. The average number of cells per millilitre was calculated to be the average count per square multiplied by both the dilution factor (2) and $10^4$.

## 2.1.3 Bacterial culture and manipulation

All bacterial work was performed at the laboratory bench. Solutions, media, glassware and plasticware were sterilised by autoclaving before use. The bench was swabbed with ethanol prior to use. A bunsen burner flame maintained

aseptic conditions in the area. Tools used, such as metal loops and glass spreading devices, were sterilised by dipping in ethanol and flaming. Bacterial cultures were grown at 37°C in an incubator (Napco Model 301).

**Media preparation** *E. coli* bacteria were grown in Luria-Bertani medium (LB, Gibco BRL). Liquid LB medium consisted of 20 g of premixed LB powder per litre of distilled water which was then autoclaved. Medium was allowed to cool to approximately 50°C before addition of the antibiotic ampicillin (Sigma) to 100 $\mu$g/ml. Agar plates were prepared using premixed LB agar powder (Gibco BRL). Thirty-two grams of powder were added per litre of distilled water and the mixture was autoclaved which, in addition to sterilisation, dissolved the agar. After adding antibiotic, as described above, the liquid was poured into sterile, 100mm plastic bacteria plates; about 33 ml of medium was used per plate. The agar plates were allowed to solidify at room temperature and were then dried, in an inverted position with covers ajar, at 37°C for 30 minutes. Plates were then either used immediately or stored at 4°C in their original plastic storage sleeves for up to one month.

For identification of bacterial colonies transformed with plasmid vector containing the beta-galactosidase gene in the polylinker region, agarose plates containing besides an appropriate antibiotic also 0.1 mM isopropyl-$\beta$-D- thiogalactopyranoside (IPTG) and 40 $\mu$g/ml of the chromogenic substrate 5-bromo-4-chloro-3-indoyl-$\beta$-D-galactopyranoside (X-Gal) were used.

**Competent bacteria preparation** Bacteria competent to absorb DNA were either purchased from Gibco BLR or made up, prepared and transformed using calcium chloride. DH5$\alpha$ bacterial strain was streaked onto an LB agar plate and allowed to grow overnight at 37°C. The next day, a single colony was selected and transferred into 5 ml of TYM medium and allowed to grow at 37°C with agitation for two to three hours. This culture was then transferred to a 250 ml Erlenmeyer flask containing 100 ml TYM media and allowed to grow until the absorbance of the suspension was approximately 0.5 OD units at 550 nm. The suspension was then snap-cooled in an iced water bath and centrifuged (GS-3 rotor, Sorvall centrifuge) in sterilised polypropylene tubes at 2600 g for ten minutes at 4°C. The resulting bacterial pellet was resuspended in 30 to 40 ml of TfbI per 100 ml original culture and incubated on ice for five minutes. Cells were centrifuged again for eight minutes at 2600 g at 4°C. The pellet was then resuspended in 4 ml of TfbII per 100 ml original culture. One hundred microlitre aliquots of competent cells in polypropylene

microcentrifuge tubes were snap-frozen in liquid nitrogen and stored at -70°C.

**Transformation of bacteria with DNA** A 100 $\mu$l aliquot of competent cells was thawed on ice for each sample of DNA to be transformed. Ten microlitres of DNA, containing between 10 to 100 ng of DNA, was added to the suspension of competent bacteria and, after gentle mixing, was incubated on ice for 15 minutes. The bacteria/DNA mixture was then "heat-shocked" by incubation at 42°C for 45-50 seconds or at 37°C for 5 minutes. Nine hundred microlitres of LB media was then added and the mixture was then incubated at 37°C for 15 minutes. A 100 $\mu$l aliquot of this mixture was plated on to LB-ampicillin/IPTG/X-Gal plates. Control transformation reactions using circular, non-recombinant plasmid vector were performed alongside experimental samples to assess transformation frequency, which was routinely determined to be between $1/10^3 - 1/10^4$ cells. Reactions eliminating plasmid DNA served as negative controls. Recombinant transformants, which have an interrupted $\beta$-galactosidase gene, grew as white colonies while non-recombinant colonies were stained blue due to reaction of $\beta$-galactosidase with X-Gal. Recombinant bacterial colonies were identified by plasmid "minipreparation", restriction digestion and electrophoresis (see below).

## 2.1.4 Nucleic acid isolation

### Extraction of total RNA

Total cellular RNA was extracted and isolated using acid phenol extraction method [75]. Cells were washed on the culture plate once with 2 ml ice-cold phosphate-buffered saline solution (PBS). PBS was removed and 500 $\mu$l (for 60 mm plate) of pre-chilled guanidinium isothiocyanate (GTC) was added. This harvest was then transferred to a sterile tube and cells were subsequently kept on ice during RNA extraction. Cells were pelleted by centrifugation at 4°C for three minutes at 900 g and the resulting pellet was homogenised in the guanidinium isothiocyanate solution by thorough vortexing.

This was then acidified by addition of 0.1 volume of 2M sodium acetate, pH 4 and then extracted to remove protein with one volume of water-saturated phenol (Rathburn Chemicals Ltd) in the presence of 0.2 volumes of chloroform:isoamyl alcohol (49:1). The solution was vortexed vigorously and after 15 min incubation on ice the sample was centrifuged at 12,000g for 20 min at 4°C. The aqueous phase, containing the RNA, was transferred to another tube. Total RNA was precipitated overnight at -20°C by adding one volume

of 100% ethanol and mixing by inversion. Overnight precipitation ensured maximum RNA yields.

RNA was pelleted by centrifugating at 4°C for 30 minutes at 8,000 g. After decanting the supernatant, the pellet was washed with 1 volume of ice-cold 75% ethanol. Pellet was resuspended by pipetting. After centrifugation and air drying, the final pellet was dissolved in DEPC-treated water. RNA samples were routinely stored as 20-50 $\mu$l aqueous solutions at -70°C.

### Isolation of plasmid DNA

**Plasmid "Minipreparation"** The alkaline lysis method [76] was used for DNA miniprep. Individual bacterial colonies were picked from agar plates using sterile plastic disposable pipette tips, placed (one colony/tube) into 30 ml sterile glass test-tubes containing 5 ml of LB/ampicillin and grown overnight with constant agitation to saturation at 37°C. Bacteria in 1.5 ml aliquots of these cultures were pelleted by centrifugation at 5,000 g for one minute. Supernatant was removed and the bacterial pellet was resuspended in 200 $\mu$l of ice-cold, 10 mM EDTA, pH 8.0. Bacteria were lysed by addition of 400 $\mu$l of 0.2 M NaOH, 1% SDS; protein was precipitated by addition of 225 $\mu$l of 10 M ammonium acetate. Following gentle mixing by inversion and subsequent flicking with the fingertips, tubes were centrifuged for five minutes at room temperature at 8,000 g and the supernatant poured into fresh microcentrifuge tubes. DNA was precipitated by adding one volume isopropanol and centrifugation for 10 minutes at 4°C. The resulting pellet was rinsed twice with 90% ethanol, air-dried and dissolved in 50-100 $\mu$l TE containing 10 $\mu$g/ml RNase A which had been preboiled to inactivate DNase.

**Plasmid "Maxipreparation"** Large-scale plasmid preparations were performed using a kit (QIAfilter Plasmid Maxi System, QIAGEN). A single colony was picked from a freshly streaked selective plate and a starter culture of 25 ml LB medium containing the appropriate selective antibiotic was inoculated for 8 h at 37°C with vigorous shaking (300 rpm). The starter culture was then diluted 1/500 to 1/1000 into selective LB medium. For high-copy plasmids 100 ml medium were inoculated and grown at 37°C for 12-16 h with vigorous shaking (300 rpm) until the culture reached a cell density of approximately 3-4 x $10^9$. A flask or vessel with a volume of at least 4 times the volume of the culture was used. The bacterial cells were harvested by centrifugation at 6000 $\times$ g for 15 min at 4°C. The bacterial pellet was resuspended in 10 ml Buffer P1

(supplied). For efficient lysis a vessel large enough to allow complete mixing of the lysis buffers was used. RNase A has been added to Buffer P1. The bacterial pellet was resuspended completely by vortexing or pipetting up and down until no cell clumps remain. 10 ml Buffer P2 (supplied) was added, mixed gently but thoroughly by inverting 4-6 times, and incubated at room temperature for 5 min. The suspension was not vortexed, as this would result in shearing of genomic DNA. During the incubation, the QIAfilter Cartridge was prepared: The cap was screwed onto the outlet nozzle of the QIAfilter Maxi Cartridge. The QIAfilter Cartridge was placed in a convenient tube. 10 ml chilled Buffer P3 (supplied) was added to the lysate, and mixed immediately but gently by inverting 4-6 times. Immediately after, the lysate was poured into the barrel of the QIAfilter Cartridge and incubated at room temperature for 10 min. A QIAGEN-tip 500 was equilibrated by applying 10 ml Buffer QBT (supplied). The column was allowed to empty by gravity flow. The cap from the QIAfilter outlet nozzle was removed. The plunger was gently inserted into the QIAfilter Maxi Cartridge and the cell lysate was filtered into the previously equilibrated QIAGEN-tip. The cleared lysate was allowed to enter the resin by gravity flow. The QIAGEN-tip was washed with 2 × 30 ml Buffer QC (supplied). DNA was eluted with 15 ml Buffer QF (supplied). DNA was precipitated by adding 10.5 ml (0.7 volumes) room-temperature isopropanol to the eluted DNA. The mixture was centrifuged immediately at 15,000 × g for 30 min at 4°C. The supernatant was decanted carefully. DNA pellet was washed with 5 ml of room-temperature 70% ethanol and centrifuged at 15,000 × g for 10 min. The supernatant was decanted carefully without disturbing the pellet. The pellet was air-dried for 5-10 min, and the DNA was redissolved in a suitable volume of buffer (e.g., TE, pH 8.0, or 10 mM Tris-Cl, pH 8.5).

### Quantification of nucleic acid

DNA or RNA was quantified spectroscopically using the DU-640B Beckman spectrophotometer. Sample absorption at 260 and 280 nm versus blank was measured and concentration determined using a predefined software. Purity of DNA/RNA was determined from $A_{260}/A_{280}$ ratio which was ideally above 1.8.

### 2.1.5 Nucleic acid manipulation

#### Phenol/chloroform extraction

Protein and/or salts were removed from solutions of DNA by extraction with phenol and chloroform [76]. One volume of phenol (equilibrated to pH 7.5 with 1M Tris, 0.2% $\beta$-mercaptoethanol, 0.1% hydroxyquinoline) was added to the DNA solution and vortexed thoroughly. An equal volume of chloroform was added to the mixture to enhance phase separation and the mix was then centrifuged at 8,000 g for 5 minutes. The upper aqueous phase containing the DNA was removed and care was taken to avoid contamination with the proteinaceous interphase.

#### Ethanol precipitation of nucleic acid

DNA or RNA was precipitated by the addition of NaCl to 0.15 M and the subsequent addition of 2.5 (for DNA) to 3 volumes (for RNA) of ethanol [76]. Precipitation was allowed to proceed at -20°C for 3-24 hours. When the amount or the size of nucleic acid to be precipitated was small, 10 $\mu$g linear polyacrylamide, or 100 $\mu$g glycogen (Boehringer Mannheim) was added to the tube to facilitate precipitation; oligonucleotides were precipitated in the presence of 10 mM $MgCl_2$ to optimise recovery [76].

### 2.1.6 DNA modification

#### Restriction enzyme digestion

DNA was digested with restriction enzymes using conditions and buffers as suggested and supplied (Gibco BRL, Promega, Boehringer Mannheim). Typically, 5-10 units of enzyme were used per microgram of DNA. Incubations were carried out for 1 hour at 37°C.

#### Dephosphorylation

Shrimp alkaline phosphatase (SAP) (U.S. Biochemicals) was used to remove the terminal 5'-phosphate group from DNA. Dephosphorylation was carried out for three hours in a reaction volume of 100 $\mu$l containing 1$\times$ buffer, digested DNA and 5 units of enzyme. The reaction was terminated by heating to 65°C for 10 minutes.

### Ligation

T4 DNA ligase (Boehringer Mannheim) was used to catalyse the formation of a phosphodiester bond between adjacent 3'-hydroxyl groups and 5'-phosphate termini in DNA [77]. A typical 10 $\mu$l reaction containing 2mM ATP, 100-500 ng DNA, 1× buffer (Boehringer Mannheim "L" buffer) and 3 units of enzyme was allowed to proceed overnight at 15-25°C. The reaction was terminated by heating to 72°C for 5-10 minutes.

## 2.1.7 DNA agarose gel electrophoresis

One to two percent agarose (SeaKem LE or FMC BioProducts) was prepared in 1× TAE and dissolved by heating in a microwave oven; 0.1 $\mu$g/ml ethidium bromide was added to both gel and running buffer to allow visualisation of the DNA under illumination with ultraviolet light at 254 nm. Gels were cast on manufactured plates with teflon well combs. Gels were electrophoresed at 70-100 V in 1× TAE buffer containing 0.1 $\mu$g/ml ethidium bromide. Molecular weight markers (*Hind* III/*Eco*R I – digested or *Sau*3A I – digested lambda DNA, *Hae* III – digested pBR322) were run alongside the samples. Gels were then photographed under ultraviolet illumination at 254 nm using Polaroid DS34 Direct Screen Instant camera and Polaroid 667 Land film. If necessary, DNA was extracted from 1× TAE-agarose gels using Gel Extraction Kit (QIAGEN).

## 2.1.8 DNA synthesis

The cDNA encoding the extracellular domain of the leptin receptor was synthesised by reverse transcription (RT) of mRNA using the cDNA Cycle® kit (Invitrogen) and amplification of cDNA using Taq/Pwo Polymerases Mix (Hybaid) or Pfu DNA Polymerase (Stratagene). In the RT step, AMV Reverse Transcriptase (Invitrogen) was used, which catalyses the polymerisation of DNA using an RNA template in the presence of $MnCl_2$. The ability of this polymerase to reverse transcribe at elevated temperatures results in increased specificity of primer hybridisation and extension and minimises problems encountered with strong RNA secondary structures since these are unstable at higher reaction temperatures. DNA Polymerases used in the PCR step are thermostable enzymes isolated from Thermus thermophilus, which catalyse the polymerisation of nucleotides into duplex DNA in the 5'-3' direction in the presence of $MgCl_2$ [78].

Reactions were performed as outlined by the manufacturer. First-strand cDNA was synthesised from 8 $\mu$g total RNA in 20 $\mu$l total volume with 1mM $MnCl_2$, 0.2 mM each of dATP, dCTP, dTTP, dGTP, 1× RT buffer (supplied), 15 pmol of RT (reverse) primer and 4-6 units of polymerase. The reaction was carried out in a thin-walled, 0.5 ml microcentrifuge tube at 70°C for 20 minutes. The reverse transcription component of the reaction was then terminated by snap-cooling the tube on ice and adding chelate buffer (supplied) which contained EGTA to remove the $Mn^{2+}$. The reaction conditions within the tube were then modified to allow for DNA polymerisation; the reaction volume was increased to 100 $\mu$l with DEPC-treated water and $MgCl_2$ to 2.5mM and 15 pmol of 5' (upstream, forward) primer were added. After gentle mixing, 40 $\mu$l of mineral oil were layered on top of the reaction mix to prevent evaporation during amplification. The tube was then subjected to cycled temperature conditions. After an initial denaturation step at 95°C for five minutes, the reaction was allowed to cycle 30 times through a sequence of temperatures: 1) denaturation of template: 92°C, 1.5 minutes; 2) primer annealing at a temperature 5 to 10°C lower than denaturing temperature (52-60°C), 1 minute; and 3) DNA polymerisation: 68°C (Taq/Pwo Mix), 70°C (Pfu), 1 minute/1 kb of template. A final elongation step at 68(70)°C for 10 minutes was also performed. Ten microlitre aliquots of the products of the reactions were size-separated by agarose gel electrophoresis. Ethidium bromide-stained DNA products in the gels were visualised under ultraviolet irradiation.

### 2.1.9 Transient transfection (SuperFect)

The following protocol was used for transfection of adherent mammalian cells in 100-mm dishes using SuperFect transfection reagent (QIAGEN). The day before transfection, $2 - 8 \cdot 10^5$ cells (depending on the cell type) were seeded per 100-mm dish in 5 ml of appropriate growth medium. The cell number seeded should produce 40-80 % confluence on the day of transfection. The cells were incubated at $37°C$ and 5% $CO_2$ in air in an incubator. 10 $\mu$g of DNA dissolved in TE, pH 7.4 (minimum DNA concentration: 0.1 $\mu g/\mu l$) were diluted with cell growth medium containing no serum, proteins, or antibiotics to a total volume of 300 $\mu$l. The solution was mixed and 60 $\mu$l of SuperFect transfection reagent was added to the DNA solution. The solution was mixed by pipetting up and down 5 times, or by vortexing for 10 seconds. The samples were incubated for 5-10 min at room temperature (20-25°$C$) to allow complex formation. While complex formation took place, the growth medium was

gently aspirated from the dish, and cells were washed once with 4 ml PBS. The 3 ml of cell growth medium (containing serum and antibiotics) was added to the reaction tube containing the transfection complexes. This was then mixed by pipetting up and down twice and was immediately transferred to the cells in the 100-mm dishes. At this stage serum and antibiotics no longer interfere with, but significantly enhance the transfection efficiency of SuperFect Reagent. Cells were incubated with the complexes for 2-3 h at 37°C and 5 % $CO_2$. Medium containing the remaining complexes was removed from the cells by gentle aspiration, and cells were washed once with 4 ml of PBS. Fresh cell growth medium containing serum and antibiotics was added. Cells were harvested 24-48 h after transfection.

### 2.1.10 Transient transfection (GenePORTER)

The following protocol was used for transfection of adherent mammalian cells in 100-mm dishes using GenePORTER transfection reagent (TSE inc.). The day before transfection, the cells were plated on 100 mm plate so that they would be 60-90% confluent on the day of transfection[3]. 8-12 $\mu$g of the DNA was diluted with serum-free medium[4] to final 500 ml. The GenePORTER solution was vortexed. 40-60 $\mu$l of the GenePORTER were diluted with serum-free medium to final 500 ml. Both the DNA and the GenePORTER solutions were mixed well. The diluted DNA was added to the diluted GenePORTER reagent, mixed rapidly and incubated at room temperature for 10-45 minutes. Further 4 ml of serum-free medium were added to the DNA/GenePORTER mixture. The culture medium was aspirated from the cells, the DNA-GenePORTER mixture was carefully added to the cells and incubated at 37°C for 3-5 hours. Then 5 ml of medium containing 20% serum was added. The incubation was continued overnight under 5-10% $CO_2$ at 37°C. 24 hours post transfection, more fresh growth medium was added as needed[5]. The assay was done 24-72 hours after the start of transfection depending on the cell type and promoter activity.

[3]Omitting antibiotics from the media during transfection can increase expression levels. This effect is cell-type dependent and usually small.

[4]Although GenePORTER consistently delivers high transfection efficiencies in a wide range of cell types, to obtain maximum efficiency in particular cell lines some optimisation may be needed. The two critical variables are the GenePORTER/DNA ratio and the DNA quantity. To optimise these two variables, first determine the best GenePORTER/DNA ratio by using 3-9 ml of reagent for each 1 mg of DNA. Use a low DNA quantity to optimise this parameter. Once the optimal ratio is determined, vary the DNA quantity over the suggested range. At this point cell number can also be optimised.

[5]For some cell types the old media can be replaced with fresh media at this step.

### 2.1.11 Transient transfection (DEAE-DEXTRAN)

The following protocol was used for transfection of adherent mammalian cells in 100-mm dishes using DEAE-DEXTRAN. 24 hours before transfection, the cells were plated on 100-mm plate so that they would be 60-90% confluent on the day of transfection. The DNA/DEAE-DEXTRAN solution was prepared by diluting DNA with 250 $\mu$l of TE to a final concentration of 0.1-4 $\mu$g/ml and adding 200 $\mu$l of DEAE-DEXTRAN. The solution was left at room temperature for 30 min. Then 5 ml of NU medium was mixed with 5 $\mu$l of 100 mM chloroquine and warmed to 37°C. Medium was removed from plates and 5 ml of warm NU medium was added to cells. Then the DNA/DEAE-DEXTRAN solution was added drop by drop. The plates were incubated at 37°C for up to 4 hours. NU medium was removed, 5 ml of 10% DMSO/1×PBS was added and cells were incubated for 2 min. Medium was promptly removed, cells were washed once with 1×PBS and 5 ml of fresh medium was added. Cells were incubated overnight and transfer to a new plate, using trypsin, to remove all traces of DEAE-DEXTRAN. The assay was done 24-72 hours after the start of transfection depending on the cell type and promoter activity.

### 2.1.12 Total protein quantification

The method of Bradford [79] (BioRad Protein Assay Dye Reagent Concentrate) was used to determine total protein concentrations. Bovine serum albumin (BSA, Sigma) was used as standard protein for calibration; calibration curves from 1-15 $\mu$g BSA were performed alongside all protein determination experiments. Typically, 5 $\mu$l of protein sample were added to plastic, 2 ml cuvettes with 0.8 ml of water. 0.2 ml of dye reagent concentrate was then added and vortexed immediately. After a period of 5 minutes to 1 hour, sample absorbance at 595 nm was assessed (DU-67, Beckman) versus reagent blank. Blank reagent contained water and dye reagent only. Absorbance values from the BSA standards were plotted against total protein to obtain a standard curve. Linear regression analysis was performed to determine the best-fit equation and this line was used to determine protein concentrations in the experimental samples which exhibited absorbance readings within the linear range of the standard curve.

### 2.1.13 Preparation of cellular membrane fraction

Cells were grown on a 100 mm dish. Medium was removed, cells were washed with 1× PBS and harvested. Cells were spun at 1000-1200 RPM for 5 min and supernatant was removed. Cells were washed again with 1× PBS and spun at 1000-1200 RPM for 5 min. The cell pellet was placed at $-80°C$ for at least 30 min. After thawing, 500-700 $\mu$l of TE was added and cells were mechanically homogenised (3 × 20). This was followed by rehomogenisation (1 × 20 with 25GA 5/8 0.5 × 16 needle). Homogenised cells were placed in an eppendorf tube and spun at 1000-1200 RPM for 5-10 min. *Supernatant 1* and *Sediment 1* were collected. *Sediment 1* was resuspended in 500-700 $\mu$l TE and rehomogenised. It was spun at 1000-1200 RPM for 5-10 min. *Supernatant 2* and *Sediment 2* were collected. *Supernatant 1* + *Supernatant 2* were then spun at 75,000 g for 30 min. The *Supernatant* and *Sediment* were collected. The *Sediment* (the membrane fraction) was resuspended in 300-400 $\mu$l TE. Samples were aliquoted and stored at -80°C.

### 2.1.14 SDS-PAGE analysis

#### Preparing SDS-PAGE gels

Glass plates were assembled according to the manufacturer's instructions.The appropriate volumes of solutions containing the desired concentration of acrylamide for the resolving gels was prepared, using the values given in Table A.1. TEMED was added as the last one. Components were vigorously mixed and without delay, the mixture was swirled rapidly and poured into the gap between the glass plates. The acrylamide solution was carefully overlaid with 0.1 % SDS solution (for gels containing $\leq 8$ %) or isobutanol (for gels containing $\geq 10$ % acrylamide). After polymerisation was completed (30 minutes), the overlay was poured off and the top of the gel was washed several times with deionised water to remove any unpolymerised acrylamide. Any remaining water was removed with the edge of a paper towel. The stacking gel was prepared as follows. In a disposable plastic tube, the appropriate volume of solution containing the desired concentration of acrylamide was prepared, using the values given in Table A.2. TEMED was added as the last one. Components were vigorously mixed and without delay, the mixture was swirled rapidly and the stacking gel solution was poured directly on to the surface of the polymerised resolving gel. A clean Teflon comb was immediately inserted into the stacking gel solution, being careful to avoid trapping air bubbles.

While the stacking gel was polymerising, samples were prepared by heating them to 100°C for three minutes in 1× SDS-gel-loading buffer (BIO RAD) to denature the proteins. After polymerisation was completed (30 minutes), the Teflon comb was removed carefully. The gel was mounted in the electrophoresis apparatus. Tris-glycine electrophoresis buffer, Table A.3, was added to the top and bottom reservoirs. Up to 100 $\mu$l of each of the samples was loaded in a predetermined order into the bottom of the wells. The gel unit was run overnight at 45-50 V according to acrylamide concentration.

### 2.1.15 Staining SDS-PAGE gels with Brilliant Blue

After electrophoresis, proteins were fixed for one hour in a solution of 7 % glacial acetic acid in 40 %(v/v) methanol, Table A.4. Four parts of 1× working solution of Brilliant Blue G-Colloidal Concentrate (SIGMA) were mixed with one part of methanol prior to staining. This solution was mixed for 30 seconds and the gel was then placed in this staining suspension for 1-2 hours. It was followed by destaining with 10% acetic acid in 25 % (v/v) methanol, Table A.5, for 60 seconds with shaking. The gel was rinsed with 25 % methanol, and then destained in 25 % methanol for up to 24 hours. Gels were stored for several months in water containing 20 % glycerol.

### 2.1.16 Protein transfer

After the protein samples were separated using gel electrophoresis, the resolving gel was rinsed in the protein transfer buffer. A sheet of Hybond ECL membrane was prepared, pre-wetted in distilled water and then equilibrated in the protein transfer buffer, Table A.3, for at least 10 min. The protein transfer from the gel to the membrane was carried out for 4-5 h (300-250 mA) or overnight (40 mA). The membrane was air dried and either stored (between sheets of 3MM paper wrapped in SaranWrap at $2 - 8°C$ for up to 3 months) or used for Western Blotting.

### 2.1.17 Western blotting

To minimise nonspecific binding, the membrane was immersed in 5% (w/v) blocking reagent (non-fat dried milk) in TBS-T or PBS-T for one hour at room temperature on an orbital shaker. The membrane was then briefly rinsed using two changes of washing buffer (TBS-T or PBS-T). It was then washed once for 15 min and twice for 5 min at room temperature (4 ml of buffer per $cm^2$). The

membrane was then incubated in diluted primary antibody for 1 hour at room temperature, followed by a brief rinse using two changes of washing buffer. It was then washed once for 15 min and twice for 5 min at room temperature. The membrane was then incubated in diluted secondary antibody for 1 hour at room temperature and washed again. To perform ECL detection, equal volumes of detection solution 1 and solution 2 were mixed to give a sufficient amount of liquid to cover the membrane (0.125 ml/cm$^2$). The excess of wash buffer was drained from the washed blots and the blots were placed with the protein side uppermost on a sheet of SaranWrap spread over the bench. The prepared ECL detection reagent was added directly to the side carrying the protein and incubated for 1 min. An excess of detection reagent was drained off and the blot was placed, protein side down, onto a fresh piece of Saran Wrap. The Saran Wrap was folded over the back of the blots to form an envelope. The blots were placed, protein side up, in the film cassette. In the dark room, a sheet of autoradiography film was put on top of the blots and exposed for 1 min. The film was developed. If required, a second exposure was performed for an appropriate length of time.

### 2.1.18 *E. coli* expression

#### Screening transformants for FLAG fusion proteins

Individual colonies were inoculated into 5 ml LB containing 50 $\mu$g/ml ampicillin and 0.4 % glucose and incubated overnight at 37°C. Overnight cultures were diluted 1:1000 into 5 ml prewarmed LB containing 50 $\mu$g/ml ampicillin and 0.4 % glucose in a 125 ml flask to ensure good aeration and incubated with shaking at 37°C. At $OD_{600}$ of 0.2, a volume of 0.5 ml of pre-induction culture was removed to a microfuge tube. Cells were pelleted in a microcentrifuge, resuspended in 25 $\mu$l of SDS-PAGE sample buffer (BIO-RAD), heated to 95°C for 5 min and stored frozen. IPTG was added to the remaining culture to final 0.5 mM concentration. At 2, 4, and 6 hours post-induction, a 0.5 ml aliquot of culture was removed. Cells were pelleted in a microcentrifuge, resuspended in 25 $\mu$l of SDS-PAGE sample buffer (BIO-RAD), heated to 95°C for 5 min and stored frozen. Protein expression levels were determined by analysis of pre- and post-induction samples by SDS-PAGE and Western blot.

#### Analysis of expression of FLAG fusion protein

Individual colonies were inoculated into 5 ml LB containing 50 $\mu$g/ml ampicillin and 0.4 % glucose and incubated overnight at 37°C. Overnight cultures

were diluted 1:1000 into 5 ml prewarmed LB containing 50 $\mu$g/ml ampicillin and 0.4 % glucose in a 125 ml flask to insure good aeration and incubated with shaking at 37°C. At $OD_{600}$ of 0.2, IPTG was added to final 0.5 mM concentration and grown at 37°C for a previously optimised time (4 hours). A 0.5 ml aliquot of culture was removed. Cells were pelleted in a microcentrifuge, resuspended in 25 $\mu$l of SDS-PAGE sample buffer (BIO-RAD), heated to 95°C for 5 min and this whole cell sample was stored frozen. The remaining culture was divided into two aliquots and each aliquot was centrifuged at 5,000 $\times$ g for 10 min at 10°C to pellet the cells. The first pellet was used to determine the presence of the FLAG fusion protein in the periplasm space by the osmotic shock procedure. This sample pellet was not frozen to prevent whole-cell lysis. The second pellet was used to determine the presence of the FLAG fusion protein in the soluble and insoluble fractions of the whole cell extract. The pellet was stored frozen until needed.

### Periplasmic fraction by osmotic shock

The unfrozen pellet was warmed to room temperature and resuspended in 40 $\mu$l of 0.5 M sucrose, 0.03 M Tris, 1 mM EDTA at a final pH of 8.0 per gram of cells. The sample was then centrifuged at 3,500 $\times$ g for 10 min at 10°C for osmotic shock. The supernatant was decanted and the pellet rapidly resuspended in 25 ml/g cell pellet ice-cold, distilled water. The mixture was then centrifuged at 3,500 $\times$ g for 10 min at 4°C. Supernatant was collected immediately. 50 $\mu$l of supernatant were mixed with 50 $\mu$l SDS-PAGE sample buffer (BIO-RAD) and heated to 95°C for 5 min. The periplasmic fraction was stored frozen until ready for electrophoresis.

### Whole cell extract: soluble and insoluble fractions

The whole cell sample was thawed at room temperature. 5 ml of *Extraction Buffer A*, section A.4, was added. The sample was incubated at room temperature for 5 min or until cells were lysed. 0.5 ml of *Extraction Buffer B*, section A.4, was added and the mixture was incubated at room temperature for 5 min or until no longer viscous. The mixture was then centrifuged at 18,000 $\times$ g for 0.5 hour. Supernatant, containing the soluble, whole cell fraction, was collected. 50 $\mu$l of supernatant were mixed with 50 $\mu$l of SDS-PAGE sample buffer (BIO-RAD), heated to 95°C for 5 min and stored frozen. Pellet containing insoluble, whole cell material, was resuspended in 5 ml of *Extraction Buffer A*, Sec. A.4. 50 $\mu$l of supernatant were mixed with 50 $\mu$l of SDS-PAGE

sample buffer (BIO-RAD), heated to 95°C for 5 min and stored frozen.

### Preparative isolation of FLAG fusion proteins

FLAG fusion proteins were isolated by the osmotic-shock method. Cells were grown according to optimised growth and induction conditions, then harvested by centrifugation at 5,000 × g for 10 min at 10°C. Cells were resuspended in 10 mM Tris-HCl (pH 8.0) diluted from a 0.1 mM stock with room temperature distilled water. 40-80 ml/g cells were used. The mixture was centrifuged at 3,500 × g for 10 min at 10°C. Supernatant was decanted and the pellet resuspended in 0.5 M sucrose, 0.03 M Tris-HCl (pH 8.0), 1 mM EDTA at room temperature. 40 ml/g cells were used. Cells were centrifuged at 3,500 × g for 10 min at 10°C. Supernatant was decanted and the cell pellet rapidly resuspended in 25-35 ml ice-cold distilled water/gram of cell pellet. The mixture was centrifuged at 3,500 × g for 10 min at 4°C and supernatant collected immediately. An equal volume of 2 × concentrated TBS (pH 7.4) was added to the supernatant. $CaCl_2$ was added to a final concentration of 1 mM. The mixture was centrifuged at 25,000 × g for 60 min at 4°C and supernatant collected immediately. Supernatant was filtered through Whatman No 1 filter paper and applied to the ANTI-FLAG M2 Affinity Gel.

### Affinity purification of FLAG fusion proteins

**Preparation of the column** The empty chromatography column was placed on a firm support. The top and bottom tab were removed and the column was rinsed twice with TBS. Buffer was allowed to drain from the column and residual TBS was left in the column to aid in packing the anti-FLAG M2 affinity gel in the next step. The vial of anti-FLAG M2 affinity gel was thoroughly suspended to make a homogenous slurry of the gel beads. The slurry was immediately transferred to the column. The gel bed was allowed to drain and the vial was rinsed with TBS. The rinse was added to the column and allowed to drain again.

**Washing the column** The gel was washed by loading three sequential 5 ml aliquots of 0.1 M Glycine-HCl (pH 3.5), followed by three sequential 5 ml aliquots of TBS, avoiding a disturbance of the gel bed while loading. Each aliquot was allowed to drain completely before adding the next.

**Binding FLAG fusion proteins to the column** The sample was loaded onto the column under gravity flow. The column was filled completely several times for larger volumes. Depending upon the protein and flow rate, all of the antigen may not bind. Multiple passes over the column improved the binding efficiency. The column was washed three times with 12 ml aliquots of TBS.

**Elution of FLAG fusion proteins** The bound FLAG fusion protein was eluted from the column with 6 $\times$ 1 ml aliquots of 0.1 M Glycine at pH 3.5 into vials containing 15 - 25 $\mu$l of 1 M Tris base at pH 8.0.

## 2.2 Surface plasmon resonance

BiaCore biosensor $BIAcore^{TM}$ 2000, CM5 research grade biosensor chips, N-hydroxysuccinimide (NHS), ethanolamine-HCl, HBS-EP buffer (10 mM Hepes, pH 7.4, 150 mM sodium chloride and 0.005% Tween 20) and N-ethyl-N'-(3-diethylaminopropyl)carbodiimide (EDC) were obtained from BiaCore AB (Uppsala, Sweden). Protein G (IgG Fc Receptor Type III) and anti-human Fc specific antibody were purchased from Sigma. Recombinant human and mouse leptin receptor-Fc chimera as well as recombinant human, mouse and rat leptin were obtained from R & D Systems.

To prepare the biosensor assay, the capturing protein G or anti-human Fc specific antibody was immobilised onto a research-grade carboxymethyl dextran chip (CM5) using the amine-coupling procedure described previously [80]. The surface was activated with NHS/EDC for 5 min. Protein G (antibody) was injected at a concentration of 200 $\mu g/ml$ in sodium acetate buffer (10 mM, pH 4.0) until 2000 resonance units (RUs) of protein were coupled. Remaining activated groups were blocked with a 5-min injection of 1 M ethanolamine (pH 8.5).

For kinetic experiments the recombinant human or mouse leptin receptor-Fc chimera was captured onto the protein G (antibody) surface by injecting typically a 10 $\mu l$ of a 50 $\mu g/ml$ solution. After 1800 s equilibrium time a 100 $\mu l$ leptin or buffer sample was injected. The leptin concentration was typically at 0.1 - 30 nM range. The dissociation phase was then monitored for 400 s, followed by two 5 $\mu l$ injections of 10 mM glycine pH 2.0 to regenerate a fully active protein G (antibody) surface. All kinetic experiments were done at 25°C in a buffer containing 10 mM Hepes, pH 7.4, 150 mM sodium chloride and 0.005% Tween 20, at a flow rate of 30 $\mu l/min$. In control experiments,

Protein G (antibody) was used instead of the leptin receptor-Fc chimera to evaluate leptin nonspecific binding.

# Chapter 3

# Results

## 3.1 Cloning of the extracellular domain of the leptin receptor

Investigation of the interaction between the leptin receptor (OBR) and its ligand was started by the construction of an effective expression system for receptor production.

The receptor was originally cloned from the human brain cDNA library [38]. However, the cloned cDNA was not initially made available to the scientific community. It was, therefore, necessary to construct the receptor from the published sequence. The clone encoding the extracellular domain of the receptor was made using human embryo kidney (HEK) cell line instead. The cDNA was ligated to an expression vector and this part of the project was finished by expression of a recombinant protein.

### 3.1.1 Isolation of the cDNA

The desired cDNA, encoding the extracellular domain of the receptor, was generated by means of the reverse transcription polymerase chain reaction (RT-PCR). To provide high quality RNA for a synthesis of the first strand cDNA in the RT step, HEK cells were grown and total RNA extracted using the acid phenol extraction method [76]. The quality of RNA was tested by gel electrophoresis, Fig. 3.1. Three intensive bands represent intact 28S and 18S been degraded by RNAses, messenger RNAs should also be intact and suitable for a synthesis of the first strand cDNA. In addition, a background "smear", extended over large molecular weights and representing mRNA species, was observed. This smear again indicated a lack of degradation.

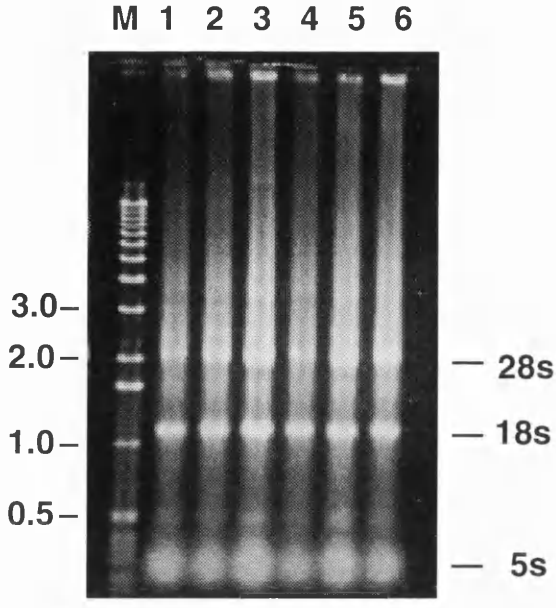


Figure 3.1: Total RNA extracted from the HEK cells. Three intensive bands correspond to the ribosomal 28s and 18s RNA and transfer 5s RNA.The background smear represents messenger RNA species of different length.

The next step was to design primers for the synthesis of the cDNA. The efficiency of the synthesis of the first-strand (a length of a synthesised product) is proportional to the purity of the mRNA used. However, only total RNA (not pure mRNA) was available. Thus, it looked very unlikely that the whole molecule (2.7 kb) could be generated at once. It was therefore decided to synthesise its two halves separately and to reconstitute the entire molecule afterwards by fragment ligation through a unique internal *Xho* I site located in the middle of the cDNA encoding predicted extracellular domain, Fig. 3.2.

Two forward primers were used to generate these fragments. The first one, F1, should generate the cDNA encoding the first half of the OBR extracellular domain. It contains an artificial *Hind* III restriction site at the 5' end for consequent cloning into an expression vector. The second primer, F2, flanks the unique internal *Xho* I site, which is located in the middle of the sequence, and should generate the cDNA encoding the second half of the extracellular domain.

Each of these forward primers was paired with the R3 and R4 reverse primers, respectively, Fig. 3.3. The R3 primer comprised the reverse complement of the sequence downstream of the unique *Xho* I site. The R4 primer was the reverse complement of sequence at the 3' end of extracellular domain and contained a *Bam*H I site to facilitate subcloning. Using these two primer

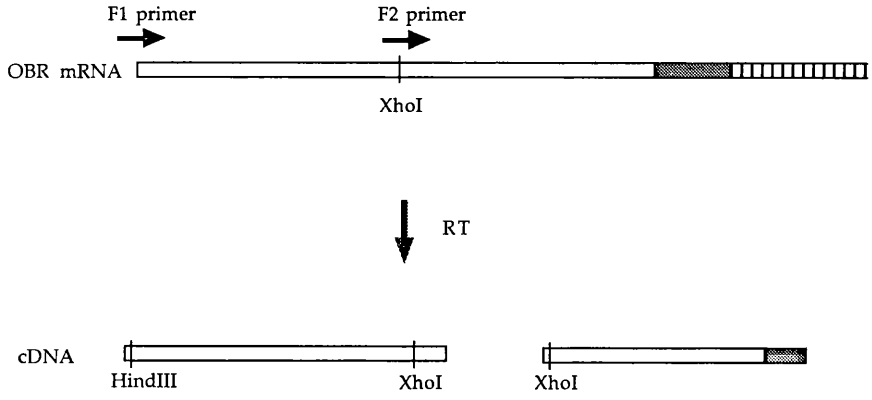


Figure 3.2: Two forward primers used in the RT reaction. Extracellular domain is in white, transmembrane is dotted and intracellular striped.

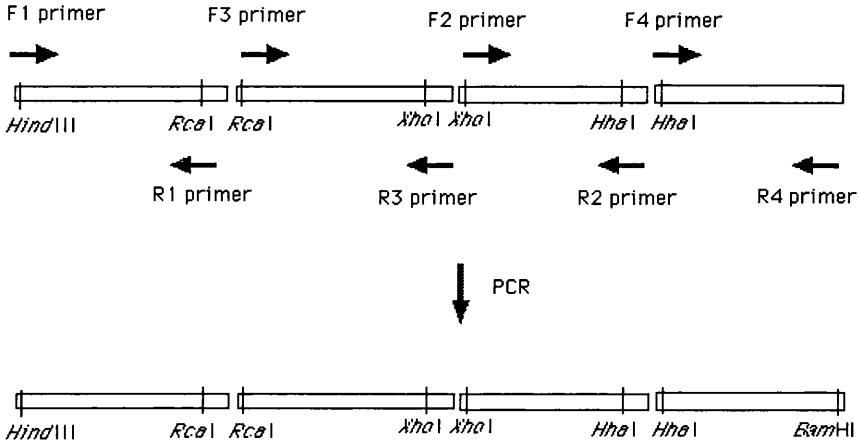


Figure 3.3: Forward and reverse primers used in PCR reaction.

pairs, no PCR products were obtained. This could be a result of the inability of Reverse Transcriptase to generate long fragments (1.3 kb) from a rare mRNA molecule. Therefore, it was decided to use four forward primers and reconstruct the molecule from four fragments (700 bp long), (Fig. 3.4)

In addition to F1 and F2 primers two additional forward primers were designed, Table 3.1. F3, containing an internal *Rca* I site, and F4, containing an internal *Hha* I site. The reverse primers used in sequential PCR reactions were: R1 with the *Rca* I site, R2 with the *Hha* I site, R3 with the *Xho* I site and R4 containing the artificial *Bam*H I site for a subsequent subcloning, (Fig. 3.3) In these experiments, the TAQ/PWO polymerase (Hybaid) with a proof-reading activity was used to overcome fidelity problems. This time, products of the expected length were generated as revealed by gel electrophoresis, (Fig. 3.5)

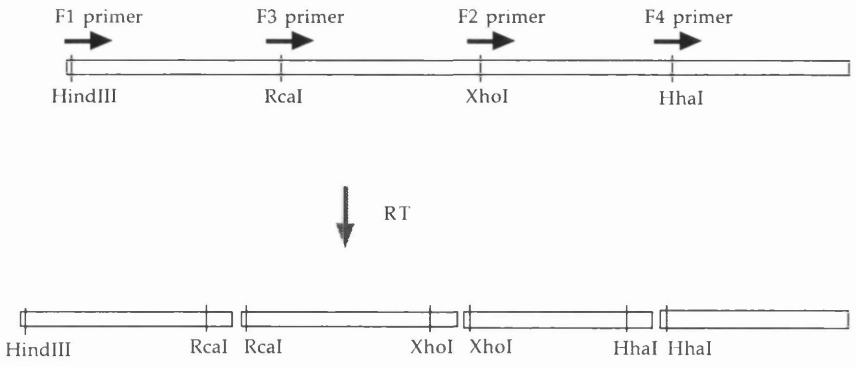


Figure 3.4: Four forward primers used in the RT reaction.

Table 3.1: Primers used in RT-PCR reaction.

| Name | Start | Sequence |
|---|---|---|
| F1 | 89 | GCGTTAAAGCTTTCGTGGCATTATC |
| F2 | 1389 | CCAAACCTCGAGGAAAGTTTACC |
| F3 | 755 | GCAGTGTTCATGAATGTTGTGAATGTCTTGTGCC |
| F4 | 2012 | TATGCTGTTCAGGTGCGCTGTAAGAGGC |
| R1 | 753 | CACAACATTCATGAACACTGCAA |
| R2 | 2021 | ATCTAGCCTCTTACAGCGCACCTG |
| R3 | 1381 | CTTTCCTCGAGGTTTGGTTTCATTC |
| R4 | 2697 | AACCTGGATCCCTCTGGTGTT |

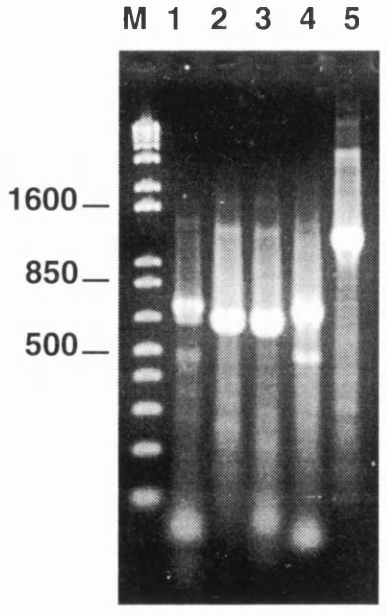


Figure 3.5: Results of RT-PCR reaction using four primers. *Lane M*, molecular weight marker, *Lane 1*, F1 and R1 primers used, *Lane 2*, F3 and R3 primers used, *Lane 3*, F2 and R2 primers used, *Lane 4*, F4 and R4 primers used, *Lane 5*, positive control.

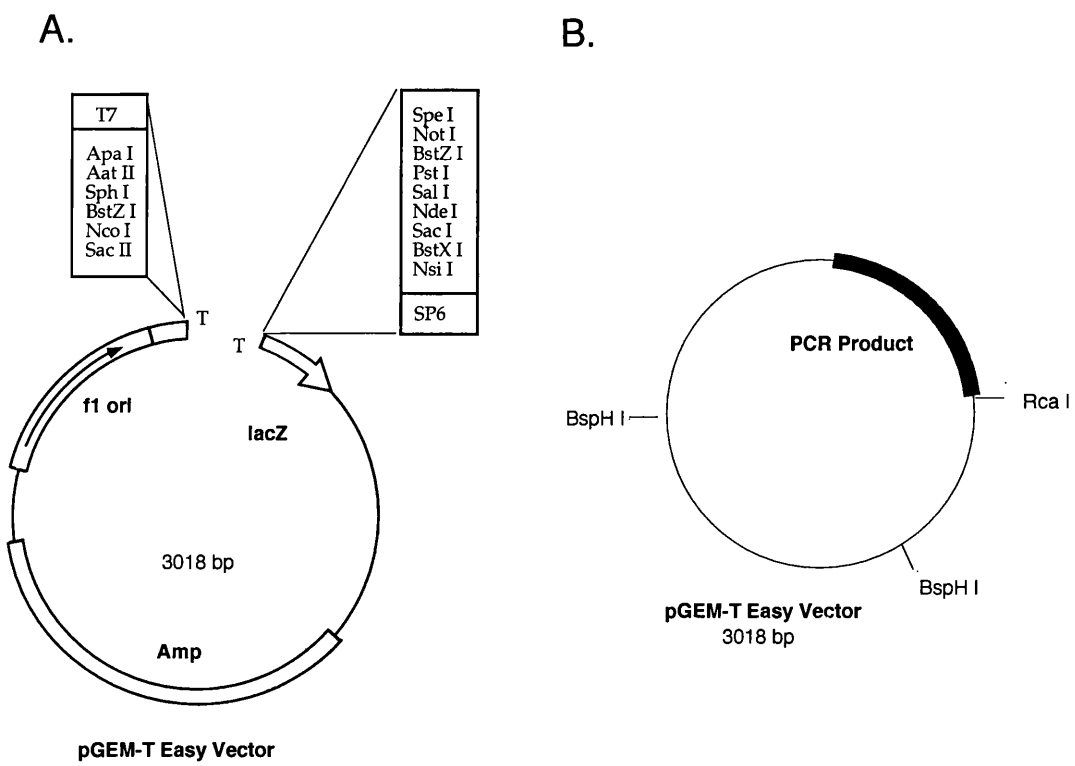


Figure 3.6: Cloning of PCR products. All four product were cloned to the pGEM-T Easy vector. A, The pGEM-T Easy vector used. A single deoxythymidine overhangs in its 3'-ends and multiple cloning sites are depicted. B, Resulting construct.

### 3.1.2 Construction of receptor clone

All four PCR products were ligated to the pGEM-T Easy Vector (Promega) to facilitate their subsequent handling. The pGEM-T Easy vector is designed for easy ligation of the PCR products with single deoxyadenosine overhang in their 3'-ends, Fig. 3.6. However, the TAQ/PWO polymerase generates blunt ends. Therefore, a post-reaction incubation with the Taq polymerase (Promega) was performed to convert the blunt ends to A-tailed ones. By this approach the advantage of proof reading was combined with ease of ligation.

The next step in the original plan called here for the digest of the cloned PCR products with appropriate restriction enzymes to ligate them together. A product generated with F1 and R1 primers (the "F1+R1" product) should be linked to the "F3+R3" product (generated with F3 and R3 primers) through the shared *Rca* I site and the "F2+R2" product (primers F2 and R2 used) to the "F4+R4" product (primers F4 and R4 used) through the shared *Hha* I site. However digests revealed that extra restriction sites were present in the pGEM-

T Easy vector. The vector contains two *Bsp*H I restriction sites. *Bsp*H I is the *Rca* I isochizomer and hence *Rca* I also cuts these sites, Fig 3.6. Moreover, another 7 copies of the *Hha* I sites are present in the vector. This means that a simple digest with *Rca* I or *Hha* I can not be used.

To link the "F1+R1" and "F3+R3" products together, a method of partial digest was used. The partial digest is based on the inability of a restriction enzyme in limiting amounts to cut all sites. 5 restriction enzyme samples with decreasing concentration were prepared: 1:1,1:3, 1:9,1:27, 1:54. Both 1:27 and 1:54 dilutions cut the clone only once, Fig. 3.7. The linearised "F1+R1" and "F3+R3" products were ligated together, Fig. 3.7.

This direct ligation resulted in a mixture of different constructs. Because there are three copies of the *Rca* I site in each cDNA/pGEM construct, the *Rca* I partial digest generated three different linear pieces, Fig. 3.7. Random ligation of two partial digest products generated 9 different potential constructs. The ligation product corresponding to the sequence of the first half of the OBR extracellular domain was separated from others by means of PCR. By using the F1 forward and R3 reverse primers, only the correctly ligated product could be amplified, Fig. 3.7. A band of the appropriate molecular length was obtained and this was then ligated to the pcDNA3.1+ vector (Invitrogen), Fig. 3.8. The ligation was verified by a restriction digest with *Xho* I and *Hind* III, Fig. 3.9.

The same strategy, the partial digest, could not be used for the reconstruction of the second half. The "F2+R2" and "F4+R4" PCR products should be ligated through *Hha* I site. However, the pGEM-T Easy vector contains more then 7 copies of the *Hha* I site. This high copy number made the use of partial digest infeasible.

It was therefore decided to ligate the PCR products "F2+R2" and "F4+R4" directly. Both PCR products were digested with *Hha* I, purified and ligated together, Fig. 3.10. The ligation result was again amplified by PCR using the forward F2 and reverse R4 primers. The complete second half of the OBR extracellular domain was then ligated to the pGEM-T Easy vector, Fig. 3.10.

To reconstitute the entire extracellular domain, the sequence encoding the second half of the receptor extracellular domain was extracted from the pGEM-T Easy vector and inserted into the pcDNA 3.1+ vector containing the first half of the extracellular domain. This was achieved by parallel digest of both plasmids with *Xho* I and *Apa* I, Fig. 3.11. The products were purified and ligated together. A restriction digest of the product with *Hind* III and *Bam*H I

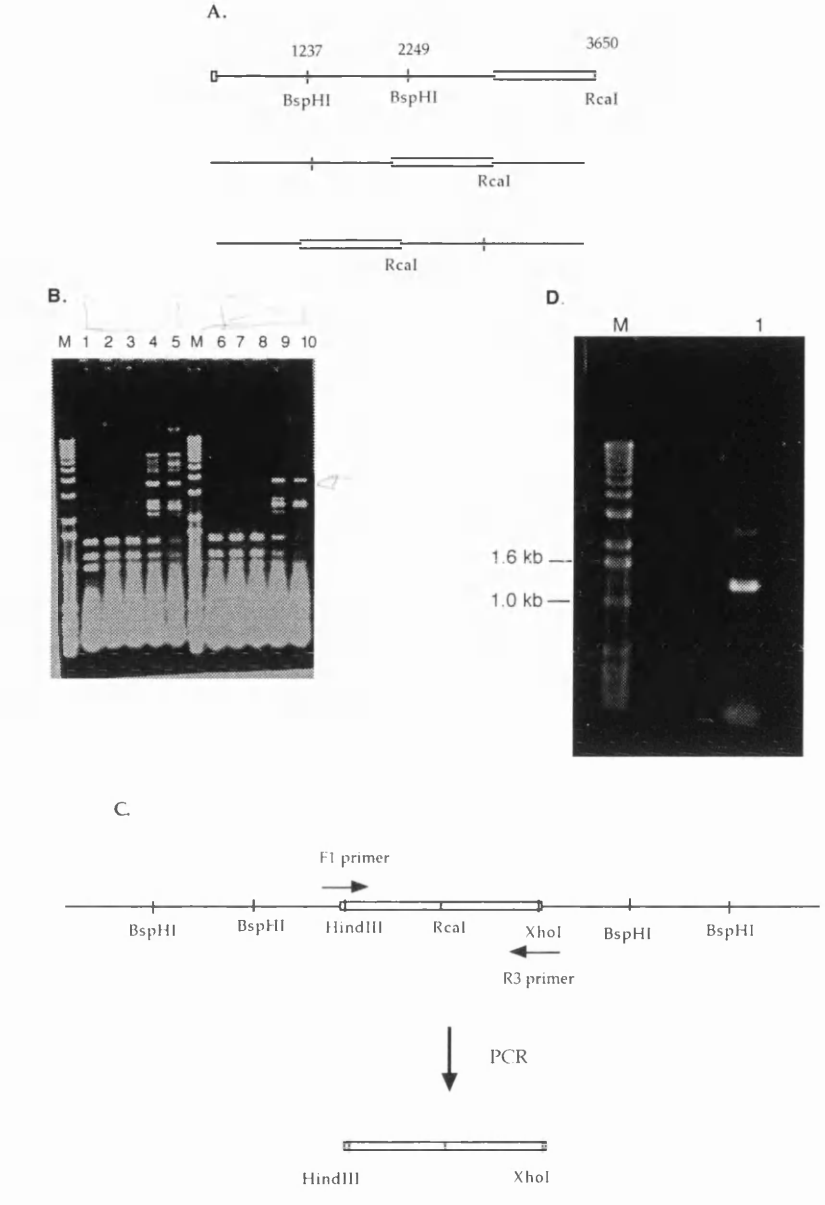


Figure 3.7: The construction of the first half of the receptor extracellular domain from the cloned "F1+R1" and "F3+R3" fragments. A, Three different products generated by a plasmid digestion with *Rca* I in partial digest. B, An electrophoresis analysis of digest results. *Lane M*, molecular weight marker, *Lanes 1, 2, 3*, all three *Rca* I sites on a single plasmid were cut. *Lanes 4, 5*, only one *Rca* I site was cut (3.7 kbp). *Lanes 6 - 10*, same as lanes 1 - 5 but the cloned "F3+R3" fragment used. C, Linearised full length fragments were ligated together. The desired construct was separated from others in PCR reaction using F1 and R3 primers. D, An electrophoresis analysis of PCR reaction. *Lane M*, molecular weight marker, *Lane 1*, the first half of the Ob-R extracellular domain (residues 1 - 1300).

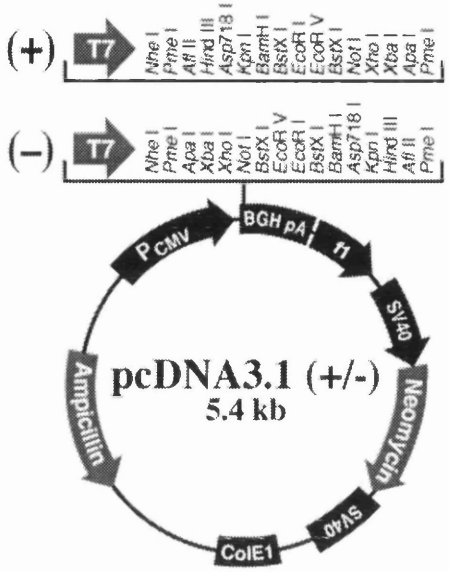


Figure 3.8: The pcDNA3.1(+) vector.

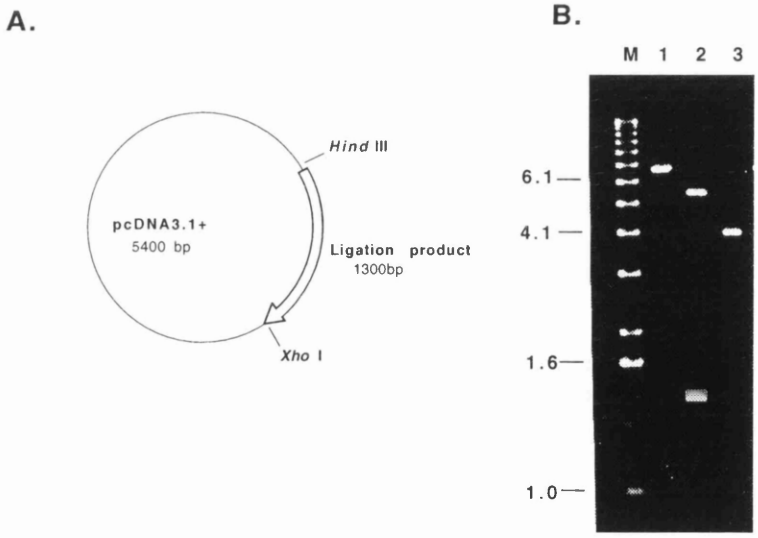


Figure 3.9: The ligation of the first half of the OBR extracellular domain to the pcDNA3.1+ vector. A, An illustration of the construct. Restriction sites used are depicted. B, An electrophoresis analysis of the ligation result. *Lane M*, molecular weight marker, *Lane 1*, linearised plasmid digested with *Xho* I. *Lane 2*, plasmid cut with *Xho* I and *Hind* III. The insert (1.3 kb, enhanced visibility) is released from the vector (5.4 bp). *Lane 3*, Supercoiled (undigested) plasmid.

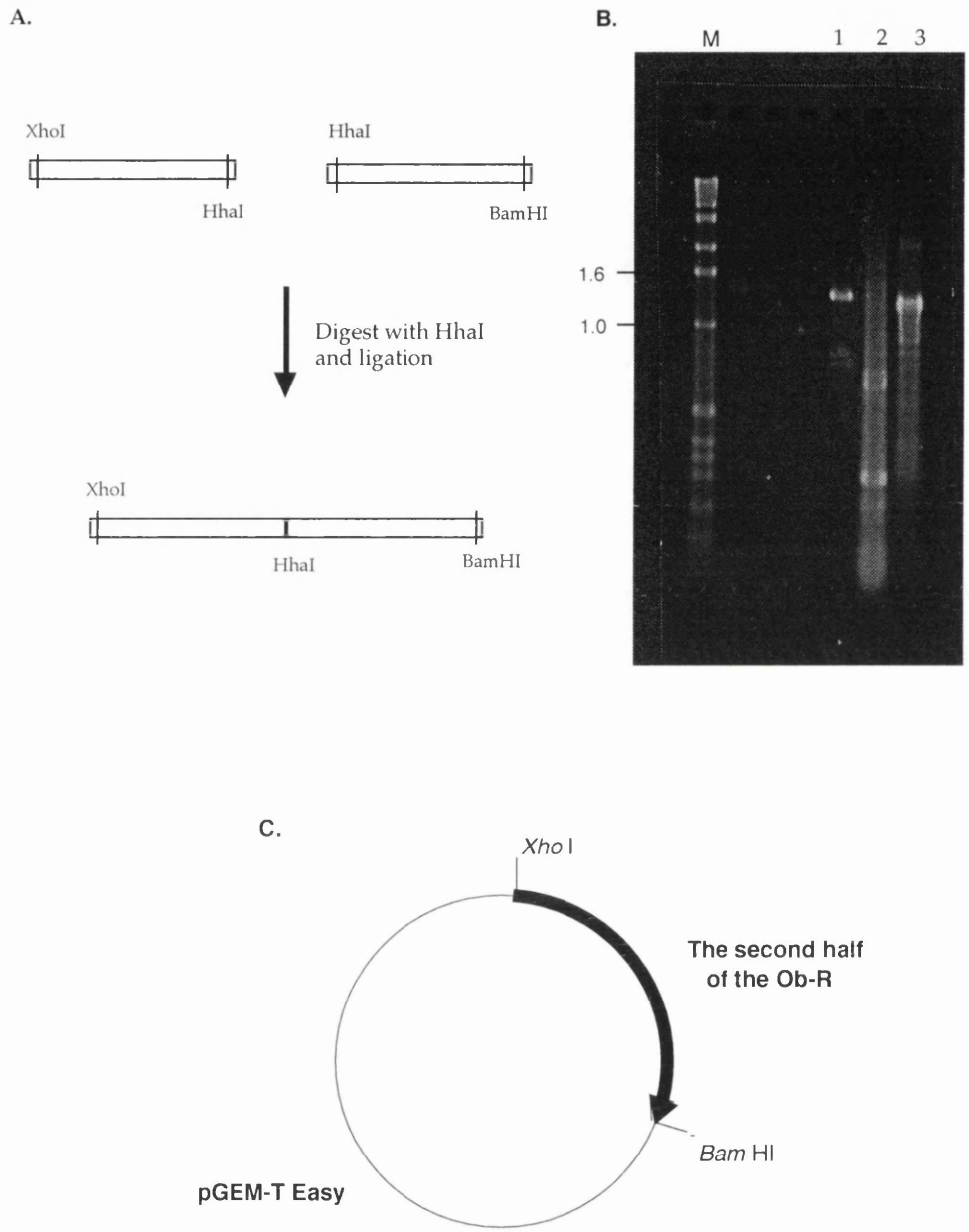


Figure 3.10: The construction of the second half of the receptor extracellular domain from the "F2 + R2" and the "F4 + R4" fragments. A, Both fragments were digested with *Hha* I and subsequently ligated together. B, An analysis of a ligation product amplified by PCR. *Lane M*, molecular weight marker, *Line 1*, PCR amplified fragment (1.3 kb). *Lane 2,3*, positive controls. C, The second half of the OBR extracellular domain ligated into the pGEM-T Easy vector.

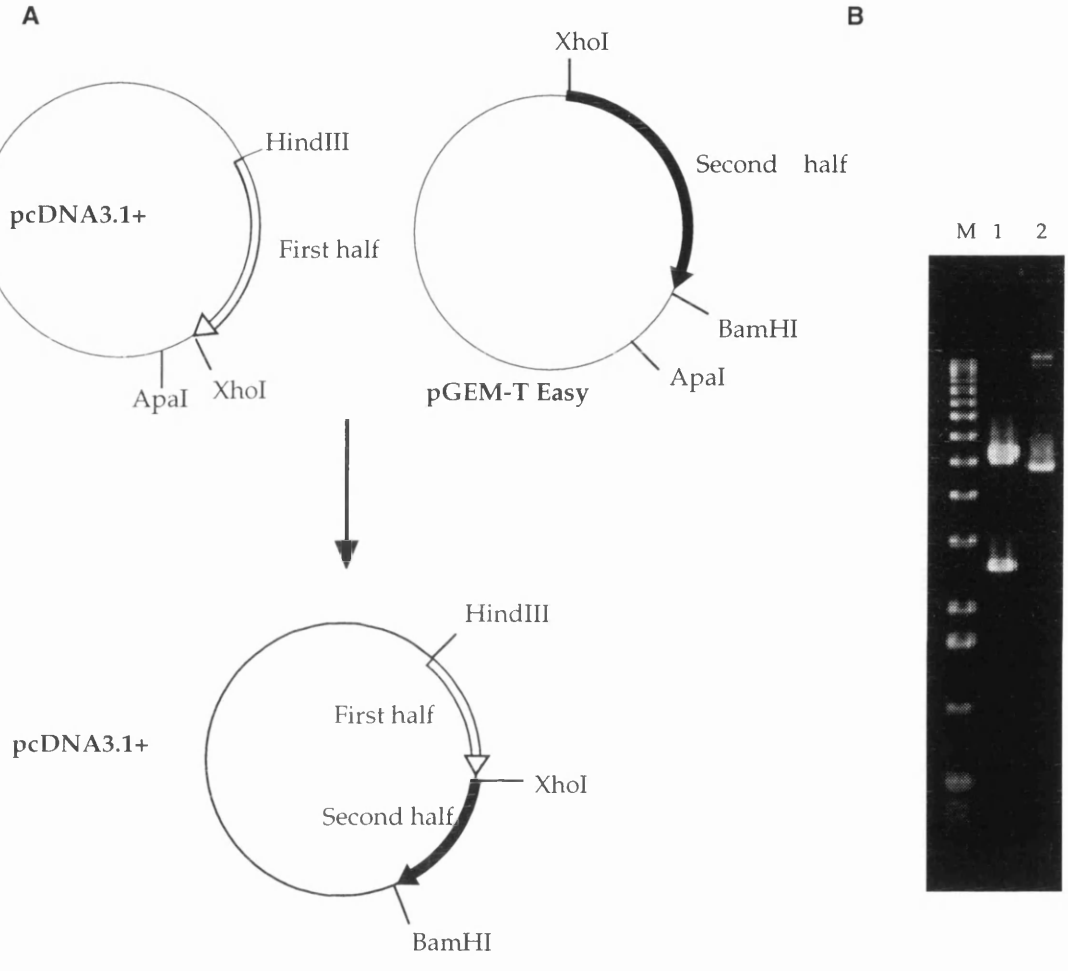


Figure 3.11: The reconstruction of the Ob-R extracellular domain. A, Both cloned fragments were digested with *Xho* I and *Apa* I. Reaction products were then ligated together. B, An electrophoresis analysis of the ligation result. *Lane M*, molecular weight marker, *Line 1*, the receptor extracellular domain (2.6 kbp) released from the pcDNA 3.1(+) vector (5.4 kbp) by a digest with *Hind* III and *Bam*H I. *Lane 2*, undigested plasmid.

GATCCGCACCACCACCACCACCACGACTACAAAGACGACGACGACAAATAGGC
GCGTGGTGGTGGTGGTGGTGCTGATGTTTCTGCTGCTGCTGTTTATCCGCCGG

*Bam* HI - H - H - H - H - H - H - D - Y - K - D - D - D - D - K - Stop-*Not* I

Figure 3.12: Sequence of the 6×His-FLAG oligonucleotide.

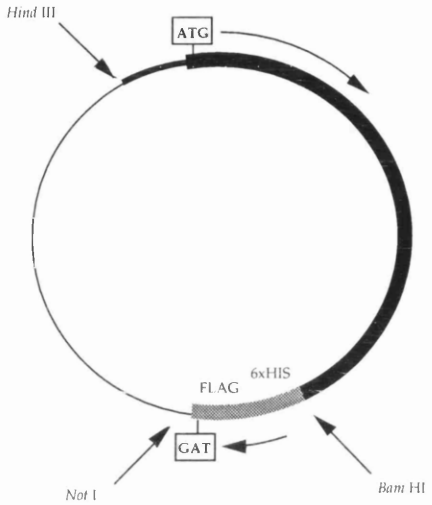


Figure 3.13: A schematic cartoon of the OBR-H-F plasmid. The sequence encoding the extracellular domain of the leptin receptor with a 6xHIS-TAG flag in its C-terminus is cloned between the *Hind* III and *Not* I sites in the polylinker of the pcDNA3.1+ vector. This plasmid was constructed from the OBR-GPI plasmid by replacing the GPI sequence with the 6xHIS-TAG flag.

confirmed that the ligation was successful, Fig. 3.11.

Paradoxically, following successful reconstitution of the extracellular domain coding region from the 4 fragments, a repeat attempt to synthesise the entire extracellular domain in one run was now successful. This was done by using a freshly prepared sample of total RNA from HEK cells which was used as a template in the RT-PCR reaction with the F1 and R1 primers. A product of desired length was obtained. This blunt ended PCR product was ligated to the pT7 Blue vector from The Perfectly Blunt Cloning Kit (Novagen). The pT7 Blue vector was very beneficial for cloning of the product, but this vector is not designed for expression, so, it was necessary to transfer the PCR product to a mammalian expression vector. The pcDNA3.1+ vector was chosen again and the insert was ligated through the *Hind* III and *Bam*H I sites. This new construct, ObR/pcDNA3.1+, encoded the complete open reading frame (ORF) of the Ob-R extracellular domain, residues $Met_1$-$Asp_{839}$. For easier manipulation with the recombinant product, the 6×His-FLAG tag, Fig. 3.12, was inserted into its C terminus via *Bam*H I and *Not* I sites, Fig. 3.13.

Table 3.2: Primers used in the sequencing of the OBR extracellular domain.

| Name | Start | $T_m$(°C) | Length | GC content (%) |
|---|---|---|---|---|
| T7 | T7 promoter | 53.7 | 20 | 55.0 |
| SF1 | 374 | 66.5 | 21 | 52.3 |
| SF2 | 896 | 51.7 | 20 | 50.0 |
| SF3 | 1394 | 51.7 | 20 | 50.0 |
| SF4 | 1911 | 47.9 | 18 | 50.0 |
| BGH | BGH poly A | 50.2 | 18 | 55.6 |
| SR1 | 1980 | 51.7 | 20 | 50.0 |
| SR2 | 1520 | 47.9 | 18 | 50.0 |
| SR3 | 1020 | 47.9 | 18 | 50 |
| SR4 | 510 | 47.9 | 18 | 50 |

Table 3.3: Mutations in the clone of the Ob-R extracellular domain

| Position | Residue | Amino acid change |
|---|---|---|
| 504 | *TTA* →CTA | L→L |
| 1283 | GAA→GGA | E→G |
| 1312 | TTA→CTA | L→L |
| 1365 | AGT→AGC | S→S |
| 1586 | TCT→TCC | S→S |
| 1598 | GTC→GTT | V→V |

### 3.1.3 Site-specific mutagenesis

To sequence both constructs, five forward and five reverse primers were designed to cover the whole region, Table 3.2. The sequencing reactions were performed externally by the Cambridge Bioscience company. Results were compared with the Gene Bank sequence of the receptor, U43168, by means of the Gene Jockey software. A preliminary analysis of the first clone, constructed from four PCR fragments, revealed that extensive use of PCR during its generation introduced several point mutations. However, in the second construct only one change in codon was identified in the entire sequence. This was a change of nucleotide at position 1238 from A to G resulting in a predicted change of amino acid from $E^{428}$ to G. Five other silent mutations were also present, Table 3.3. It was thus decided to correct the single mutation in the second construct and use this construct for protein expression.

The U.S.E. Mutagenesis kit (Pharmacia Biotech) was used to correct the $A^{1283} \rightarrow G$ point mutation. This method of site-specific mutagenesis employs the unique site elimination (U.S.E.) procedure [81], Fig. 3.14. This is based on fact that circular plasmid DNA is more efficient in transforming bacteria then

linear DNA. Here, a two-primer system is utilised to generate site-specific mutations. One primer, designated the target mutagenic primer MP1, introduces the desired mutation into a known sequence of the plasmid DNA. A second primer, the SEM selection primer, eliminates a unique non-essential restriction site in the plasmid, which subsequently serves as the basis for selection of mutated plasmids. Since both primers anneal to the same strand of the denatured double-stranded plasmid, it is possible to synthesise a new strand of DNA containing both mutations.

The target mutagenic primer MP1 was designed so that it introduced the desired mutation as well as a new unique restriction site *Bst*Z17 I (Fig. 3.15.) This new restriction site could be used for a rapid analysis of mutagenesis products. The SEM selection primer was chosen to replace a unique non-essential restriction site *Pst* I with the *Sac* II site. *Pst* I is present in the pcDNA3.1+ plasmid in two copies. However, it is unique in the ObR-H-F/pcDNA3.1+ plasmid because one site, located in the pcDNA3.1+ polylinker, was removed during the subcloning of the ObR-H-F insert. The second copy of the*Pst* I site is in the nonutilised Neomycin gene.

The ObR-H-F/pcDNA3.1+ plasmid contains two *Bst*Z17 I sites at positions 1901 and 5834 bp (the total length of the plasmid is 8024). A successful mutagenesis reaction should introduce both a reversal of the mutation $G \rightarrow A$ and an addition of another *Bst*Z17 I site at the position 2194. Mutated and parental plasmids should be easily distinguishable in a digest with *Not* I[6] and *Bst*Z17 I . The digest of parental plasmid should generate 3 fragments (1675, 2258, 4096 bp) whereas four fragments of length 334, 1341, 2258 and 4096 bp should be produced from mutated plasmid. Thus, an appearance of a 1341 bp fragment instead of the 1675 bp fragment in the pattern of digested products is a proof of successful mutation,(Fig 3.16.)

This corrected version of the cDNA encoding the receptor extracellular domain was used for generation of several variants, (Table 3.4) In the ObR-GPI plasmid, Fig. 3.17, the 6×His-FLAG tag was replaced with the GPI anchor [82] through *Bam*H I and *Not* I sites. This plasmid encoded a version of the receptor where the extracellular domain is anchored to the membrane through a glycosyl phosphatidyl inositol anchor (GPI) through post translational processing of the nascent protein [82]. Cell surface expressed protein can be cleaved from its anchor by the enzyme PIPLC to release Ob-R into the cell supernatant [82]. The anchored protein mimics the wild-type receptor which is anchored in the

[6]In the ObR-H-F/pcDNA3.1+ plasmid there is one copy of *Not* I site at position 3575.

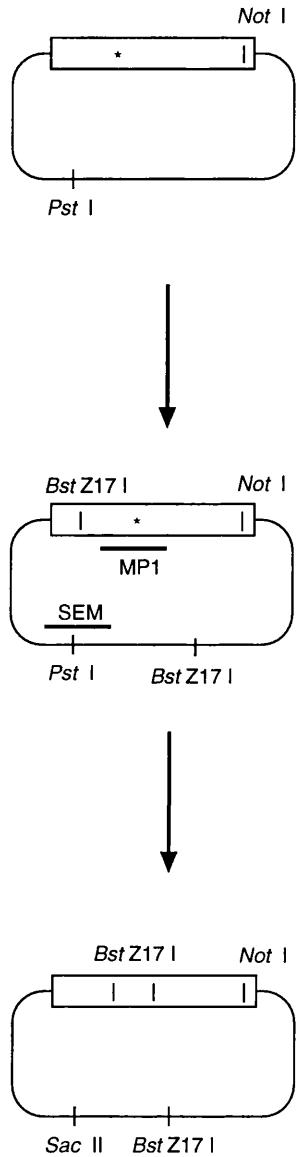


Figure 3.14: Site-specific mutagenesis, based on the unique site elimination (U.S.E.) procedure [81]. A two-primer system is utilised to generate site-specific mutations. One primer, designated the target mutagenic primer MP1, introduces the desired mutation into a known sequence of the plasmid DNA. A second primer, the SEM selection primer, eliminates a unique non-essential restriction site in the plasmid, which subsequently serves as the basis for selection of mutated plasmids. Since both primers anneal to the same strand of the denatured double-stranded plasmid, it is possible to synthesise a new strand of DNA containing both mutations.

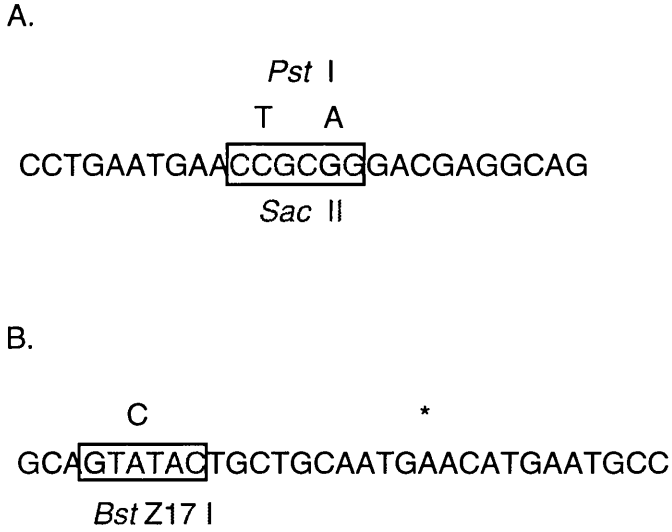


Figure 3.15: Sequence of the U.S.E. primers. A., the SEM selection primer replaces a unique non-essential restriction site *Pst* I with the *Sac* II site. B., the target mutagenic primer MP1 designed to introduce the desired mutation(*) together with a new *Bst*Z17 I site.

cell membrane through its transmembrane domain. In the KOZAK plasmid, Fig. 3.18, the flanking region of the Ob-R starting codon was replaced by the Kozak consensus translation initiation sequence [83], CCAACC**ATG**G, to maximise the efficiency of translation. In the KOZ-H-GPI plasmid, Fig. 3.19, the 6×His-FLAG tag was replaced by 2×6His-GPI sequence. This modification should again result in anchoring of the protein into the membrane surface. Furthermore, 6×His could be used for purification of a recombinant protein after its easy cleavage from the membrane using PIPLC [82].

### 3.1.4 Short form of the receptor

It is important to mention that at this stage when these several DNA constructs were generated we received a clone of the wild-type receptor (the short form, [84]) from Dr de Sauvage (Genentech Inc.). In this construct, the OBR open reading frame was inserted to the pRK5tkneo vector via *Bam*H I site. To make the manipulation of the clone easier, it was released from the pRK5tkneo vector by a restriction digest with *Bam*H I and ligated into the pcDNA3.1+ vector. A clone in correct orientation relative to plasmid was selected by restriction digest with *Xba* I, Fig. 3.20. One *Xba* I site is in the insert, 6 bp downstream from the 5' *Bam*H I. The second one is in the vector, 62 bp downstream from the 3' *Bam*H I site. Thus, the digest of the plasmid with *Xba* I

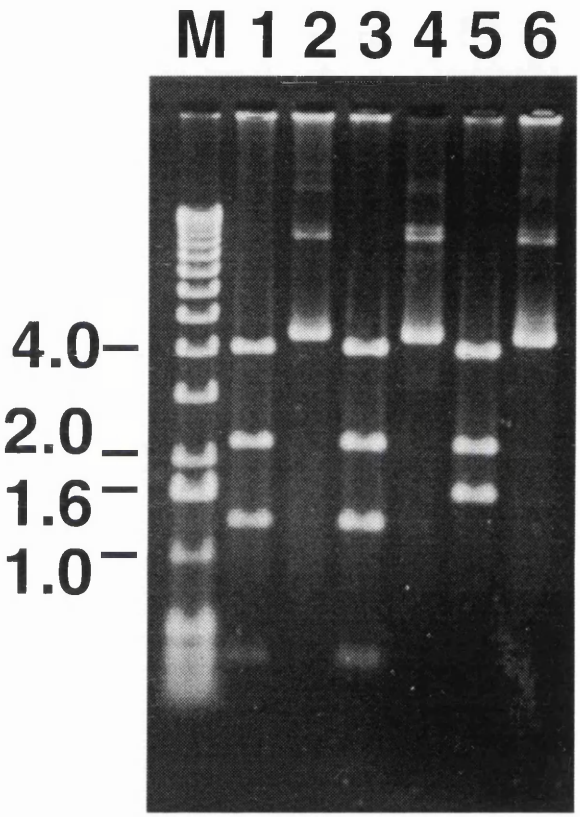


Figure 3.16: The analysis of the mutagenic reaction by restriction digest. Plasmids were digested with *Not* I + *Bst*Z17 I. This digest should generate 3 fragments (1675, 2258, 4096 bp) from a parental plasmid or four fragments (334, 1341, 2258 and 4096 bp) from mutated plasmid. Samples 1 and 3 represent mutated plasmids.

Table 3.4: Different constructs encoding the extracellular domain of Ob-R

| Plasmid | Features |
|---|---|
| OBR-H-F | Sequence of extracellular domain of Ob-R with 6xHis-FLAG tag in C-terminus |
| ObR-GPI | Sequence of extracellular domain of Ob-R with a GPI anchor in C-terminus |
| KOZAK | Sequence of extracellular domain of Ob-R with the Kozak consensus translation initiation sequence and 6xHis-FLAG tag in C-terminus |
| KOZHGPI | Sequence of extracellular domain of Ob-R with the Kozak consensus translation initiation sequence and 6xHis tag and GPI anchor in C-terminus |

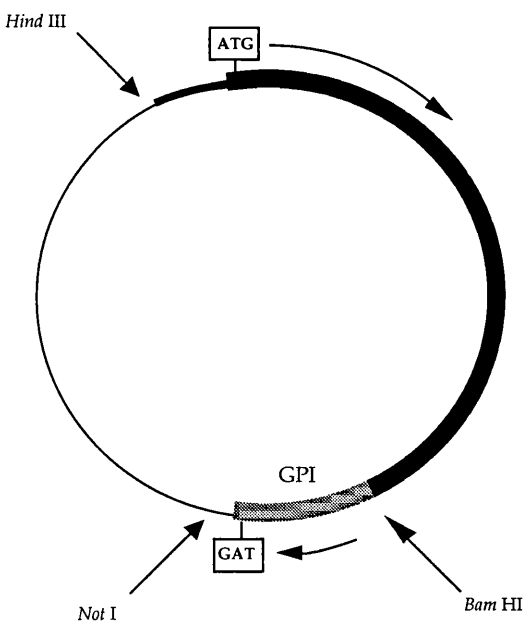


Figure 3.17: A schematic cartoon of the OBR-GPI plasmid. The sequence encoding the extracellular domain of the leptin receptor with a GPI anchor in its C-terminus is cloned between the *Hind* III and *Not* I sites in the polylinker of the pcDNA3.1+ vector.

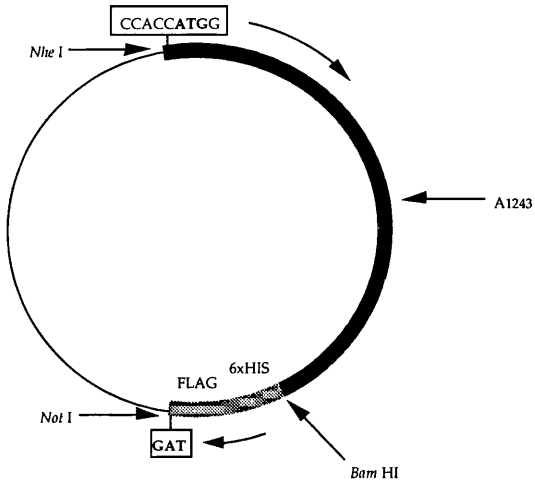


Figure 3.18: A schematic cartoon of the KOZAK plasmid. The sequence encoding the extracellular domain of the leptin receptor linked in its C-terminus to the 6xHis-FLAG tag is cloned between the *Nhe* I and *Not* I sites in the polylinker of the pcDNA3.1+ vector. In this construct, the flanking region of the starting codon was replaced with the Kozak consensus translation initiation sequence [83], CCAACC**ATG**G, to maximise the efficiency of translation.

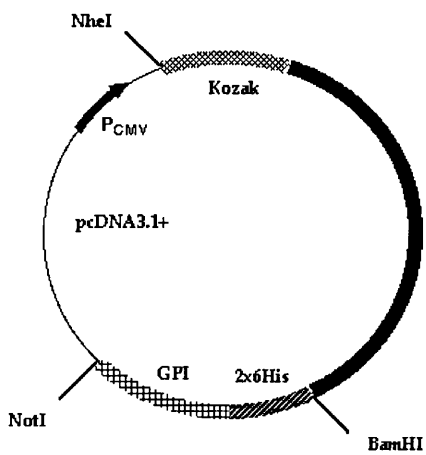


Figure 3.19: A schematic cartoon of the KOZ-H-GPI plasmid. The sequence encoding the extracellular domain of the leptin receptor with two copies of the 6xHis tag and GPI anchor in its C-terminus is cloned between the *Nhe* I and *Not* I sites in the polylinker of the pcDNA3.1+ vector. The clone has the Kozak consensus translation initiation sequence [83], CCAACC**ATG**G, to maximise the efficiency of translation.

should release 3794 bp fragment (when the clone has correct orientation).

To enhance translation, the consensus Kozak sequence was introduced to the clone. This was done by PCR. Here, the forward primer, called FNHEI, was used which introduced an *Nhe* I site and the consensus Kozak sequence at the beginning of the sequence. The reverse primer, called HR1, introduced the *Bam*H I site at the end of the nucleotides encoding the extracellular domain. This construct was sequenced.

Sequencing reactions were carried out by The C.M.H.T, University of Leicester. The whole OBR extracellular domain was sequenced using supplementary primers (Table 3.2). The consensus sequence was generated from sequencing fragments using Fragment Assembly System (FAS) from GCG programme package. The FAS is a series of programs designed to assemble the overlapping fragment sequences from a sequencing project. A generation of consensus sequence from individual fragments is shown in Fig. 3.21.

The consensus sequence was aligned with the hOBR cDNA (Gene Bank accession U43168) using the programme LINEUP from the GCG package. Mismatches between the consensus and template sequences were identified at following positions: 4, 1956, 1957, 2323, 2367, 2484, where position 1 corresponded to A of the initiation codon, methionine. Because a correct residue was present in at least one fragment in all except two positions (4 and 2514), it was decided that these mismatches are due to incorrect gel reading and that the analysed and the GeneBank sequences are identical also at these positions. The mismatches at positions 4 and 2514 result from the introduction of the consensus Kozak sequence (position 4) and an artificial restriction site *Bam*H I (position 2514). Thus, the obtained clone truly encodes the extracellular domain of the OBR (the GeneBank sequence U43168).

## 3.2 Expression of the receptor clone

### 3.2.1 Mammalian expression of the leptin receptor

After successful cloning, the expression work was started. The plan was to express the recombinant protein first in the mammalian expression system, COS cells, and then in the Baculovirus (BV) expression system. The rationale for this is that the mammalian expression system is easier to setup and the recombinant protein should have the same post-translation modifications as the authentic protein in the native environment. The disadvantage of the mammalian system is the relatively low level of recombinant protein expres-

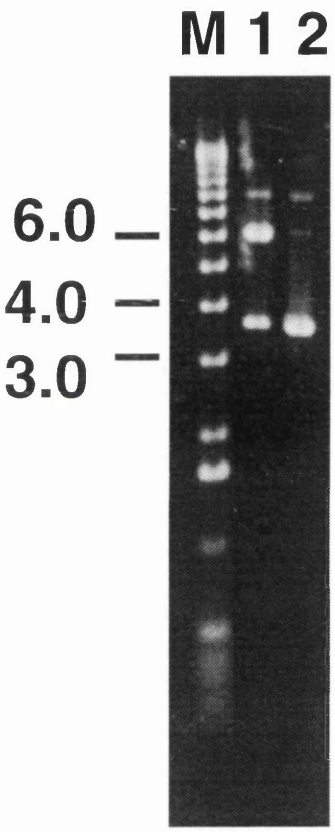


Figure 3.20: The clone of the short form of the hOb-R. M, molecular weight ladder; 1, the plasmid digested with *Xba* I ; 2, undigested plasmid.

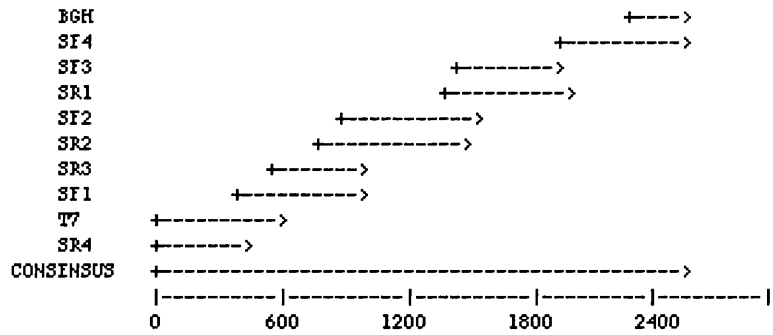


Figure 3.21: An alignment of sequencing fragments generated by the FAS.

sion. Expression in COS cells should produce enough protein for the BiaCore experiments as it requires only micrograms of protein. However, much more protein is necessary for microcalorimetry and other biophysical techniques such as analytical centrifugation. Typically milligrams of protein are required for these, and could be obtained by employing the Baculovirus (BV) expression system which results in very high expression levels. Unfortunately, this system has one crucial disadvantage over mammalian systems. In the BV system, fast production may overwhelm the ability of the cell to modify the protein product. Thus, although most of the post-translational modifications occur in the BV system, and the sites where these modifications happen are often identical to those of the authentic protein in its native cellular environment, the levels of glycosylation or phosphorylation are often lower. Thus, comparison of the BV and mammalian products in BiaCore experiments would be very useful for a validation of the BV system for the Ob-R expression.

The expression work was started with *in vitro* analysis of translation products generated from constructed plasmids. Their size was evaluated in *in vitro* translation experiments using the TNT Coupled Reticulocyte Lysate System (Promega). This system couples *in vitro* RNA synthesis from T7 RNA polymerase promoter with rabbit reticulocyte lysate translation. In this way, the TNT System generates a translation product from any insert ligated to a vector bearing T7 promoter such as the pcDNA3.1+ vector. Taking advantage of the $^{35}S$ incorporation, translation products can be evaluated directly by the radiography of the SDS-PAGE results.

The SDS-PAGE analysis of TNT products from different Ob-R clones[7] is shown in Fig 3.22. Lane 1 represents the short form of the wild-type receptor; lane 2 is ObR-H-F; lane 3 is Kozak-H-GPI; lane 4 is KOZAK; lane 5 is ObR-

[7]The constructed clones are summarised in Table 3.4.

GPI; lane 6 is uncorrected ObR-H-F and lane 7 is Luciferase, positive control. A negative control was not included in this particular experiment, but it had been performed previously and the results showed that in the absence of DNA template, the TNT system does not generate any detectable protein.

All Ob-R products migrate as 80-100 kDa proteins. This is in agreement with the predicted molecular weight of the short form of the Ob-R which should be 102.5 kDa as calculated from its primary sequence (U50748) using the Peptidesort programme from the GCG package. The extracellular domain alone (residues 1 - 839) has a predicted size of 96 kDa. Small variation in position of bands is due to different C-terminus in these constructs. The similar length of the wild-type (896 residues) and recombinant proteins suggests that the constructed plasmids encode the whole extracellular domain as was previously confirmed by sequencing.

The next step was expression of these clones in mammalian system. COS, CHO and HEK cells were transfected with target plasmids using DEAE-DEXTRAN, Transfectin (Qiagen) and GenePORTER (TSE inc.) transfection reagents. Unfortunately, the level of expression was very low in all these systems. The only product obtained was from COS cells transfected with a clone of the wild-type receptor using the GenePORTER reagent, (Fig. 3.23.) This product had a size of ≈120 kDa. The difference in size compared to *in vitro* expression is likely due to glycosylation [85].

### 3.2.2 Baculovirus expression of the leptin receptor

Because the level of the Ob-R expression in mammalian systems was so low it was not possible to make enough protein for BiaCore experiments. It was decided, therefore, to switch to Baculovirus expression and concentrate only on this system. The Baculovirus expression system is one of the most powerful eukaryotic systems available. It is a helper-independent viral system which has been used to express heterologous genes from many different sources in insect cells. Since the Baculovirus genome is too large to easily insert foreign genes, heterologous genes are cloned into a transfer vector. Co-transfection of the transfer vector, bearing the gene of interest, and the *Autographa californica* nuclear polyhedrosis virus (AcNPV) DNA into *Spodoptera frugiperda* (*Sf*) cells allows recombination between homologous sites, transferring the target gene to the viral genome.

It was decided to use the Bac-N-Blue$^{TM}$ system (Invitrogen). This virus has a functional *lacZ* gene and produces blue plaques which are easily purified.

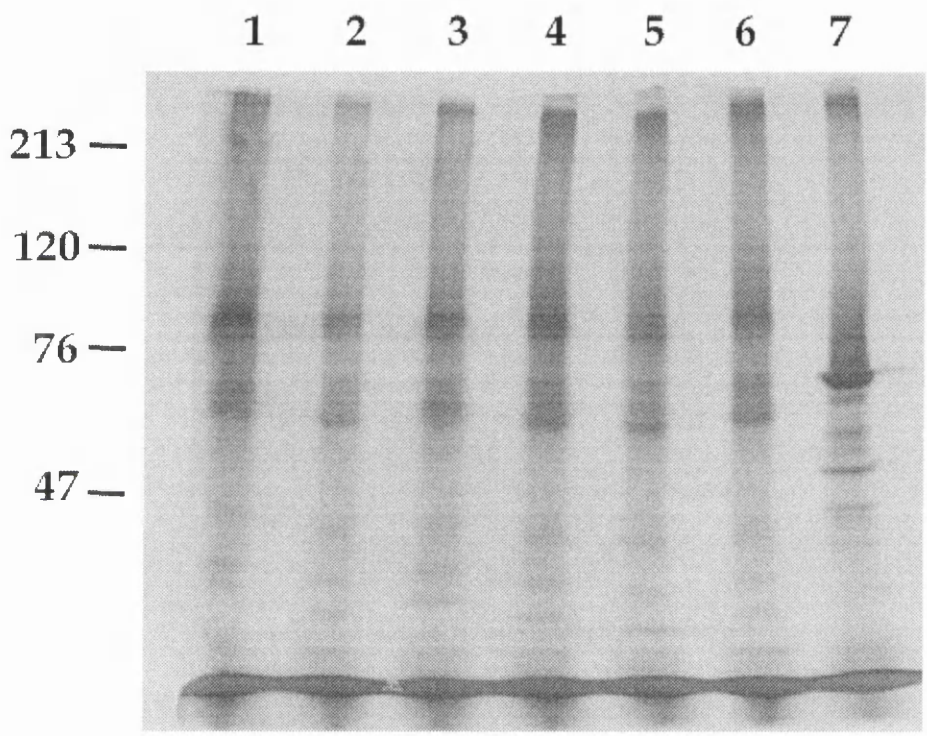


Figure 3.22: The SDS-PAGE analysis of *in vitro* translation products from different Ob-R clones. Lane 1 represent the wild-type receptor, the short form; Lane 2 is ObR-H-F; Lane 3 is Kozak-H-GPI; Lane 4 is KOZAK; Lane 5 ObR-GPI; Lane 6 is uncorrected ObR-H-F and Lane 7 is Luciferase, a positive control.

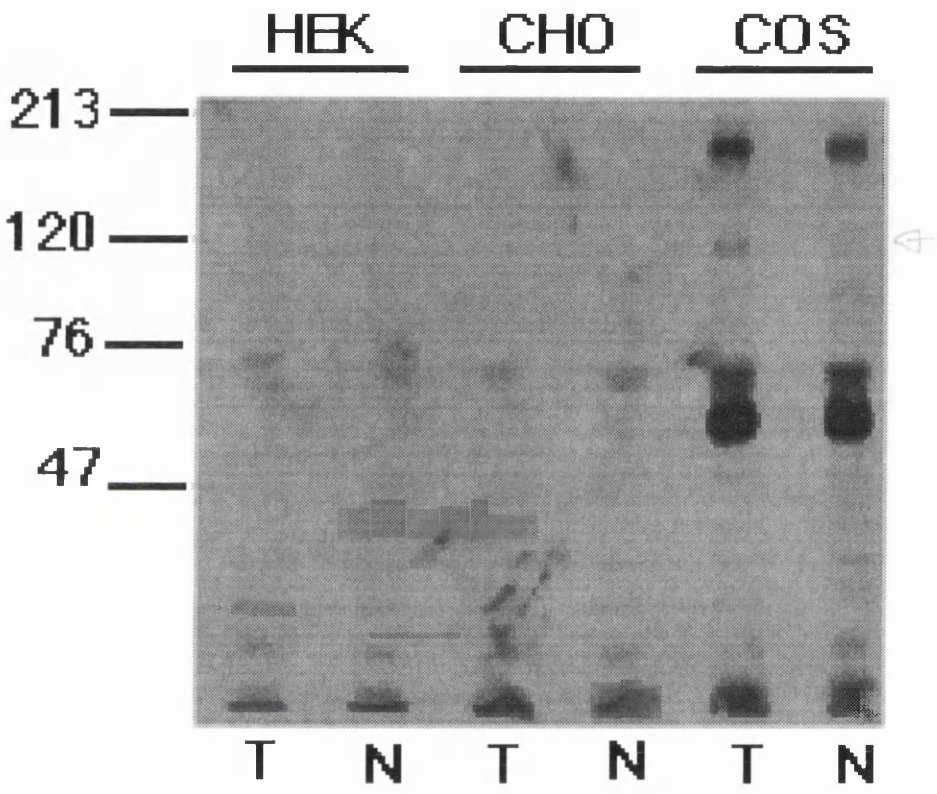


Figure 3.23: The SDS-PAGE analyses of the wild-type receptor expression in different mammalian systems. HEK, COS, and CHO cells were used. Cell lysate samples from transfected (T) and nontransfected (N) cells were compared. The GenePORTER transfection reagent was used in these experiments. Western analysis: Blots were probed with anti-Leptin Receptor antibody (R & D Systems)(1:1000 dilution) in a combination with the HRP conjugated anti-goat antibody (Sigma) (1:5000 dilution) and visualised using ECL.


Figure 3.24: The Baculovirus transfer vector encoding the Ob-R extracellular domain. The original leading sequence was replaced by the honeybee melittin (HBM) sequence to facilitate protein secretion to medium. In the C-terminus, 6×His-FLAG tag was added for easy purification.

Baculovirus infection of *Sf* cells results in the shut-off of host gene expression allowing for a high rate of recombinant mRNA and protein production. Recombinant proteins can be produced at high levels reaching 50 % of the total insect cell protein.

The pMelBac baculovirus transfer vector (Invitrogen) was chosen for cloning of the Ob-R extracellular domain. The pMelBac vector is designed for direct secretion of recombinant protein into the extracellular medium. This is achieved by using the honeybee melittin signal sequence which has been found to drive high protein expression as well as very efficient secretion to the medium [86]. This vector exists in three copies: A, B and C [87]. The version B was used because it had the most useful polylinker.

The construction of the Ob-R transfer vector required transfer of the sequence of the Ob-R extracellular domain from the pcDNA3.1+ vector to the pMelBac vector, downstream and in-frame with its starting Met, Fig. 3.24. To achieve this, it was decided to introduce a *Sac* I site directly before Asparagine at position 23 ($N^{23}$) of the Ob-R sequence. In this way the original signal peptide of Ob-R would be replaced by the honeybee melittin one. The honeybee melittin sequence is cleaved after protein secretion. Because the residues 1-22 of Ob-R are cleaved after transport of the authentic protein to the cell membrane, the BV recombinant protein should have a very similar N-terminal sequence with its authentic counterpart. The only difference would be due to a introduction of the *Sac* I site. However, this would introduce a minimum number of new residues because the *Sac* I site is the second site in the pMelBac multiple cloning site. The first one, the *Bam*H I site, could not be used because it is also present in the clone.

The pcDNA3.1+ and pMelBac polylinkers do not share a restriction site downstream of the Ob-R insert, which could be used as a second site for clone transfer. However, *Sal* I and *Xho* I restriction enzymes produce compatible

ends. There is a *Sal* I site in the pMelBac polylinker which lies at the extreme 3' end of the linker. There is an *Xho* I site present in the pcDNA3.1+ polylinker and this site lies 3' to the *Not* I site which was used as a second site for insertion of the Ob-R clone to the vector. The only disadvantage of the *Xho* I site is that a second site exists in the Ob-R clone as there is also an internal *Xho* I site in the Ob-R sequence. Thus, *Xho* I can be used only in a partial digest of the ObR/pcDNA3.1+ plasmid.

The procedure for the construction of the ObR/pMelBac plasmid is depicted in Fig.3.25. It was started with a modification of the N-terminus of the clone for its in-frame insertion to the pMelBac vector. The *Sac* I site was introduced in front of the $N^{23}$ by PCR. New primers were designed. The forward primer introduces the *Sac* I site in front of the $N^{23}$. The reverse primer contains the unique *Eco*R I site, some 800bp downstream of the methionine start codon.

The *Pfu* Polymerase (Stratagene) was used in the PCR reaction. This is a proofreading DNA polymerase, isolated from *Pyrococcus furiosus*, which exhibits the lowest error rate of any thermostable DNA polymerases commercially available. The polymerase is supplied with two buffers, Native and Native Plus. The Native Plus buffer produces higher product yields for certain amplification, while maintaining high fidelity. Both buffers were tested.

This variation in reaction conditions was further multiplied by varying the dNTP concentration. Because high dNTP concentration leads to the greatest product yield while specificity and fidelity is highest at low dNTP concentrations, both high (1 mM) and low (0.4 mM) concentrations were used. The results of the PCR reaction are shown in Fig. 3.26.

From the intensity of the bands it is clear that the yield of product did not significantly differ in the various reaction conditions. Because the highest fidelity should be obtained for low dNTP concentration, the product No. 1 was used for subsequent ligation to the pMelBac vector. The purified PCR product as well as the vector were digested with the *Sac* I and *Eco*R I and ligated together. The ligation product was analysed by restriction digest. Because there is no common buffer in which *Sac* I and *Eco*R I enzymes work effectively, other enzymes were used instead: *Bam*H I , in front of the *Sac* I, and *Hind* III following *Eco*R I in the pMelBac polylinker, Fig 3.27.

To reconstruct the entire extracellular domain of the receptor, the second part of the clone from the ObR/pcDNA3.1+ (sequence that lies 3' to *Eco*R I site) was released and inserted into the newly created plasmid, Fig. 3.25. To

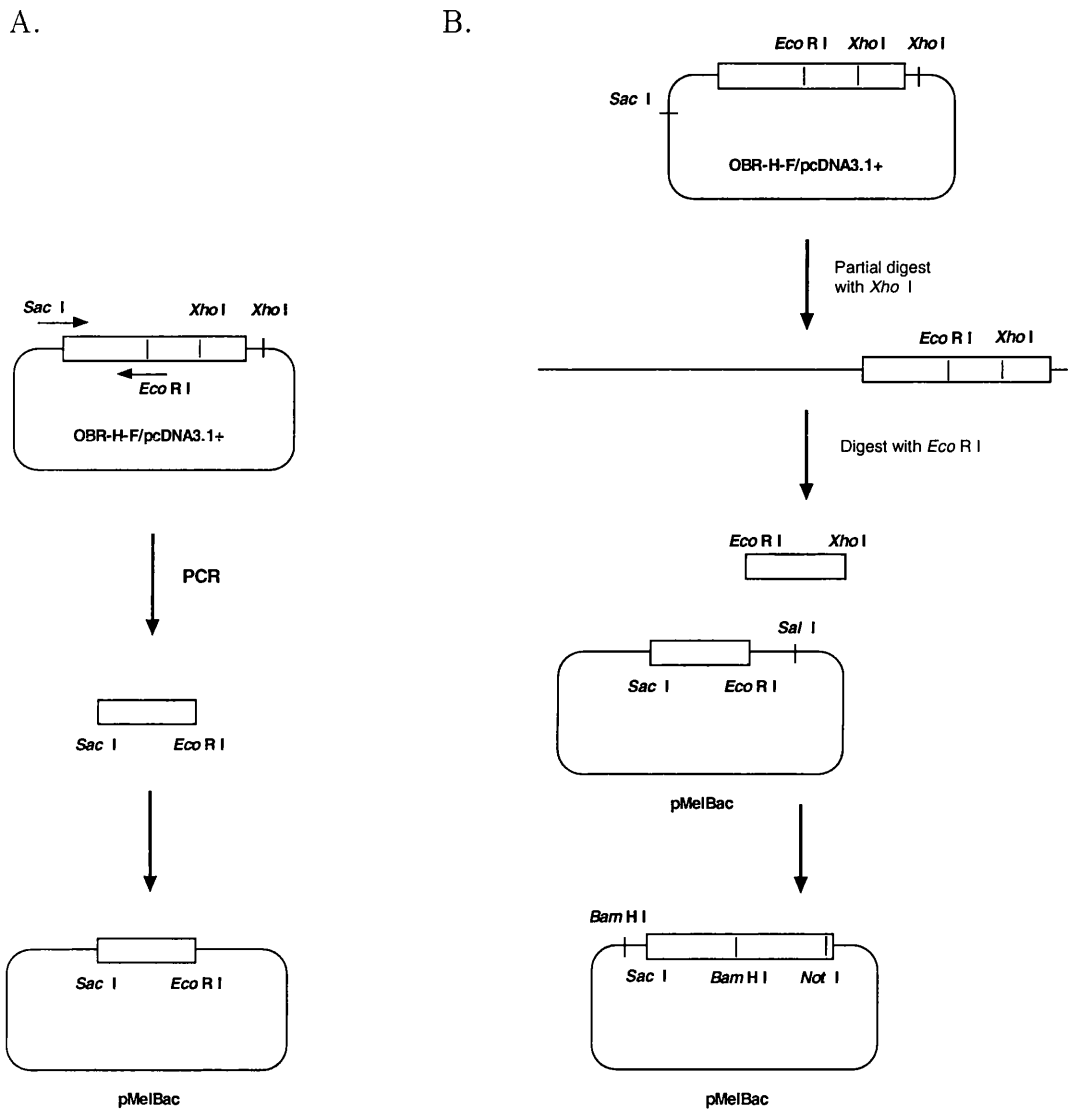


Figure 3.25: Cartoon representing a protocol for a construction of Baculovirus transfer vector encoding the Ob-R extracellular domain. A, A generation of the first part of the clone. The PCR product was ligated to the pMelBac vector through *Sac* I and *Eco*R I sites; B, The second part was released by a partial digest of a plasmid with *Xho* I followed by a digest with EcoR I. The product was inserted to the plasmid generated in step A.

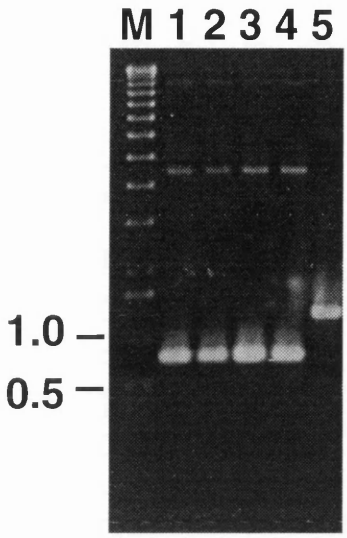


Figure 3.26: PCR of the first part of the clone done to introduce the *Sac* I site at $N^{23}$ of Ob-R. M, molecular weight ladder; 1; Native Buffer, 0.4 mM dNTP; 2; Native Buffer, 1.0 mM dNTP; Plus Buffer, 0.4 mM dNTP; Plus Buffer, 1.0 mM dNTP; 5, positive control

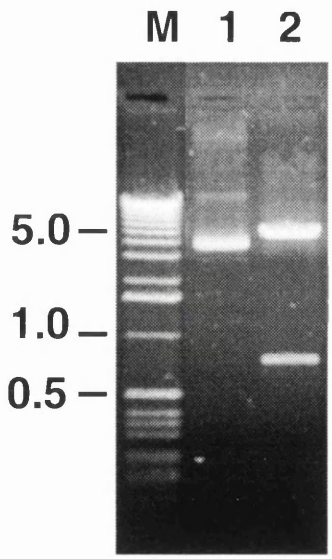


Figure 3.27: The restriction digest analysis of a ligation of the first half of the Ob-R clone to the pMelBac vector. M, molecular weight ladder, 1, undigested plasmid; 2, plasmid digested with *Hind* III and *Bam*H I .

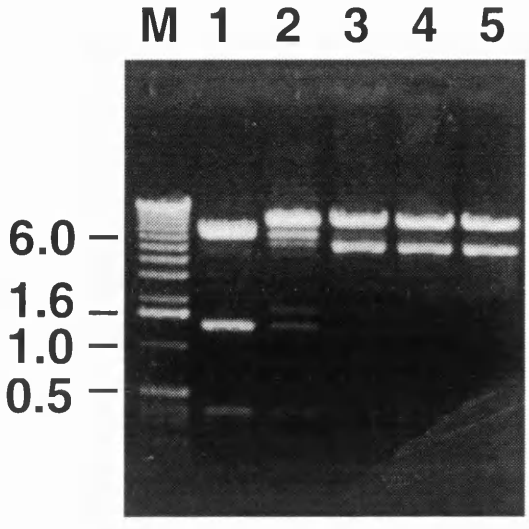


Figure 3.28: The partial digest of the ObR/pcDNA3.1+ with *Xho* I. A serial dilution of the enzyme was used in 1. - 5. reactions. The digest was performed for 15 min at 37°. Reaction products were then digested with *Eco*R I. Because *Xho* I cuts the plasmid at 2211 and 3582 positions and *Eco*R I at 1834 position, when only the second *Xho* I site is cut in the partial digest, the subsequent digest with *Eco*R I should release a 1748 bp product. This product is obtained in reaction 2. The total *Xho* I digest released a 1371 bp product.

do this the appropriate fragment between the *Eco*R I and the second *Xho* I site in the ObR/pcDNA3.1+ plasmid was obtained by first performing a partial *Xho* I digest of the ObR/pcDNA3.1+ plasmid. The reaction product was then digested with the *Eco*R I , Fig. 3.28.

A purified product of appropriate size was ligated to the pMelBac vector containing the first part of the extracellular domain, Fig. 3.25. This was digested with the *Eco*R I and *Sal* I. The *Sal* I enzyme produces ends compatible with *Xho* I. Therefore, the fragment of Ob-R released with the *Eco*R I and *Xho* I could be inserted to the plasmid digested with the *Eco*R I and *Sal* I. The *Sal* I site is lost in this process.

The ligation product was analysed by restriction enzyme digest with several different enzymes, Fig. 3.29. The first digest was with *Bam*H I. Two *Bam*H I sites should be present in the final construct; one in the polylinker in the front of the insert (cut position 158) and the second inside the insert (position 2618). Thus, a digest with the *Bam*H I should release a fragment of 2460 bp as observed in Fig. 3.29a.

The second digest was with *Eco*R I and *Not* I to provide further evidence for successful cloning, particularly to show that the second of the two original *Xho* I sites was cut in the partial digest. In the correct construct, the *Eco*R I

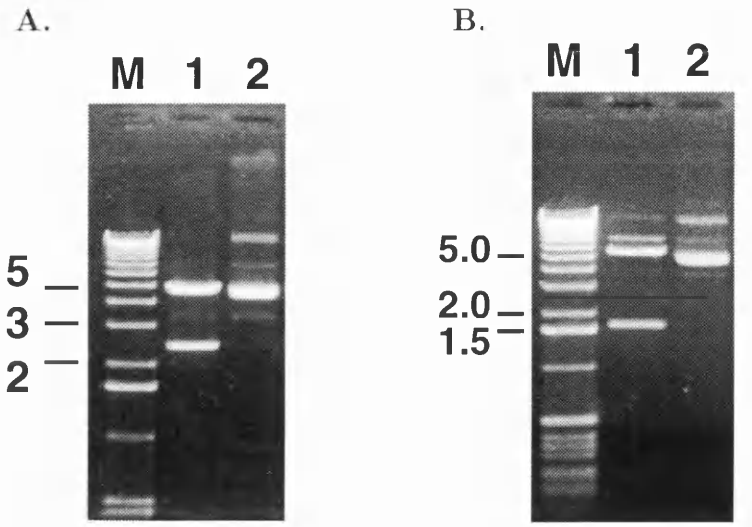


Figure 3.29: The restriction digest of the ObR/pMelBac plasmid. A, The *Bam*H I digest. The *Bam*H I site should be present in two copies in the final construct. One is in the polylinker in the front of the insert (cut position 158) and the second is inside the insert (position 2618). M, molecular weight ladder; 1, a digest with the *Bam*H I released a 2460bp long fragment; 2, undigested plasmid; B, The *Eco*R I and *Not* I digest. M, molecular weight ladder; 1, the digested plasmid released a insert of correct size: 1742 bp. The *Eco*R I site cut at 929 bp position while the *Xho* I at 2671. 2, undigested plasmid.

site should be cut at 929 bp position while the *Xho* I at 2671. The *Eco*R I + *Not* I digest should release a fragment of 1742 bp. The digest released this fragment, Fig 3.29b. These results suggests that the ligation procedure was successful.

The region between the *Sac* I and *Eco*R I sites was sequenced. Four sequencing reactions with two forward and two reverse primers, which cover this region, Fig. 3.30, were performed by the C.M.H.T, University of Leicester. The consensus sequence was generated from the obtained sequences using the Fragment Assembly System (FAS) from the GCG programme package. The derived consensus sequence was compared with the template, designed using the SeqEd programme (GCG package) from the Ob-R (U50748) and pMelBac sequences, using the Bestfit programme (GCG package). It revealed 100% identity of the cloned sequence and the template. This result confirmed that no mutations were introduced by PCR.

The constructed transfer vector was sent to Invitrogen. A recombinant baculovirus encoding the Ob-R extracellular domain with the 6×His-FLAG tag in its C terminus was generated by a co-transfection of the transfer vector with the Bac-N-Blue$^{TM}$ DNA into *Sf*21 cells. Four clones of the ObR-pMelBac

construct were purified. The DNA purified from a viral stock of each clone was analysed by PCR (data not shown). A PCR product of approximately 3.2 kb, corresponding to 2.8 kb of the insert, and 0.316 kb of the pMelBac vector, indicated that these are recombinants containing the desired gene.

In Glasgow, the clones were analysed for protein expression by Western Blot (data not shown) and the best one was returned to Invitrogen for the generation of a high titer stock. The high titer stock was completed to a titer of $3.1 \times 10^8$ pfu/ml.

A time course of protein expression was carried out (Invitrogen). The 250 ml of High Five™ cells used for the time course were grown to a density of $2.0\text{-}2.5 \times 10^6$ cells/ml in a spinner flask. A 1.5 ml baseline sample, 0 hr, was removed. The content of the spinner flask was then infected with the 8.9 ml of the high titer stock generated previously. Samples were then taken at 24 hour intervals up to 96 hours. Each time point sample was separated into cell pellet and cell supernatant by centrifugation for 4 min at 2,500 rpm.

Both supernatant and cell pellets were analysed for protein expression (Glasgow) by Western Blot. Data from the analysis of the supernatants indicated, that the recombinant protein is expressed and effectively secreted into the medium 72 hours post-infection, (Fig. 3.31)

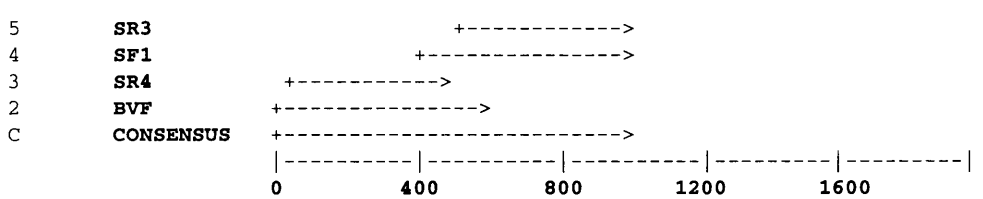


Figure 3.30: Determination of the ObR/pMelBac sequence. The consensus sequence was generated from the sequencing results using the Fragment Assembly System (FAS) from the GCG programme package.

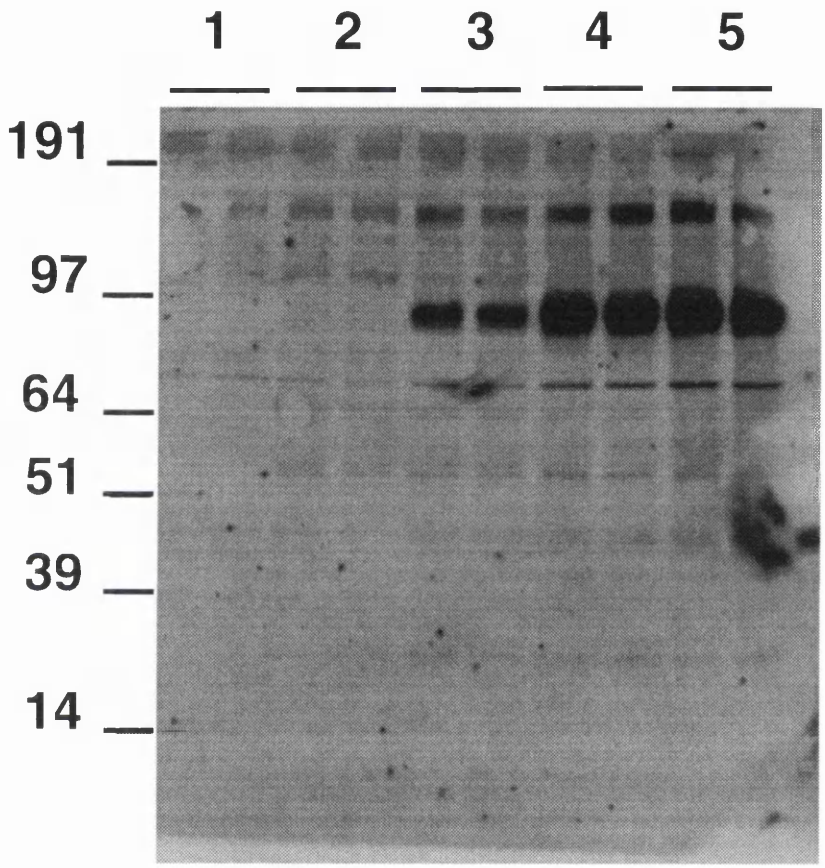


Figure 3.31: Time course study of Ob-R expression in High Five™ cells. 1, 0 hr post-infection sample; 2, 24 hr; 3, 48 hr; 4, 72 hr, 5, 96 hr. In the Western blot analysis, anti-leptin receptor antibody (R&D Systems) (1:1,000 dilution) was used in a combination with the HRP conjugated anti-goat antibody (SIGMA) (1:5,000 dilution) in ECL detection.

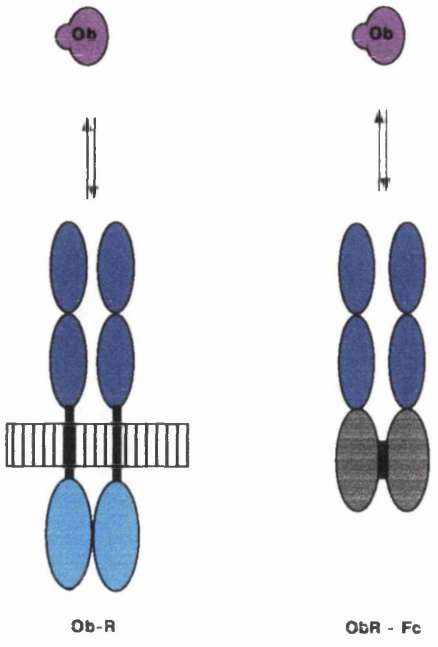


Figure 3.32: Leptin receptor chimera (ObR-Fc) used in the BiaCore experiments. The chimera consists of two extracellular domains of the receptor fused to the Fc region of $IgG_1$. The chimeric receptor used mimics the dimerised leptin receptor expressed on the cell surface.

## 3.3 BiaCore analysis of Ob-ObR interaction

The leptin - leptin receptor interaction was studied using recombinant human, mouse and rat leptin and recombinant human and mouse receptor chimeras (ObR-Fc). These chimeras consist of two extracellular domains of the receptor fused to the Fc region of $IgG_1$. The chimeric receptors used mimic the dimerised leptin receptor expressed on the cell surface, Fig. 3.32. The possibility that the leptin receptor exists as a dimer has been proposed recently [71]. This contradicts the common model of cytokine receptor activation, in which a ligand-free receptor exists as a monomer and its dimerisation is introduced by the ligand binding, Fig 1.11.

### 3.3.1 Real-time BIA technology

The interaction between leptin and its receptor was studied using the biosensor BIAcore™ 2000 from Pharmacia. BIAcore™ 2000 is a fully automated flow-cell instrument based on the Biomolecular Interaction Analysis (BIA) system. This system exploits the optical phenomenon of surface plasmon resonance (SPR) to monitor biomolecular interactions, Fig. 3.33.

SPR arises in thin metal films under conditions of total internal reflection.

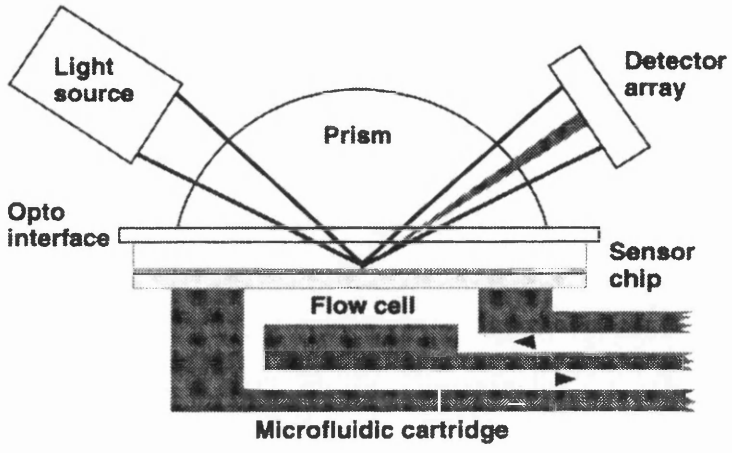


Figure 3.33: BiaCore detection system. The optical system and flow cell in the BiaCore analytical instrument. The figure taken from the BIAtechnology Handbook [88].

The phenomenon produces a sharp dip in the intensity of reflected light at a specific angle, the *resonance angle*. The position of this refractive angle depends partly on the refractive index of the medium close to the metal film. The refractive index of the medium is directly correlated to the concentration of dissolved material. Thus, SPR is used in BIA to measure changes in the surface layer of solution in contact with the sensor surface. This information is then processed to obtain the molecular concentration in the medium close to the metal film. This concentration determines the mass bound to the surface and thus formation of the molecular complex in real time.

In real-time monitoring, continuous-flow technology is used to measure chip-bound molecular mass during the course of interaction. The experimental-geometry of the system is as follows. One interactant is immobilised on the sensor surface, which forms one wall of a micro-flow cell. Solution containing the other interactant flows continuously over the sensor surface. As molecules from the solution bind to the immobilised interactant, the resonance angle changes and a response is registered.

Results from real-time BIA are presented in the form of a *sensorgram*. The sensorgram is a plot of the resonance-signal change as a function of time, Fig. 3.34. The signal change is marked in arbitrary resonance units (RU). Kinetic data are extracted from the rate of the signal change.

The BiaCore has several advantages over other techniques, the most important being real-time monitoring and label-free detection. The real-time

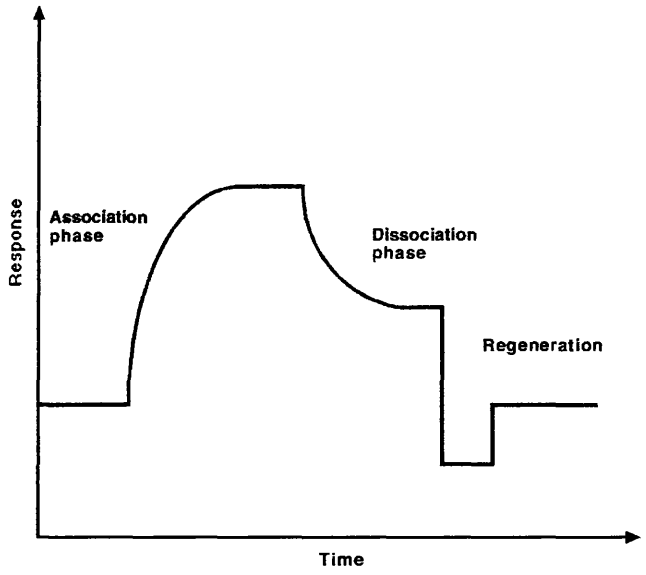


Figure 3.34: BiaCore sensorgram. During *association phase*, analyte is exposed to the chip and binding is monitored. If the reactions proceed long enough, equilibrium may be achieved. When the chip is washed with buffer, *dissociation phase*, the dissociation of the analyte-ligand complex is monitored. The chip can be reused after *regeneration* with mild acid or base.

monitoring of interaction is the ideal way to obtain kinetic data. The absence of a need to label molecules results in minimal interference with the interaction being studied.A problem of the interaction alteration due to the immobilisation of one of the interactants onto the chip is routinely eliminated by a coupling the interactant on the chip surface via a monoclonal antibody with a binding site different from that involved in the interaction(Section 3.3.3.)

## 3.3.2 Sensor chip

The metal film on the sensor chip is essential for generation of an SPR signal(3.35). Gold is used in real-time BIA because it gives an SPR signal at a convenient combination of reflectance angle and light wavelength, and is also chemically inert to solvents and solutes typically used in biochemical contexts.

The gold film on the sensor chip is covered with a surface matrix (covalently attached through an inert linker layer) on which biomolecules may be immobilised using well-defined chemistry. The sensor chip, CM5, has a matrix consisting of carboxymethylated dextran, which provides an environment suitable for studies of biomolecular interactions and enhances the interactant-immobilisation capacity of the surface.

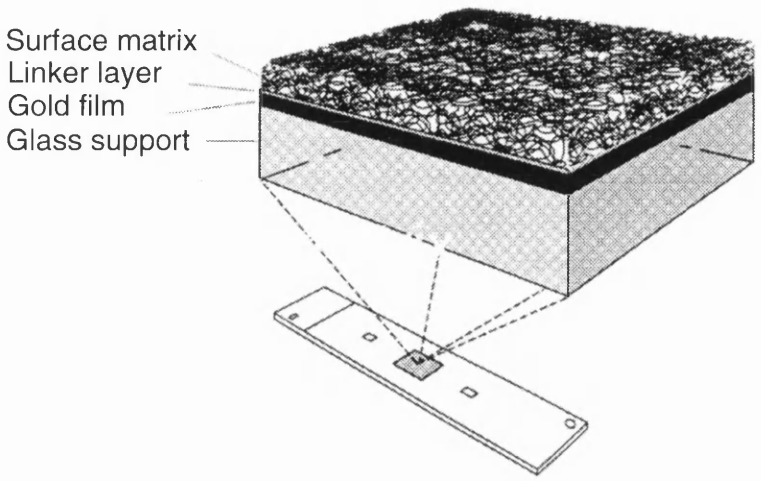


Figure 3.35: Sensor chip. The surface of Sensor Chip CM5 consists of three layers: glass, a thin gold film, and a matrix layer. The matrix is bonded to the gold film through an inert linker layer. The figure taken from the BIAtechnology Handbook [88].

### 3.3.3 Ligand immobilisation

In BiaCore experiments one molecule (ligand) is immobilised on the sensor surface, while the other (analyte) is injected in continuous flow over the surface. The ligand can be coupled to the surface either directly or indirectly by capturing via immobilised antibody. Direct coupling creates a stable surface. However, coupling procedures, such as primary amine coupling [80], can introduce heterogeneity in the surface bound molecule.

Alternatively, capturing methods e.g. using monoclonal antibodies [89] or nickel chelating surfaces [90, 91] orient molecules on the surface, thus minimising the effects of surface heterogeneity. Unfortunately, the capture step does not always create a stable complex with the first molecule which artificially increases the complexity of the binding responses for the second molecule [92].

A capturing assay shown in Fig. 3.36 was used for receptor immobilisation. Leptin receptor was captured on the chip surface via one of two molecules: Protein G or anti human (Fc specific) antibody, which were covalently linked to the chip surface by amine coupling using reactive esters.

Amine coupling introduces N-hydroxysuccinimide esters into the surface matrix by modification of the carboxymethyl groups with a mixture of N-hydroxysuccinimide (NHS) and N-ethyl-N'-(dimethyl-aminopropyl)- carbodiimide (EDC). These esters then react spontaneously with amines and other

nucleophilic groups on the ligand to form covalent links [80].

The desired amount of the capturing molecule (2000 RU of Protein G or 7000 RU of anti-human antibody) was amino-coupled to all four cells of the chip. An important feature of the capturing molecule is the stability of its binding capacity for ligand over a large number of repeated experiments. For each experimental cycle the ObR-Fc is first captured on the surface via the capturing molecule Protein G or anti-human antibody. Leptin is then injected over the surface. At the end of the experiment ObR-Fc and leptin are removed during surface regeneration. Good regeneration of the surface is important because residual surface-bound residues after each regeneration would affect the subsequent analyte response.

A 1 min pulse of glycine pH 2.0 was used to regenerate the surface. It effectively disrupted interaction between the ObR-Fc and the capturing molecule. However, repeated use of glycine pH 2.0 might lead to degradation of the capturing molecule. We monitored Protein G as well as the anti-human antibody degradation by measuring an amount of ObR-Fc bound in repeated experiments (Fig. 3.37, 3.38). It was clear from the comparison that Protein G created a much more stable surface than anti-human antibody, so, we used Protein G in subsequent experiments.

### 3.3.4 Mass transport

We continued with an evaluation of mass transport. Mass transport refers to the transport of analyte from bulk solution $Ob_{flow}$ to the chip surface $Ob_{surf}$. This can be described by the following equation

$$Ob_{flow} \overset{k_m}{\rightleftharpoons} Ob_{surf} + ObR \overset{\overset{k_a}{\rightleftharpoons}}{k_d} Ob : ObR$$

Mass transport can significantly affect binding if the interaction between analyte and ligand is much faster than the transport of analyte from bulk solution to the surface. For a given analyte, there are two factors affecting mass transport: the flow rate and the concentration of surface binding sites. The flow rate affects the mass transport rate constant $k_m$ but has no effect on the interaction kinetics. Increasing the flow rate increases $k_m$, but this effect is relatively low. On the other hand, the concentration of surface binding sites affects the absolute interaction rate but has no effect on mass transport. This is the more important parameter because increasing the surface binding capacity increases the initial interaction rate, so that mass transport is more likely to be limiting.

To minimise mass transport, it is important to keep surface binding capacity as low as possible. Immobilisation levels of 50-250 RU are recommended. Mass transport can be ignored if the initial binding rate does not increase more than 5-10 % when the flow rate is raised from 15 to 75 $\mu$l/min.

To verify whether or not the leptin-leptin receptor interaction was mass-transport limited, a control experiment was carried out. 180 RU of the ObR-Fc was immobilised. The flow rate was changed from 15 to 100 $\mu$l/min and the binding rate was monitored for an initial 100 s, (Fig. 3.39.) Because no increase was observed, mass transport was treated as not limiting and not considered in data analysis.

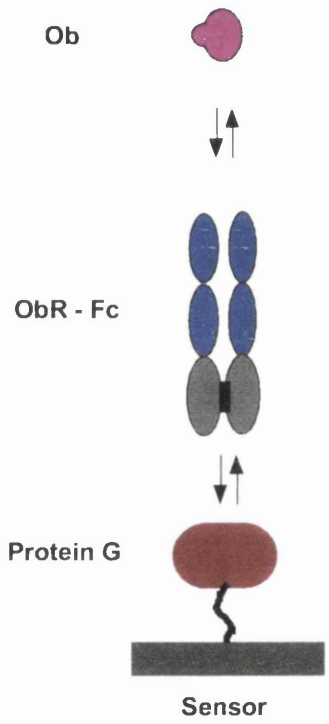


Figure 3.36: Schematic of the biosensor capturing assay. The ObR-Fc was captured onto the chip surface via protein G, which was covalently bound to the dextran matrix of the chip. In this configuration a homogenous receptor surface is formed and its interaction with Ob can be monitored.

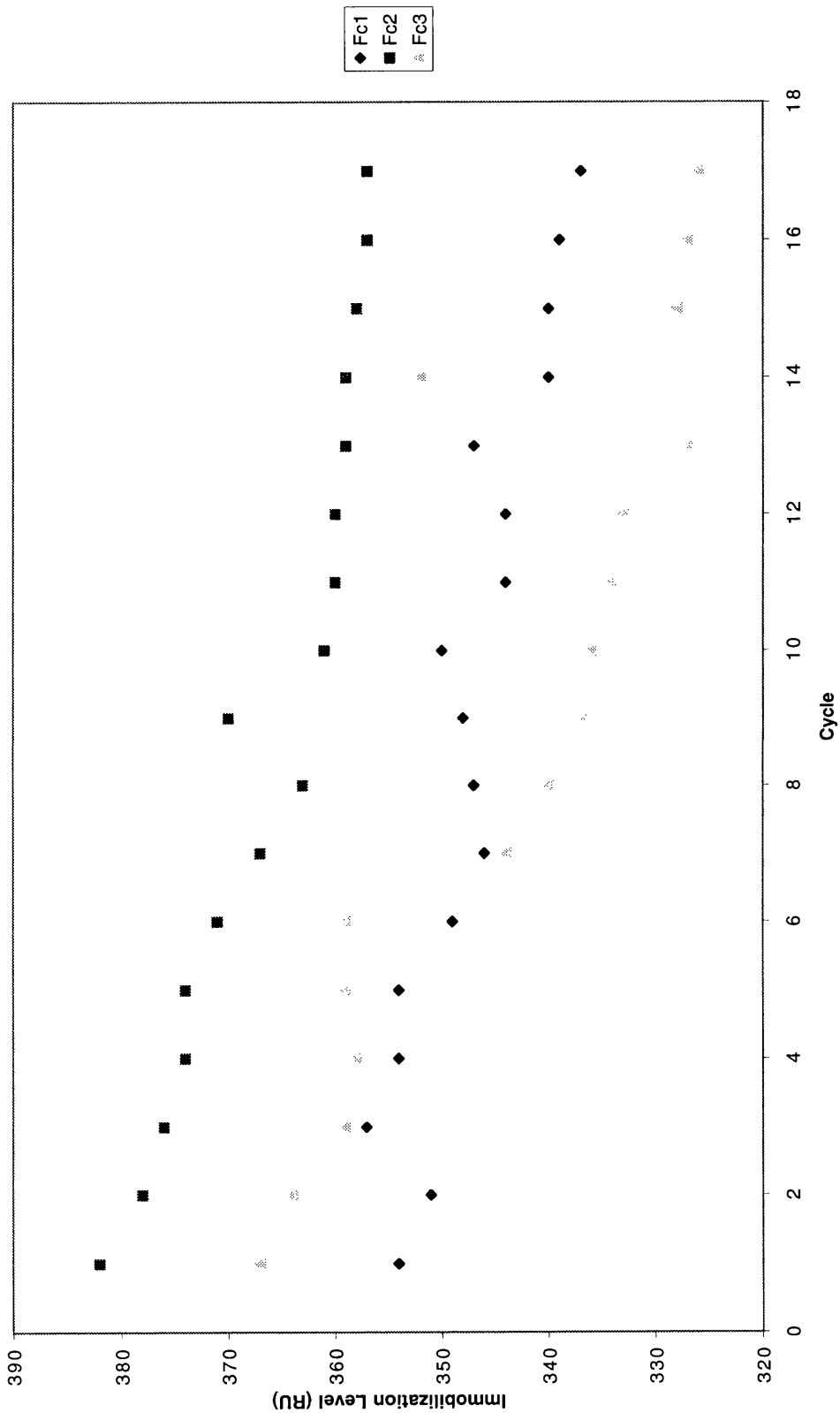


Figure 3.37: Regeneration of anti-human (Fc specific) antibody surface of Fc 1, Fc 3 and Fc 4 channels.

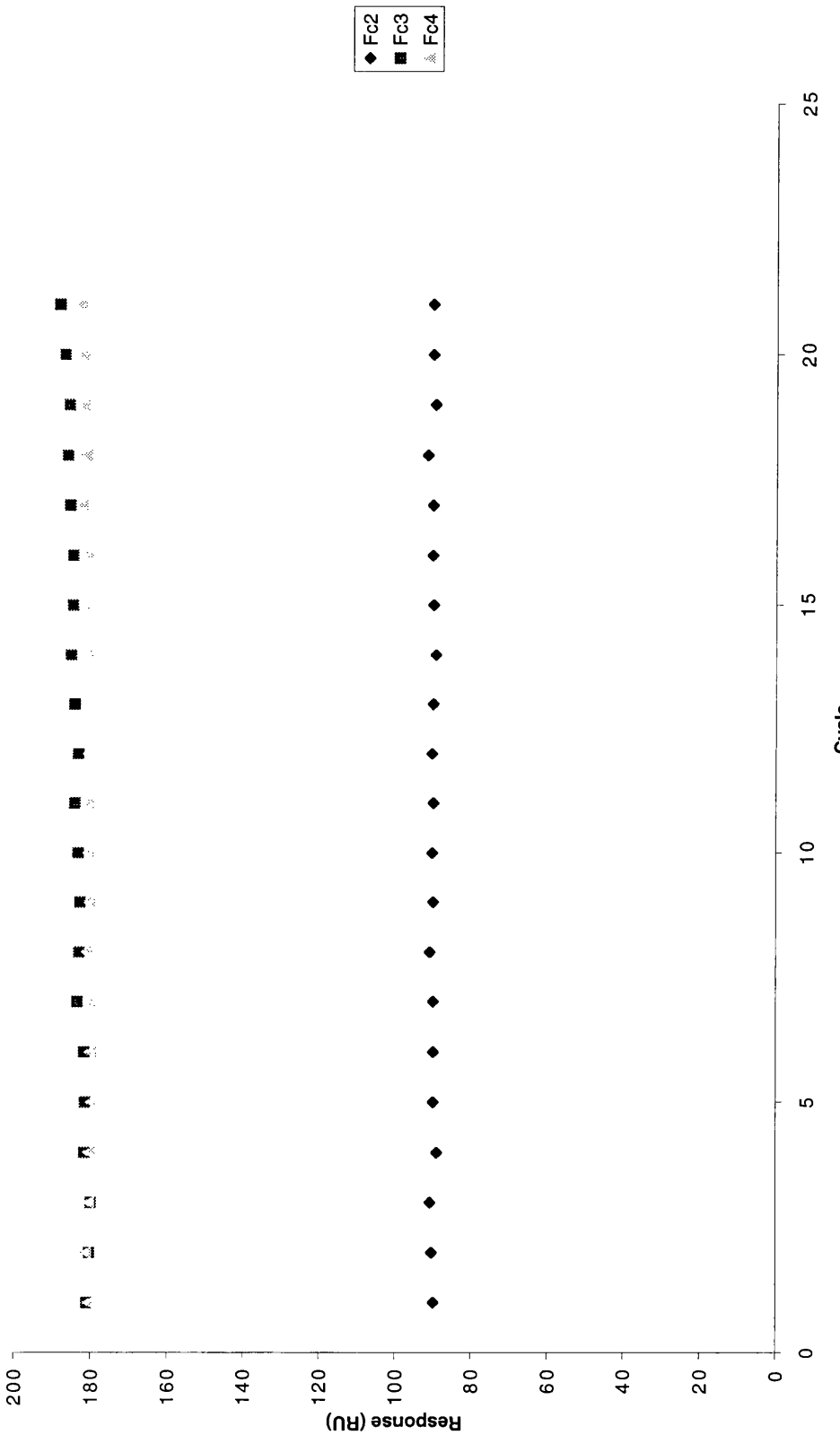


Figure 3.38: Regeneration of Protein G surface of Fc 2, Fc 3 and Fc 4 channels.

### 3.3.5 Experimental design

To measure leptin-leptin receptor interaction, an active surface was created on flow cells 2, 3 and 4 by immobilising the receptor chimera (human or mouse). The flow cell 1 was used as a control surface to measure leptin nonspecific binding. In this case Protein G alone was used instead of ObR-Fc.

In a typical experiment, 50-3000 RU of one of the two receptor chimeras was immobilised on flow cells 2, 3 and 4. After equilibrating for 100 s, leptin injection was passed over all four flow cells and leptin binding to active (Fc 2, 3 and 4) and control (Fc 1) surfaces was measured. This procedure was repeated several times with different leptin concentrations.

Examples of collected binding data are shown in Fig. 3.40. The higher traces show an overlay of six repeated leptin (0.1 - 30 nM) or buffer alone (0 nM) injections on to an active surface (Fc 2). The lower traces represent control experiments in which leptin from the same injection passed over a control cell (Fc 1). The rapid rise in signal at the start of each injection is due to the difference in bulk refractive index of the injection and running buffer, as well as instrument noise. It is followed by a slow increase representing leptin binding to the chip surface.

Generation of good quality data for kinetic analysis was achieved classically as follows. To remove contributions of non-specific binding and refractive index, the control responses from Fc 1 were subtracted from binding data obtained from active cells (Fc 2, 3 and 4). Results are shown in Fig. 3.41. A minor baseline drift was observed as shown in Fig 3.42A. This was a disadvantage of the capturing method used. Using Protein G to capture the ObR-Fc resulted in the correct orientation of the receptor relative to the chip and the analyte thereby minimising surface heterogeneity. On the other hand, the complex between the ObR-Fc and the Protein G slowly dissociated. This could be corrected by subtraction of a bulk injection (0 nM) from (0.1-30 nM) binding data, Fig. 3.42B.

First, the compatibility of flow cells was analysed. For initial chip-activation, the predefined BiaCore application wizard, Immobilisation, was used to link 2000 RU of Protein G covalently on to all four flow cells. The final values of 1505, 1117, 1593 and 1606 RU on flow cells 1, 2, 3, and 4, respectively, were obtained. This difference in Protein G levels on different cells raised a question of their compatibility. This problem was investigated by injecting the same amount of the human ObR-Fc (12 $\mu$l of 0.5 $\mu$g/ml solution) on each of the four flow cells and monitoring the hOb (0.1 - 30 nM) binding. Data were pro-

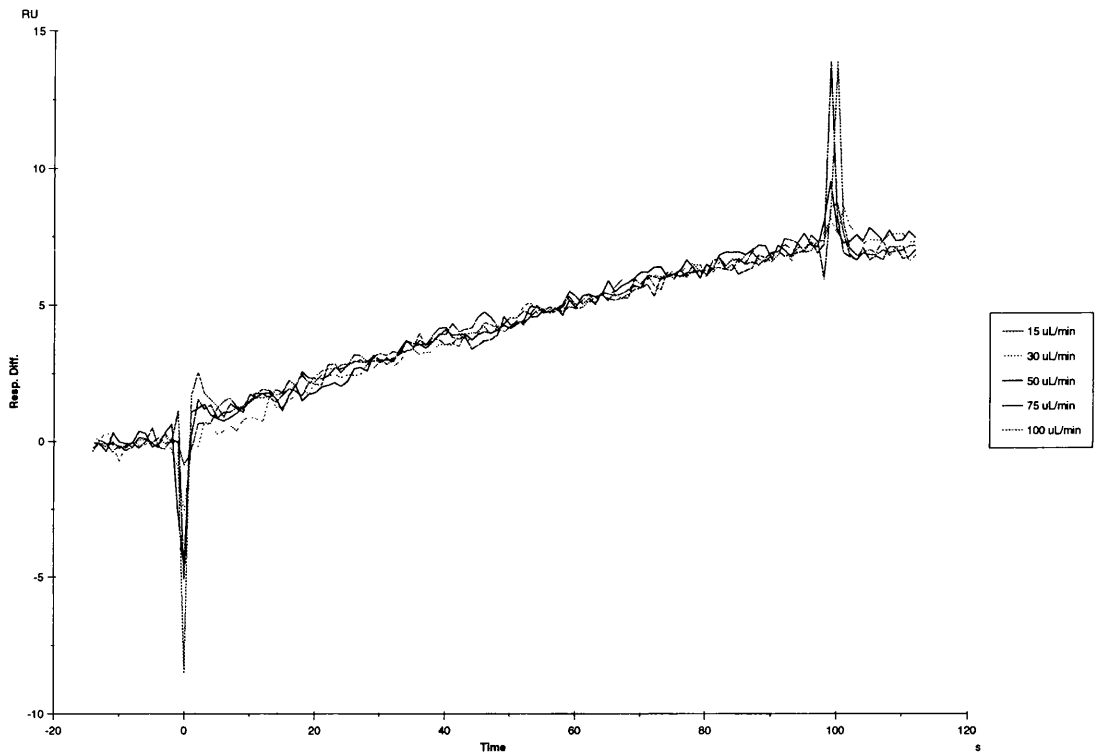


Figure 3.39: Mass transport evaluation. The flow rate was changed from 15 to 100 $\mu l/min$ and the binding rate was monitored for initial 100 s.

| Cell | $k_a/10^6$ | $k_d/10^{-4}$ | $\chi^2$ |
|---|---|---|---|
| 2 | 1.26 | 4.05 | 0.110 |
| | 1.53 | 3.92 | 0.103 |
| | 1.47 | 4.74 | 0.106 |
| 3 | 1.58 | 2.78 | 0.097 |
| | 1.61 | 3.56 | 0.0843 |
| | 1.68 | 4.23 | 0.0864 |
| 4 | 1.42 | 3.56 | 0.0931 |
| | 1.43 | 4.19 | 0.0901 |
| | 1.42 | 4.37 | 0.0969 |

Table 3.5: Flow cells compatibility; $k_a$ and $k_d$ are the association and dissociation rate constants, $\chi^2$ describes the closeness of fit.

cessed as described above and fitted to the 1:1 Langmuir model. The derived values for $k_a$and $k_d$ are summarised in Table 3.5. They clearly demonstrate that despite different levels of hObR-Fc immobilised on individual cells, the reaction kinetics are very similar.

To obtain binding data for all possible combinations of human and mouse ObR-Fc and human, mouse and rat Ob a simple macro for controlling the BiaCore instrument was written, Appendix C. An execution of this macro performed the following tasks in three subsequent repeats. All four cells were first regenerated with two injections of a 1 min pulse of glycine pH 2.0. The hObR-Fc was then immobilised on Fc 3 (12 $\mu$l of 0.5 $\mu$g/ml , 3 $\mu$l/min) and the mObR-Fc on Fc 2 (5 $\mu$l of 0.5 $\mu$g/ml, 3 $\mu$l/min) and Fc 4 (10 $\mu$l of 0.5 $\mu$g/ml, 3 $\mu$l/min). Different injection volumes for mObR-Fc were used to compare data from surfaces with different immobilisation levels $R_l$. After 180 s of equilibration, a 100 $\mu$l of Ob was injected (20 $\mu$l/min) and the binding was monitored. Thus, performing one such macro on the BiaCore instrument generated 3 sets of data for leptin (human, mouse or rat) binding to human leptin receptor and 6 sets of data for mouse leptin receptor (one cell used for h ObR-Fc and two for mObR-Fc). Performing the described macro three times with different leptin molecules generated data for all possible combinations of Ob and Ob-R molecules available. This macro with small modifications was used in all experiments.

### 3.3.6 Data analysis

Association and dissociation phases of all corrected sensorgrams (0.1 - 30 nM) from one data set were simultaneously fitted to a predefined 1:1 binding model

from the BIAevaluation 3.1 software. This is a simple model for 1:1 interaction between analyte and immobilised ligand, which is equivalent to the Langmuir isotherm for adsorption to surface. Experimental data were fitted to the model by means of non-linear regression analysis. Equation B.5 was used for fitting the association phase of a single sensorgram while equation B.7 was exploited for fitting of the dissociation phase.

Association and dissociation rate constants $k_a$, $k_d$, and the analyte maximum binding capacity $R_{max}$ were determined as fitting parameters. The rate constants $k_a$ and $k_d$ were fitted globally to all six sensorgrams. $R_{max}$ was fitted locally for each sensorgram. Local fitting of $R_{max}$ was used to reflect possible minor differences due to ObR-Fc dissociation from the Protein G complex.

Fitted data are presented in Fig 3.43 - 3.48. The quality of the fitting model was assessed from residual plots, which represent a difference between theoretical and experimental data for each sensorgram. The residual plots for all six sensorgrams are present in Fig. 3.49- 3.54. In all cases the difference between experimental and theoretical data is smaller than 2 RU, which is a level of instrumental noise, indicating that the 1:1 Langmuir model approximates kinetic processes on the chip surface very accurately.

To minimise experimental errors, especially those arising from pipetting, data were collected for several independently prepared samples. Kinetic data obtained are summarised in Tables 3.7 - 3.12. Single lines separate data obtained from different samples.

There was a good overall agreement between data, but some discrepancies were also observed, especially for the dissociation rate constant, $k_d$. If one or two values did not fit into the numerical range determined by the values from a given set, these were considered as a consequence of experimental and data

| Ob-R | Ob | $k_a/10^6$ $M^{-1} \cdot s^{-1}$ | $k_d/10^{-4}$ $s^{-1}$ | $K_D/10^{-10}$ M |
|---|---|---|---|---|
| h | h | 1.9 ± 0.4 | 4.6 ± 0.9 | 2 ± 1 |
| h | m | 1.1 ± 0.2 | 1.3 ± 0.6 | 1.2 ± 0.8 |
| h | r | 2.9 ± 0.1 | 2.8 ± 0.2 | 1.0 ± 0.8 |
| m | h | 1.2 ± 0.3 | 6.8 ± 0.6 | 6 ± 2 |
| m | m | 0.7 ± 0.1 | 1.4 ± 0.6 | 2 ± 1 |
| m | r | 1.1 ± 0.3 | 3.2 ± 0.9 | 3 ± 1 |

Table 3.6: Kinetic constants for the Ob–Ob-R interaction. Data represent the average value ± standard deviation derived from values obtained in repeated experiments; $k_a$ and $k_d$ are the association and dissociation rate constants, $K_D$ is the equilibrium dissociation constant.

processing errors and excluded from a calculation of the average values of $k_a$ and $k_d$. The dissociation constant, $K_D$, was determined as $k_d/k_a$. Its standard deviation S.D.($K_D$) (% ) was calculated as $S.D.(K_a) + S.D.(K_d)$. The kinetic constants obtained from this analysis are summarised in Table 3.6.

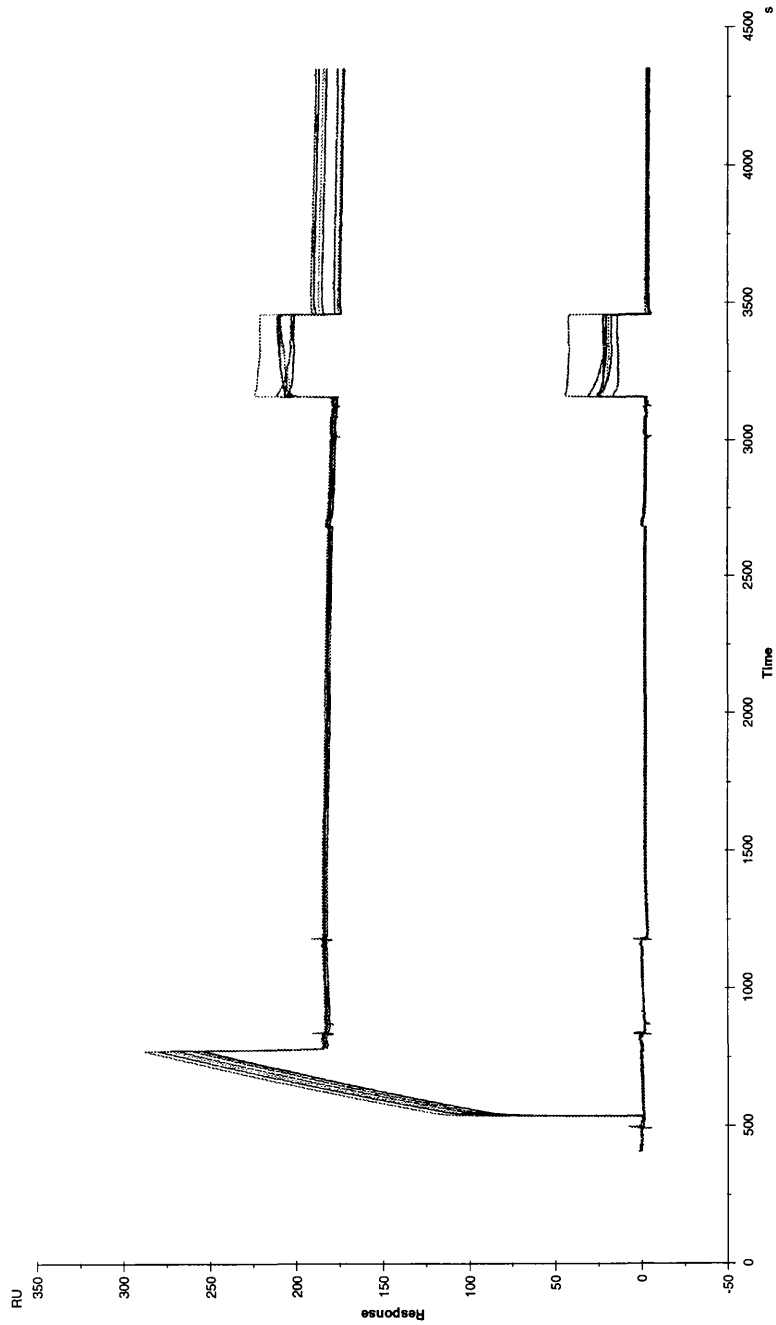


Figure 3.40: Collected binding data. Top traces show the immobilisation of the ObR-Fc on to the Fc3, a cell activation, followed by leptin (0.1 - 30 nM) or bulk buffer (0 nM) injections. Bottom traces represent a control experiment when molecules from the same injection passed over the control cell, Fc 1, with the Protein G instead of the ObR-Fc.

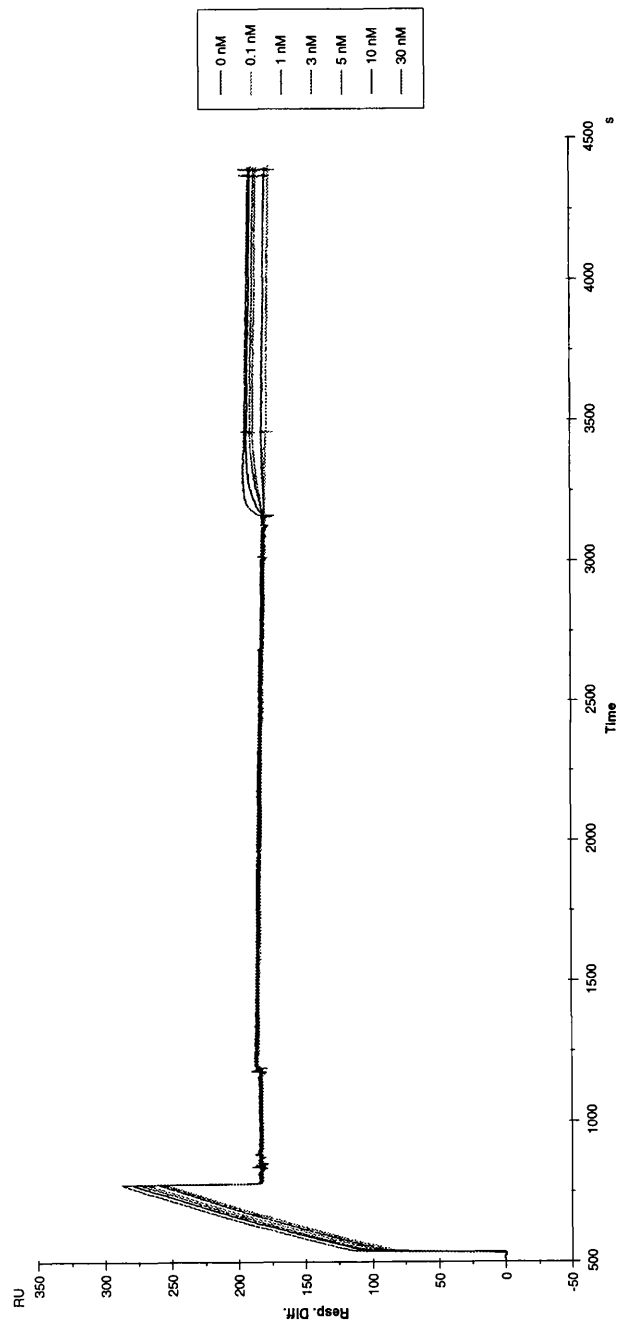


Figure 3.41: Nonspecific binding correction. To remove contributions of non-specific binding and refractive index a response from the control cell Fc 1 was subtracted from responses from the active cell Fc 3.

A.

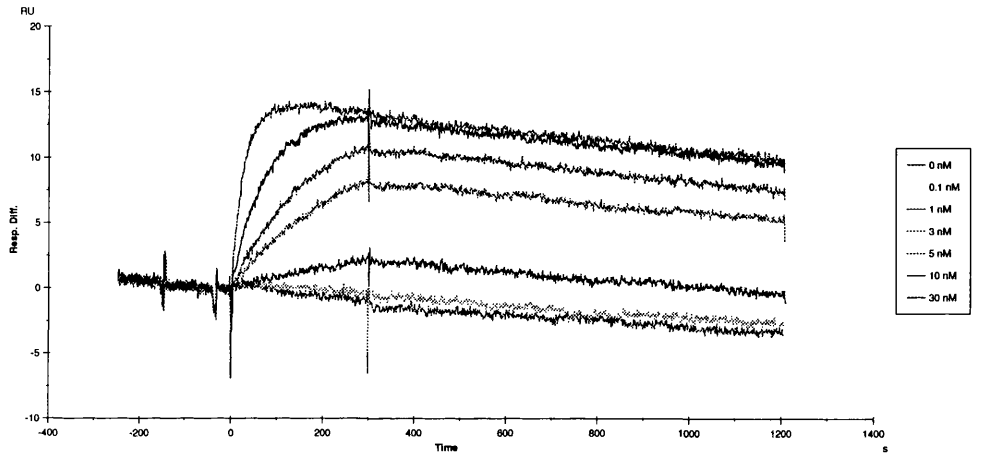


B.

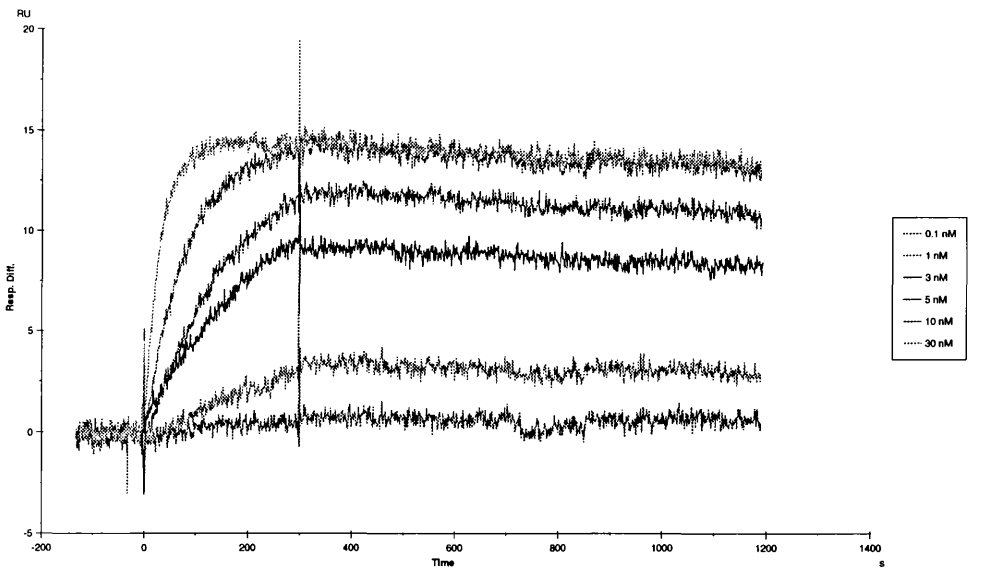


Figure 3.42: Drifting baseline correction. A. A demonstration of a baseline decay due to a dissociation of the complex between ObR-Fc and Protein G. B. The baseline decay was corrected by subtracting the 0 nM injection.

| Experiment No. | $k_a/10^6$ $M^{-1} \cdot s^{-1}$ | $k_d/10^{-4}$ $s^{-1}$ | $\chi^2$ | Cell |
|---|---|---|---|---|
| 1 | 1.59 | 5.41 | 0.100 | Fc3 |
| 2 | 2.14 | 6.21 | 0.112 | Fc3 |
| 3 | 2.36 | 5.59 | 0.114 | Fc3 |
| 4 | 1.53 | 3.92 | 0.103 | Fc2 |
| 5 | 1.61 | 3.56 | 0.084 | Fc3 |
| 6 | 1.43 | 4.19 | 0.090 | Fc4 |
| 7 | 2.11 | 3.92 | 0.113 | Fc2 |
| 8 | 2.32 | 3.44 | 0.153 | Fc3 |
| 9 | 2.40 | 5.00 | 0.121 | Fc4 |

Table 3.7: Kinetic constants for hOb-R/hOb interaction determined from repeated experiments; $k_a$ and $k_d$ are the association and dissociation rate constants, $\chi^2$ describes the closeness of fit and *Cell* corresponds to the chip flow cell used.

| Experiment No. | $k_a/10^6$ $M^{-1} \cdot s^{-1}$ | $k_d/10^{-4}$ $s^{-1}$ | $\chi^2$ | Cell |
|---|---|---|---|---|
| 1 | 0.95 | 0.78 | 0.096 | Fc3 |
| 2 | 1.08 | 0.88 | 0.087 | Fc3 |
| 3 | 1.24 | 1.81 | 0.097 | Fc3 |
| 4 | 1.18 | 2.04 | 0.085 | Fc3 |
| 5 | 1.18 | 1.08 | 0.088 | Fc3 |

Table 3.8: Kinetic constants for hOb-R/mOb interaction determined from repeated experiments; $k_a$ and $k_d$ are the association and dissociation rate constants, $\chi^2$ describes the closeness of fit and *Cell* corresponds to the chip flow cell used.

| Experiment No. | $k_a/10^6$ $M^{-1} \cdot s^{-1}$ | $k_d/10^{-4}$ $s^{-1}$ | $\chi^2$ | Cell |
|---|---|---|---|---|
| 1. | 2.62 | 2.41 | 0.093 | Fc3 |
| 2. | 2.75 | 2.66 | 0.099 | Fc3 |
| 3. | 3.20 | 3.01 | 0.099 | Fc3 |
| 4 | 2.68 | 2.84 | 0.119 | Fc2 |
| 5 | 2.82 | 3.36 | 0.111 | Fc2 |
| 6 | 2.78 | 3.18 | 0.118 | Fc2 |
| 7 | 2.71 | 2.91 | 0.097 | Fc 3 |
| 8 | 3.06 | 2.67 | 0.087 | Fc 3 |
| 9 | 3.41 | 2.43 | 0.092 | Fc 3 |

Table 3.9: Kinetic constants for hOb-R/rOb interaction determined from repeated experiments; $k_a$ and $k_d$ are the association and dissociation rate constants, $\chi^2$ describes the closeness of fit and *Cell* corresponds to the chip flow cell used.

| Experiment No. | $k_a/10^6$ $M^{-1} \cdot s^{-1}$ | $k_d/10^{-4}$ $s^{-1}$ | $\chi^2$ | Cell |
|---|---|---|---|---|
| 1 | 0.86 | 7.26 | 0.114 | Fc2 |
| 2 | 0.97 | 6.10 | 0.098 | Fc3 |
| 3 | 0.88 | 5.80 | 0.104 | Fc4 |
| 4 | 1.24 | 7.17 | 0.136 | Fc2 |
| 5 | 1.05 | 6.21 | 0.140 | Fc3 |
| 6 | 0.92 | 7.87 | 0.161 | Fc4 |
| 7 | 1.70 | 6.73 | 0.126 | Fc2 |
| 8 | 1.62 | 6.78 | 0.115 | Fc3 |
| 9 | 1.43 | 7.02 | 0.127 | Fc4 |

Table 3.10: Kinetic constants for mOb-R/hOb interaction determined from repeated experiments; $k_a$ and $k_d$ are the association and dissociation rate constants, $\chi^2$ describes the closeness of fit and *Cell* corresponds to the chip flow cell used.

| Experiment No. | $k_a/10^6$ $M^{-1} \cdot s^{-1}$ | $k_d/10^{-4}$ $s^{-1}$ | $\chi^2$ | Cell |
|---|---|---|---|---|
| 1 | 0.82 | 2.47 | 0.098 | Fc2 |
| 2 | 0.75 | 2.02 | 0.089 | Fc3 |
| 3 | 0.95 | 1.36 | 0.107 | Fc4 |
| 4 | 0.65 | 0.78 | 0.121 | Fc2 |
| 5 | 0.73 | 1.09 | 0.097 | Fc3 |
| 6 | 0.57 | 1.74 | 0.112 | Fc4 |
| 7 | 0.65 | 0.43 | 0.107 | Fc2 |
| 8 | 0.54 | 0.95 | 0.103 | Fc3 |
| 9 | 0.46 | 1.73 | 0.120 | Fc4 |

Table 3.11: Kinetic constants for mOb-R/mOb interaction determined from repeated experiments; $k_a$ and $k_d$ are the association and dissociation rate constants, $\chi^2$ describes the closeness of fit and *Cell* corresponds to the chip flow cell used.

| Experiment No. | $k_a/10^6$ $M^{-1} \cdot s^{-1}$ | $k_d/10^{-4}$ $s^{-1}$ | $\chi^2$ | Cell |
|---|---|---|---|---|
| 1 | 1.41 | 4.33 | 0.113 | Fc2 |
| 2 | 1.52 | 3.17 | 0.102 | Fc3 |
| 3 | 1.47 | 3.33 | 0.113 | Fc4 |
| 4 | 0.98 | 2.62 | 0.136 | Fc2 |
| 5 | 0.89 | 1.87 | 0.133 | Fc3 |
| 6 | 0.76 | 2.06 | 0.146 | Fc2 |
| 7 | 0.79 | 3.32 | 0.146 | Fc3 |
| 8 | 0.77 | 4.62 | 0.151 | Fc4 |

Table 3.12: Kinetic constants for mOb-R/rOb interaction determined from repeated experiments; $k_a$ and $k_d$ are the association and dissociation rate constants, $\chi^2$ describes the closeness of fit and *Cell* corresponds to the chip flow cell used.

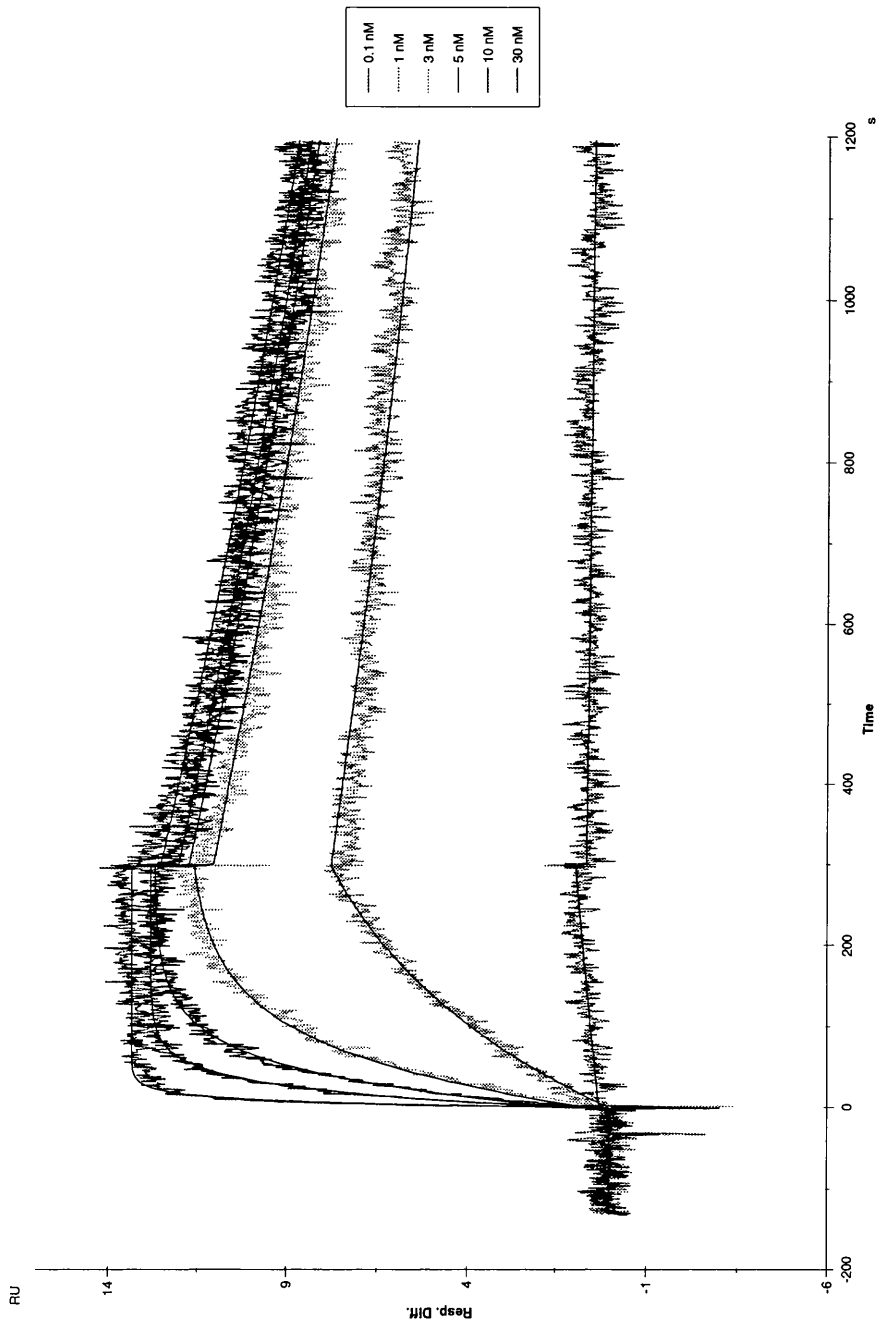


Figure 3.43: Fitting of corrected data for hOb-R/hOb interaction to a 1:1 (Langmuir) binding model.

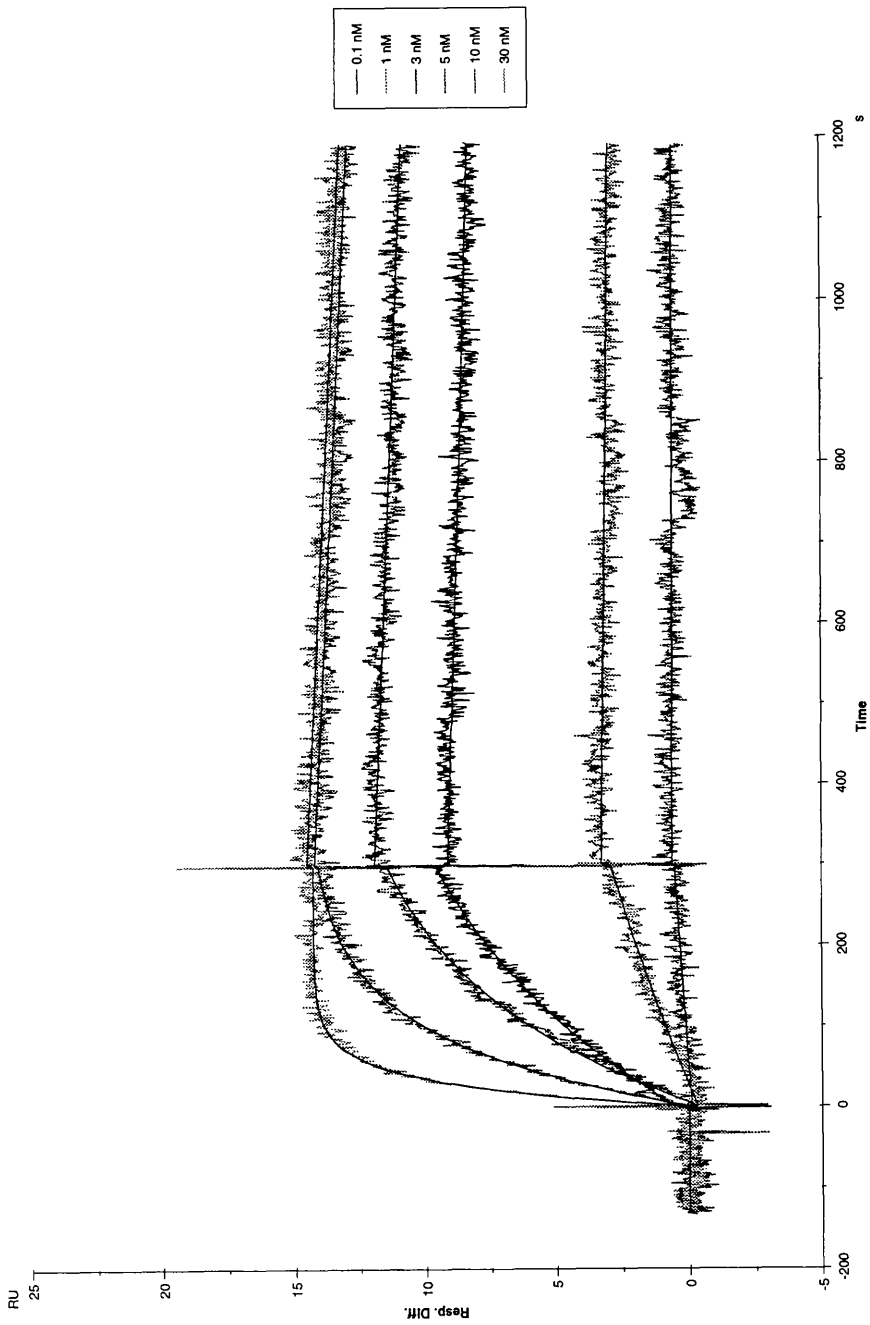


Figure 3.44: Fitting of corrected data for hOb-R/mOb interaction to a 1:1 (Langmuir) binding model.

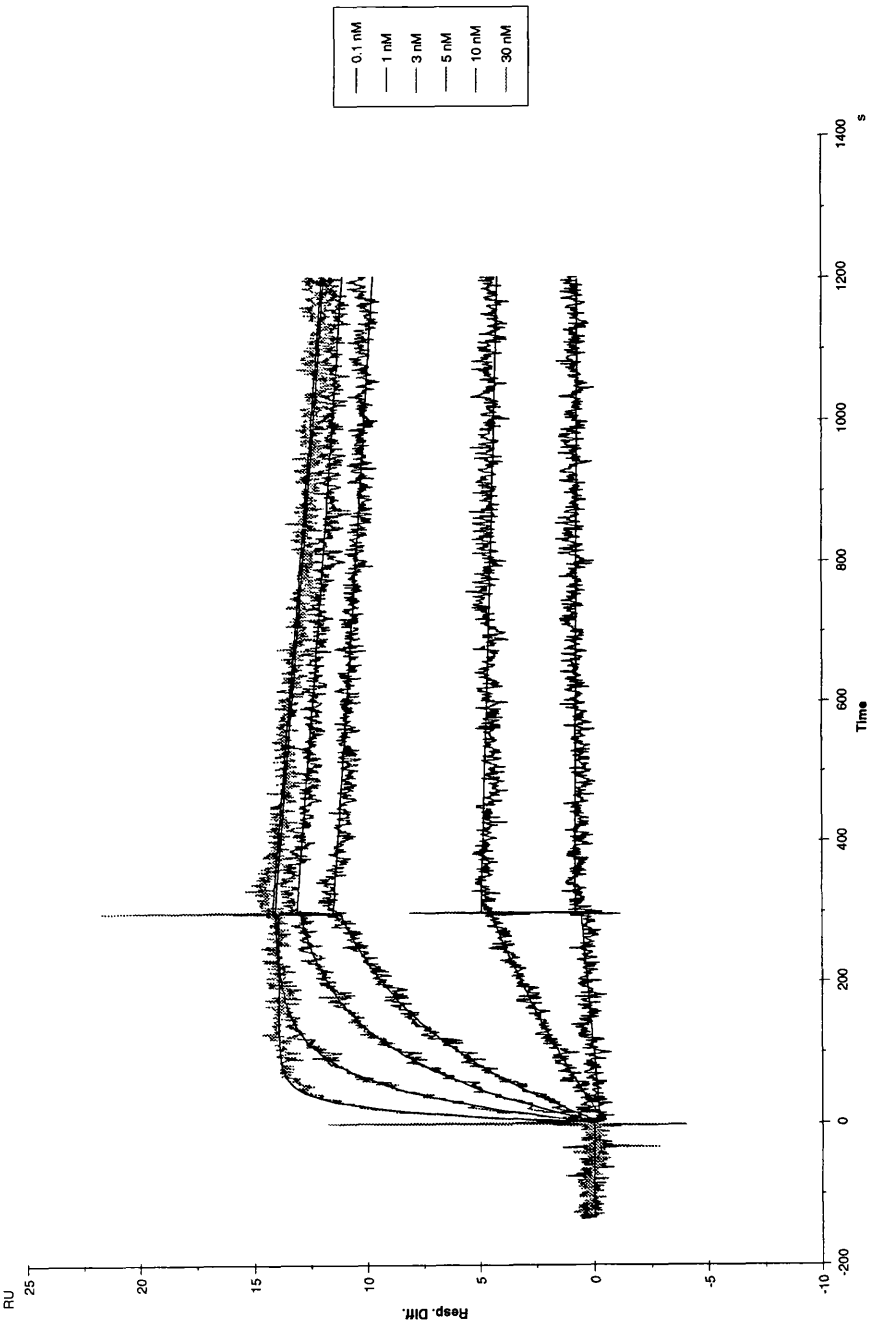


Figure 3.45: Fitting of corrected data for hOb-R/rOb interaction to a 1:1 (Langmuir) binding model.

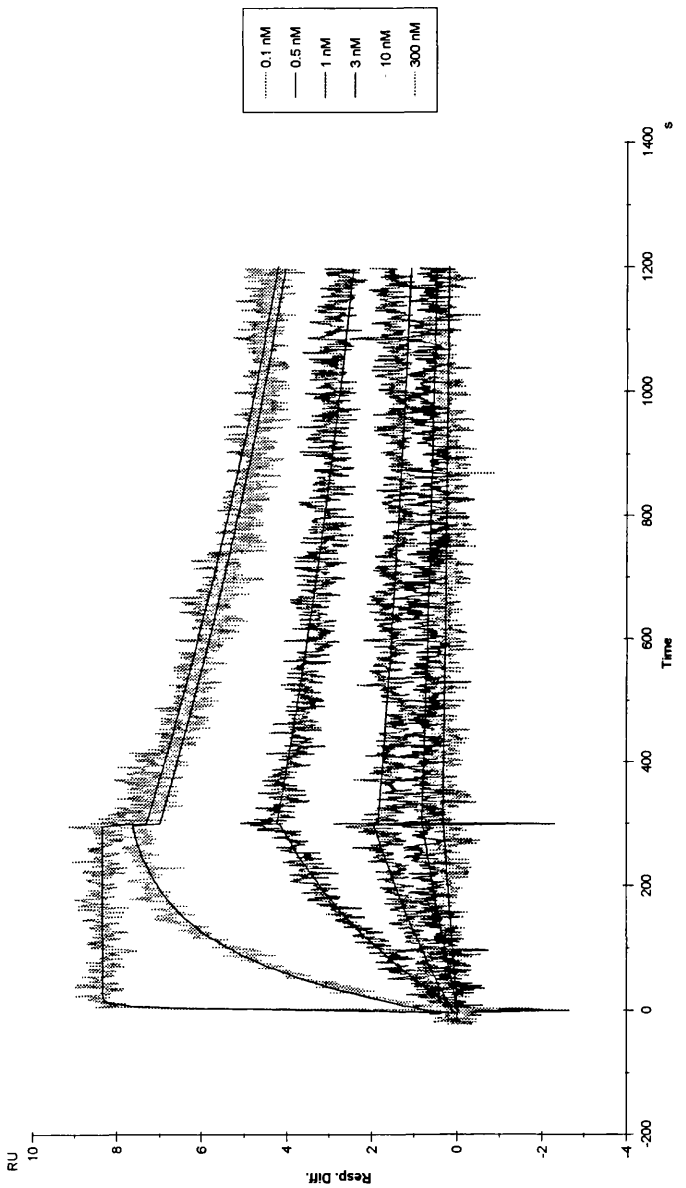


Figure 3.46: Fitting of corrected data for mOb-R/hOb interaction to a 1:1 (Langmuir) binding model.

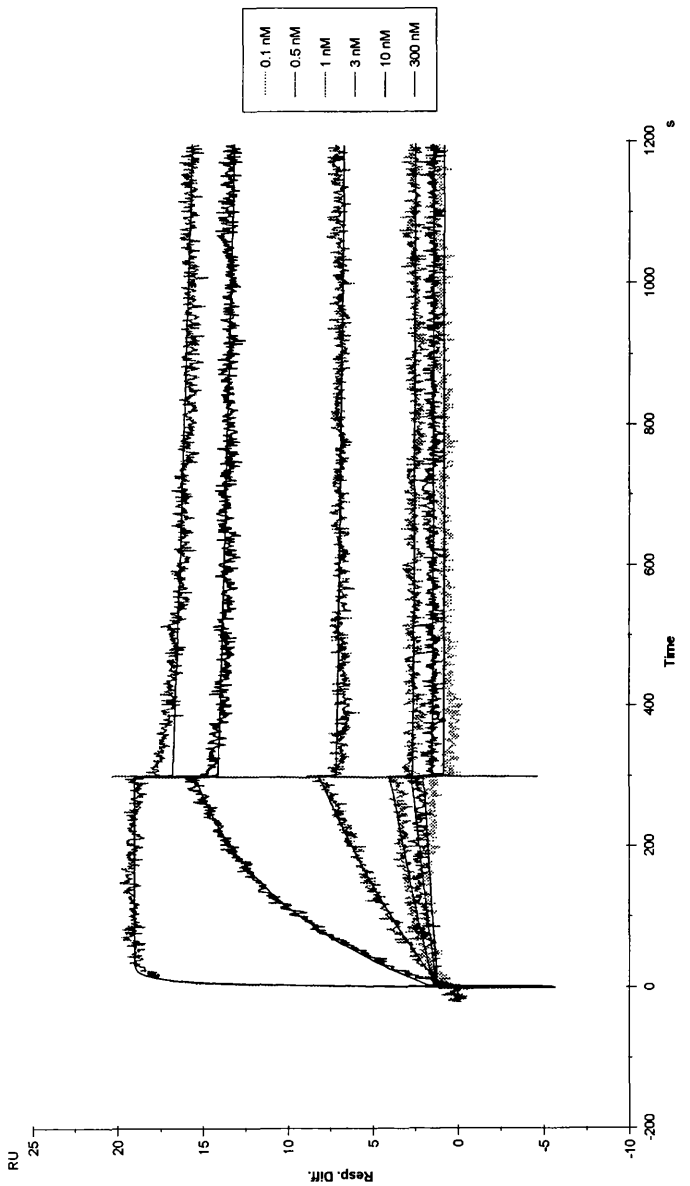


Figure 3.47: Fitting of corrected data for mOb-R/mOb interaction to a 1:1 (Langmuir) binding model.

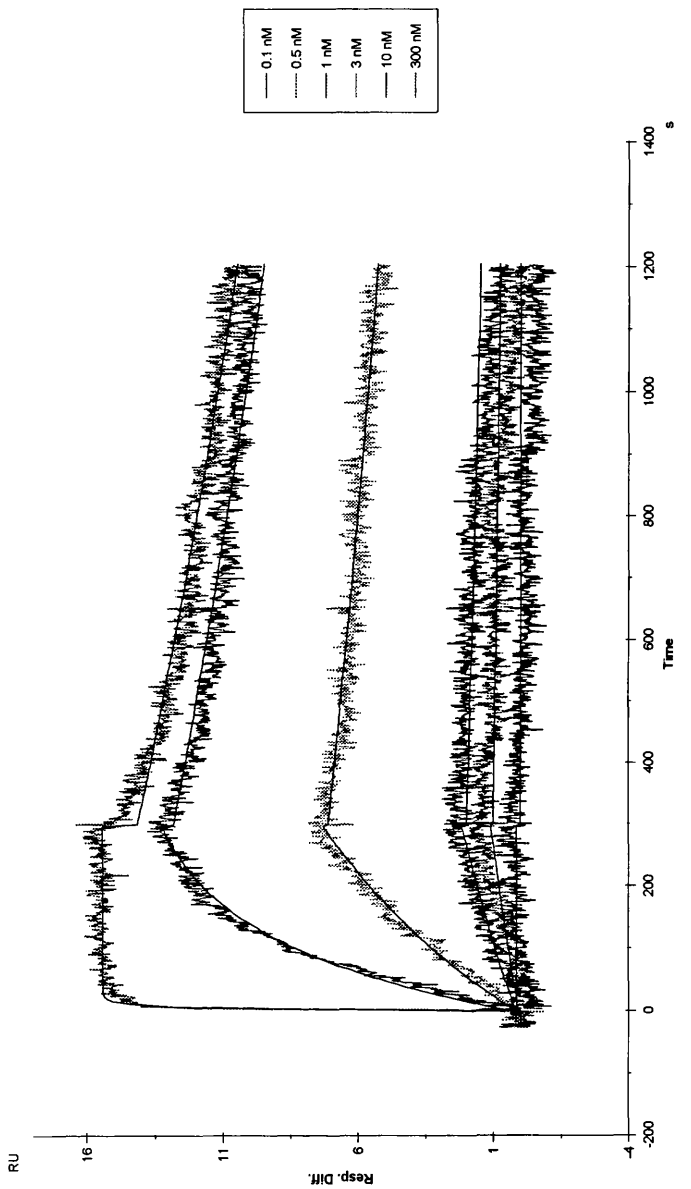


Figure 3.48: Fitting of corrected data for mOb-R/rOb interaction to a 1:1 (Langmuir) binding model.

| Ob-R | Ob | Stoichiometry | | |
|---|---|---|---|---|
| | | 3000 RU | 1300 RU | 300 RU |
| h | h | 0.49 | 0.75 | 1.11 |
| h | m | 0.52 | 0.81 | 1.11 |
| h | r | - | 0.82 | 1.12 |
| m | m | 0.81 | 1.00 | 1.00 |
| m | h | 0.77 | 0.91 | 0.91 |
| m | r | - | 0.99 | 1.01 |

Table 3.13: Stoichiometry of the Ob - Ob-R interaction determined from the BiaCore experiments with human and mouse leptin receptor chimera and human, mouse and rat leptin.

### 3.3.7 Stoichiometry

The BiaCore instrument measures the mass of molecules bound to the sensor surface. Thus, the stoichiometry of the surface molecular complex can be determined from the following equation

$$stoichiometry = \frac{R_{max} \cdot MW_{ligand}}{MW_{analyte} \cdot R_l} \tag{3.1}$$

where $R_{max}$, analyte binding capacity, can be extrapolated from experimental data and $R_l$ is given directly from a sensorgram recorded during ligand immobilisation.

The stoichiometry of ObR-Fc–Ob interaction was determined using the following values: $MW_{hObR-Fc} = 220\ kDa, MW_{mObR-Fc} = 160\ kDa, MW_{hOb} = MW_{mOb} = MW_{rOb} = 16\ kDa$. All these numbers refer to monomeric molecules. Therefore, that the derived stoichiometry represents the number of Ob molecules bound to a monomeric ObR-Fc molecule. The obtained values for different species are summarised in Table 3.13.

Apart from some of the data obtained on a very dense surface (about 3000 RU receptor immobilised), the observed stoichiometry is around 0.9 i.e. describing a 1:1 configuration. Thus, one monomeric ObR-Fc molecule interacts with one Ob molecule (one dimerised ObR-Fc molecule interacts with two Ob molecules). Lower stoichiometry (around 0.5) was observed when large amounts of hObR-Fc (3000 RU) were immobilised. This phenomenon is probably due to steric hindrance on the sensor surface which hinders Ob molecules from binding to all presented binding sites.

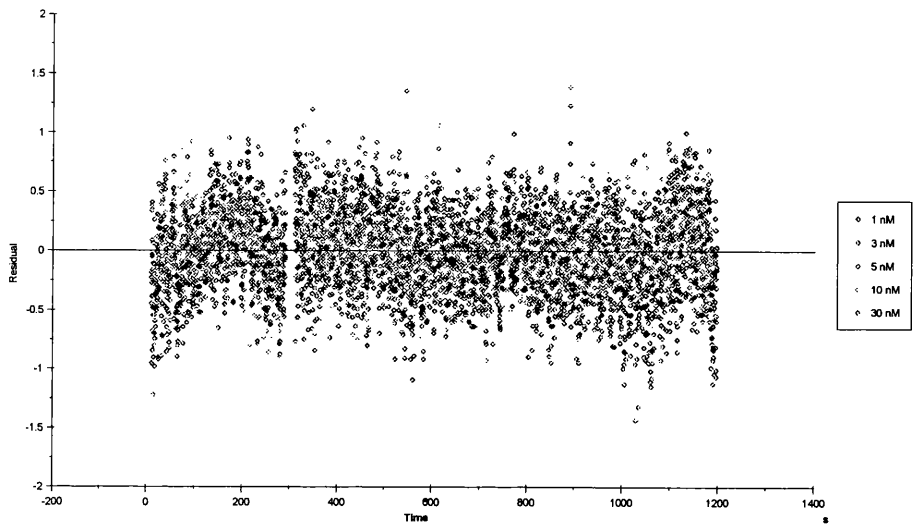


Figure 3.49: Residual plots for hOb-R/hOb interaction.

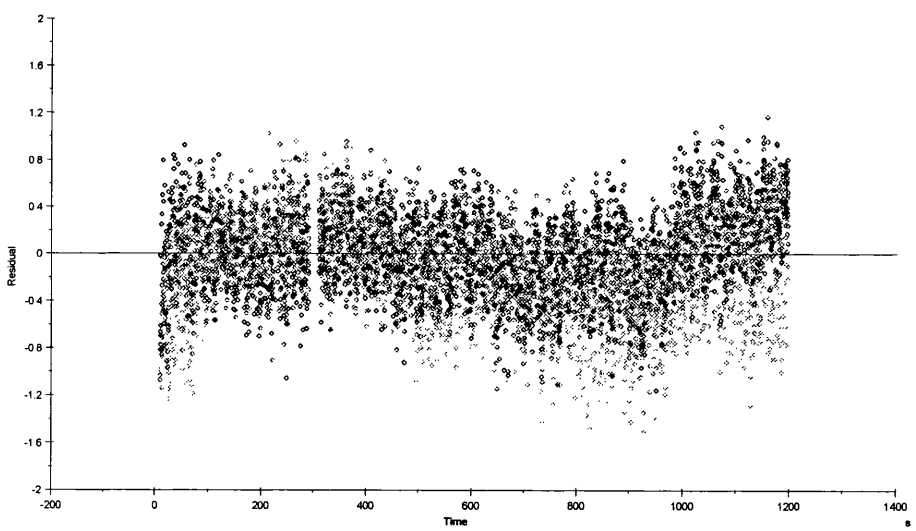


Figure 3.50: Residual plots for mOb-R/hOb interaction.

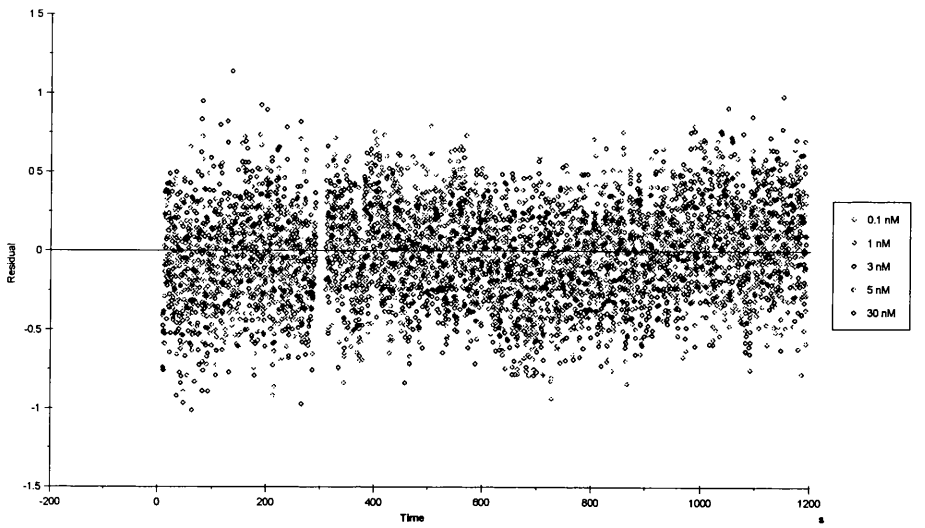


Figure 3.51: Residual plots for hOb-R/mOb interaction.

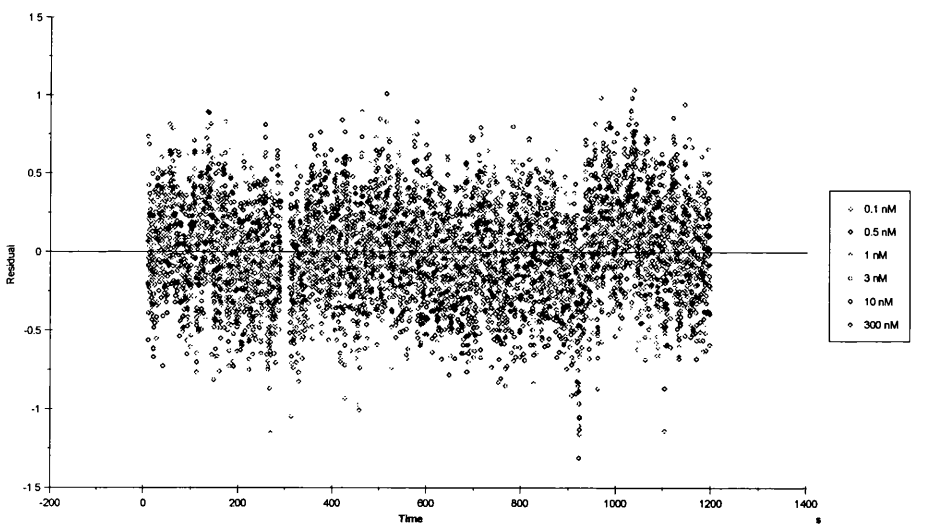


Figure 3.52: Residual plots for mOb-R/mOb interaction.

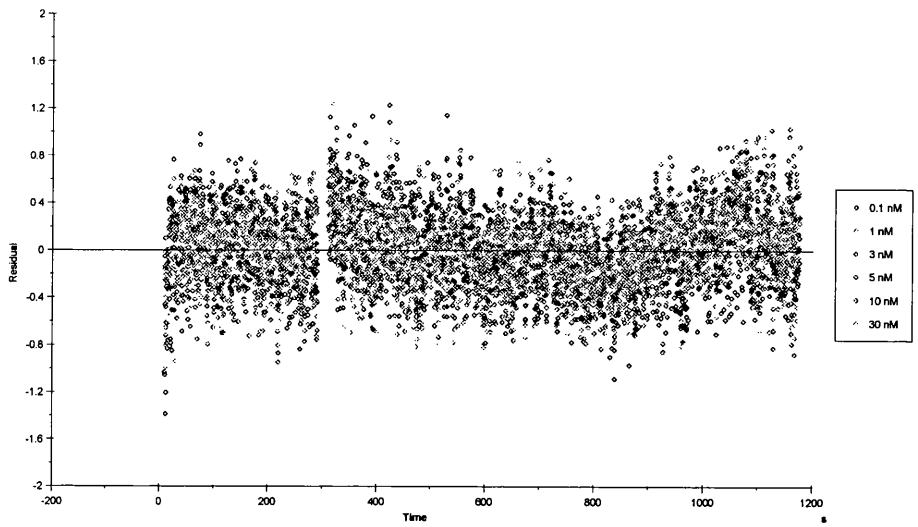


Figure 3.53: Residual plots for hOb-R/rOb interaction.

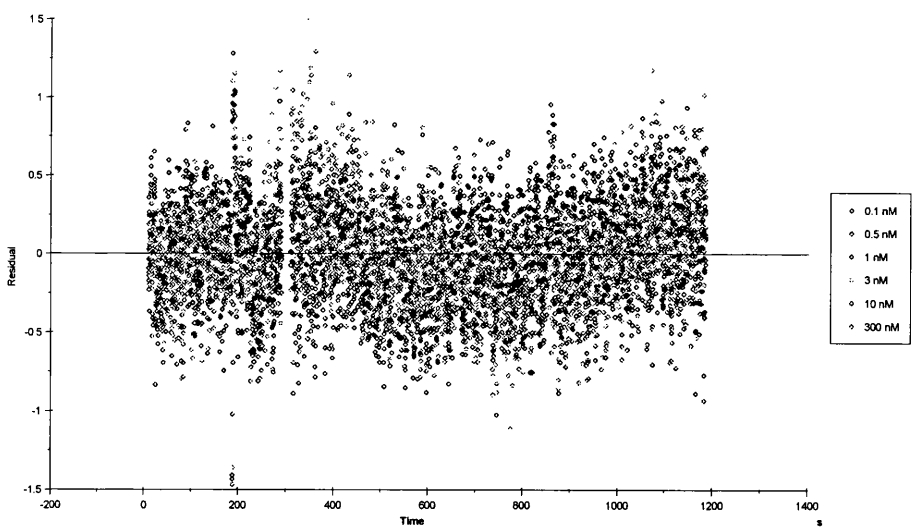


Figure 3.54: Residual plots for mOb-R/rOb interaction.

## 3.4 Binding properties of a truncated leptin

### 3.4.1 Construction of expression vectors

A clone of human leptin was kindly provided by Dr. Masuzaki [93]. The sequence analyses revealed that glutamine 28 ($Q^{28}$) was deleted from the sequence. This is an interesting feature as $Q^{28}$ is localised in the AB loop that is predicted to be involved in receptor binding,(Fig 4.1.)

Therefore, it was decided to overexpress this clone, encoding leptin with the $Q^{28}$ deletion, in *E. coli* and use the recombinant protein for the BiaCore analysis and to determine the potential role of $Q^{28}$ in receptor binding.

The FLAG system (SIGMA) designed for fusion of the FLAG peptide to proteins and expression in *E. coli* was used. The open reading frame (ORF) of leptin lacking $Q^{28}$ ($\Delta$Q28) was cloned into an amino-terminal FLAG expression vector. Two expression vectors were used: pFLAG-MAC and pFLAG-ATS. The pFLAG-ATS vector codes for the OmpA signal peptide which allows for expression of amino-terminal FLAG fusion protein within periplasm. The pFLAG-MAC lacks the coding sequence for the OmpA signal peptide and is useful for the expression of Met-amino-terminal FLAG fusion proteins within the cytoplasm.

The leptin cDNA was engineered for subcloning to both pFLAG-MAC and pFLAG-ATS vectors. Its leading sequence, $Met^{1}$-$Val^{22}$, was removed and the sequence encoding the processed protein was inserted into the vectors in-frame with respect to the ATG translation start codon. PCR was used to introduce the relevant restriction sites,(Fig. 3.55 A, B) The forward and reverse primers were designed. The forward primer introduced a *Sma* I site in front of $Pro^{23}$ in-frame with respect to the vector ATG translation start codons. The reverse primer contained the *Bgl* II site directly after the stop codon. The PCR product was subcloned into the pFLAG-MAC and pFLAG-ATS vectors digested with the *Sma* I and *Bgl* II restriction enzymes,(Fig. 3.56 A, B)

The two constructs encoding FLAG-leptin expressed either in the cytoplasm (ob-ATS) or periplasm (ob-MAC) were sequenced to check for any mutations introduced by PCR and were found to encode desired proteins.

### 3.4.2 Screening transformants for FLAG fusion proteins

Anti-M2 monoclonal antibody, which binds to the FLAG tag at any location on FLAG fusion protein, was used to screen for the presence of fusion proteins encoded by the ob-ATS or ob-MAC plasmids in bacterial transformants. Pro-

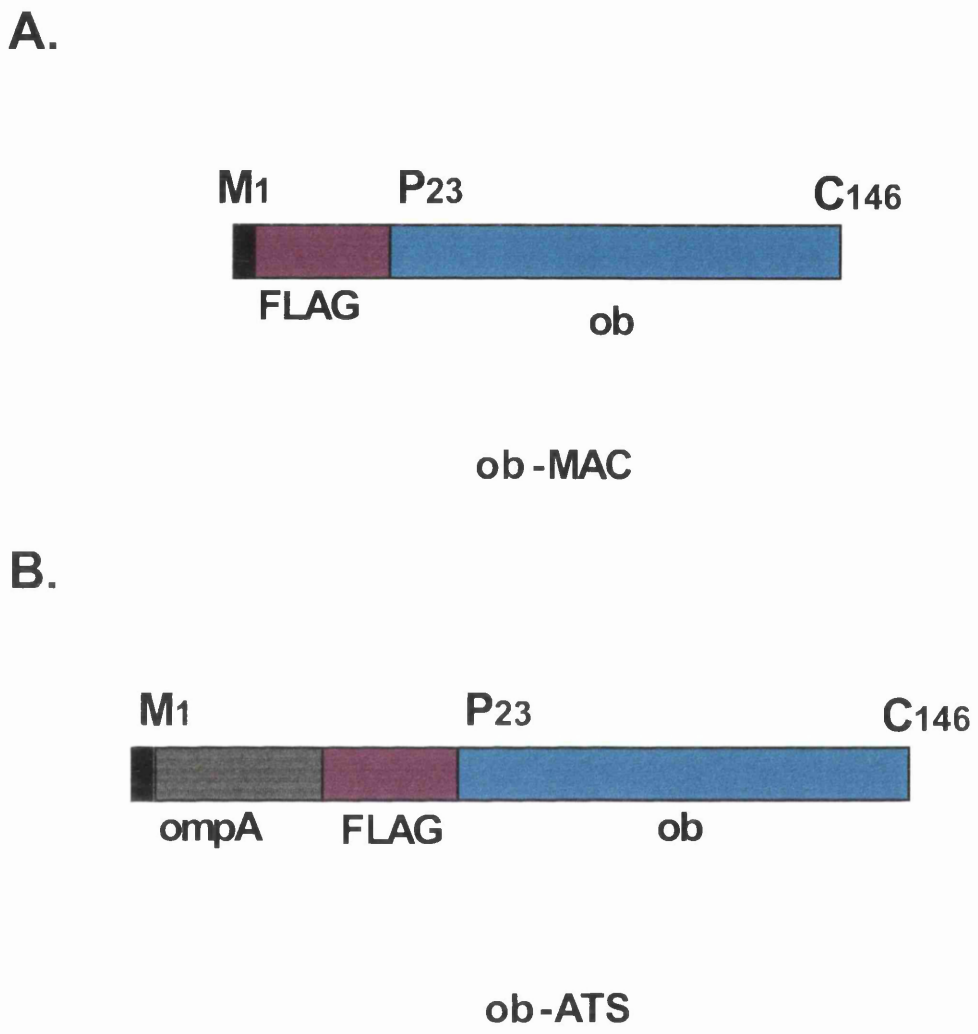


Figure 3.55: Design of FLAG-leptin fusion proteins. A. The ob-MAC plasmid designed for the expression of Met-amino-terminal FLAG fusion leptin within the cytoplasm. B. The ob-ATS plasmid designed for the expression of amino-terminal FLAG fusion leptin within periplasm.

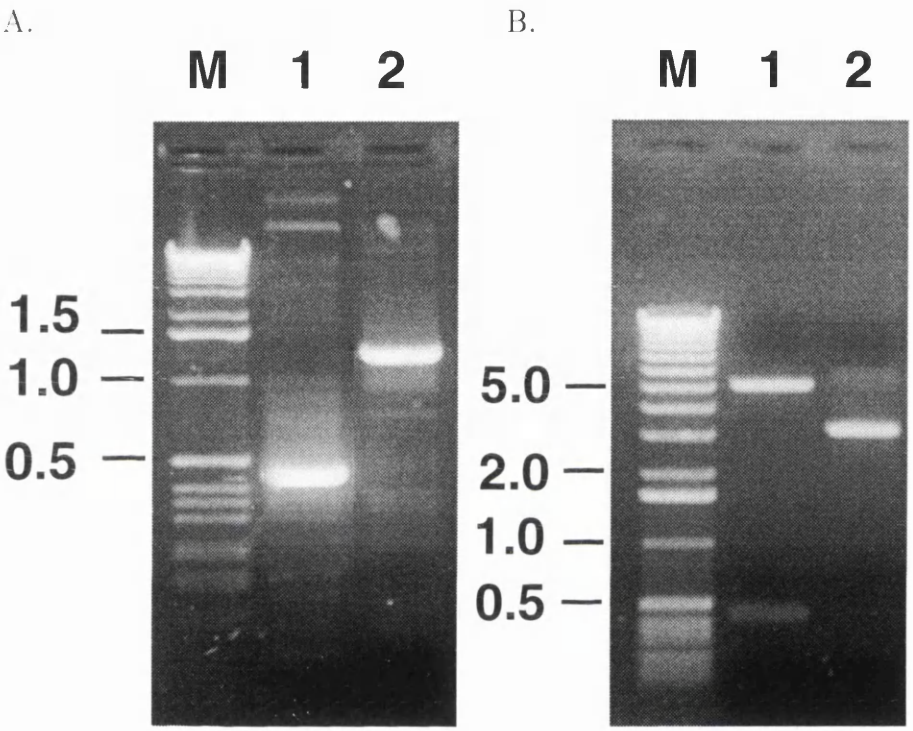


Figure 3.56: PCR of FLAG-leptin. (A.) The cDNA encoding processed leptin protein was amplified by PCR. The forward primer introduced the *Sma* I site in front of $Pro^{23}$ in-frame with respect to the vector ATG translation start codon. The reverse primer contained the *Bgl* II site directly after the stop codon. M, molecular weight ladder; 1, PCR product; 2, positive control. (B.) The PCR product was subcloned into the pFLAG-MAC and pFLAG-ATS vectors. M, molecular weight ladder; 1, The ob-ATS digested with *Sma* I and *Bgl* II ; 2, undigested plasmid.

tein expression levels at 0, 2 and 4 hours post-induction were analysed. The expression of proteins with expected molecular weight (14 kDa) and specificity was confirmed by SDS-PAGE and Western blot, Fig. 3.57 A, B.

The doublet observed for the ob-ATS corresponds to the processed and non-processed protein without or with the OmpA signal peptide which is cleaved after protein transport to the periplasm. The BAP-ATS plasmid expressing the BAP (Bacterial Alkaline Phosphatase) gene as a 49 kDa FLAG fusion protein was used as positive control. The pFLAG-ATS plasmid (ATS) was used as negative control.

### 3.4.3 Analysis of expression of FLAG fusion proteins

Western blot analysis was used to determine whether the expressed FLAG fusion proteins are found in the periplasm, soluble whole cell fraction or insoluble whole cell fraction, Fig. 3.58.

The doublet observed for the ob-ATS in the whole cell sample corresponds to the processed and non-processed protein without or with the OmpA signal peptide which is cleaved after protein transport to the periplasm. The majority of the processed protein is found in the periplasm, while the unprocessed protein is localised in the insoluble fraction. The pFLAG-ATS plasmid (ATS) was used as negative control. The results indicate, that the transcript from the ob-ATS is expressed in the periplasm. The transcription product of the ob-MAC vector was not detected in any of the subcellular fractions although it was present in the whole cell sample.

### 3.4.4 Immuno-affinity purification of FLAG-leptin

To purify the protein encoded by the ob-ATS plasmid localised in the insoluble fraction, it would be necessary to solubilise it with a detergent or chaotropic agent prior to affinity purification with the anti-FLAG M2 affinity gel. However, the protein found in the periplasm fraction could be simply isolated using osmotic shock. The isolated ob-ATS protein was then purified using immuno-affinity purification with the anti-FLAG M2 affinity gel, Fig. 3.58 A, B.

SDS-PAGE analysis, Fig. 3.59 A, indicated, that the purified recombinant FLAG-leptin protein had no detectable contamination. This protein was used in the BiaCore experiments to examine the effect of deletion of the glutamine 28 ($Q^{28}$) on the affinity of binding to the receptor.

A.

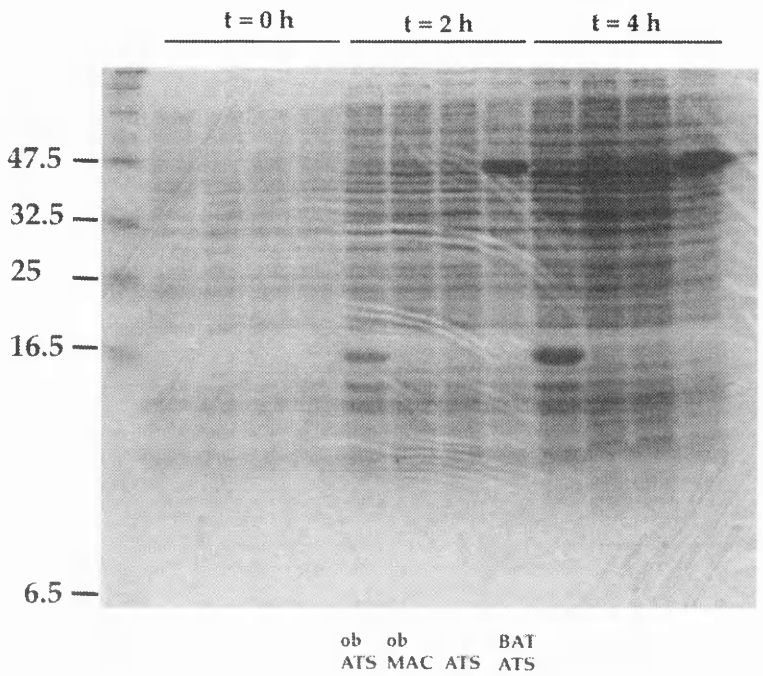


B.

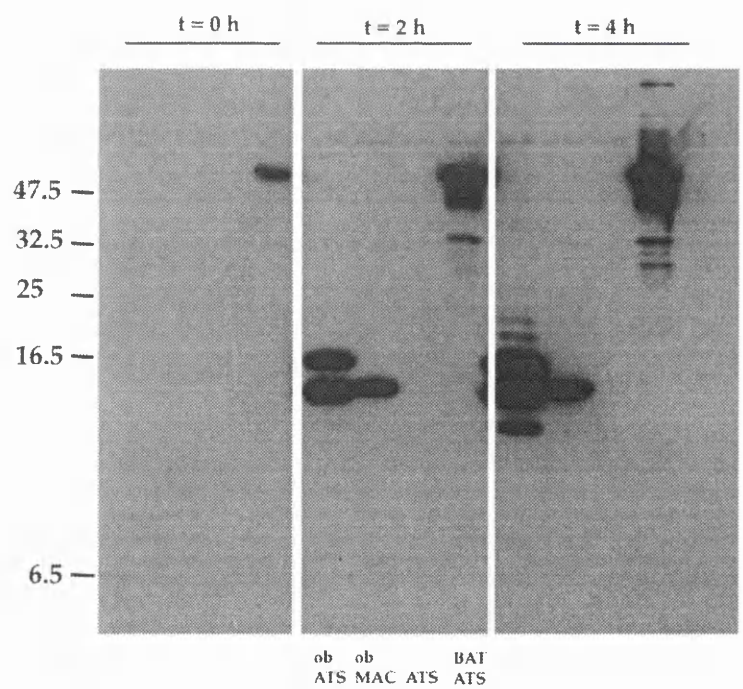


Figure 3.57: Optimisation of protein expression. The expression levels of the ob-ATS, ob-MAC, FLAG-BAP (positive control) and pFLAG-ATS (negative control) at 0, 2 and 4 hours post-induction were analysed by Brilliant Blue staining of SDS-PAGE (A.) and Western blot (B.). The doublet observed for the ob-ATS corresponds to processed and non-processed protein. In the Western blot analysis, anti-FLAG M2 antibody (SIGMA) (10 $\mu$g/ml) was used in a combination with the HRP conjugated anti-mouse antibody (SIGMA) (1:15,000 dilution) in ECL detection.

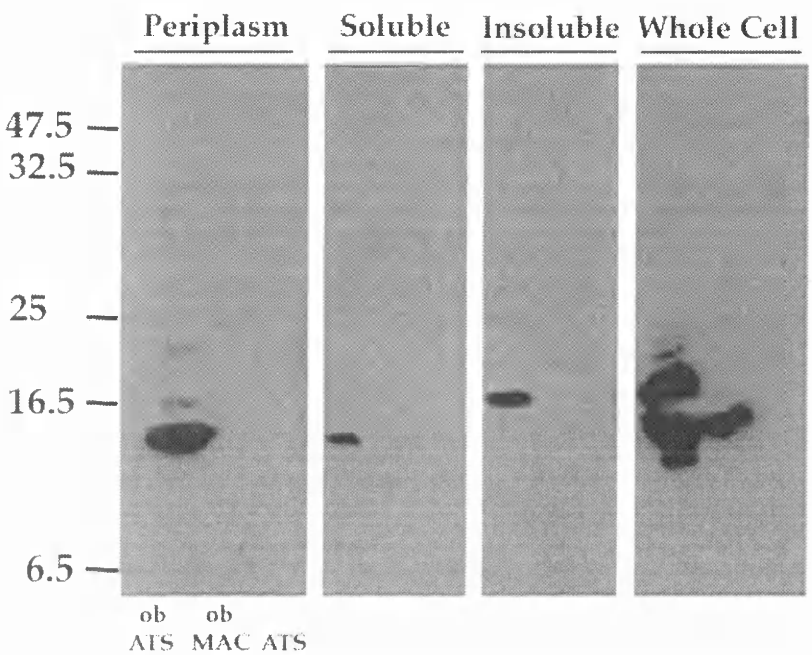


Figure 3.58: Fractionation of FLAG fusion proteins. The fractionation of the FLAG fusion proteins to the periplasm, soluble whole cell fraction or insoluble whole cell fractions was analysed by Western blot. The doublet observed for the ob-ATS in the whole cell sample corresponds to the processed and non-processed protein. The processed protein is identified in the periplasm, while the unprocessed protein is localised in the insoluble fraction. The pFLAG-ATS plasmid (ATS) was used as negative control. In the Western blot analysis, anti-FLAG M2 antibody (SIGMA) (10 $\mu$g/ml) was used in a combination with the HRP conjugated anti-mouse antibody (SIGMA) (1:15,000 dilution) in ECL detection.

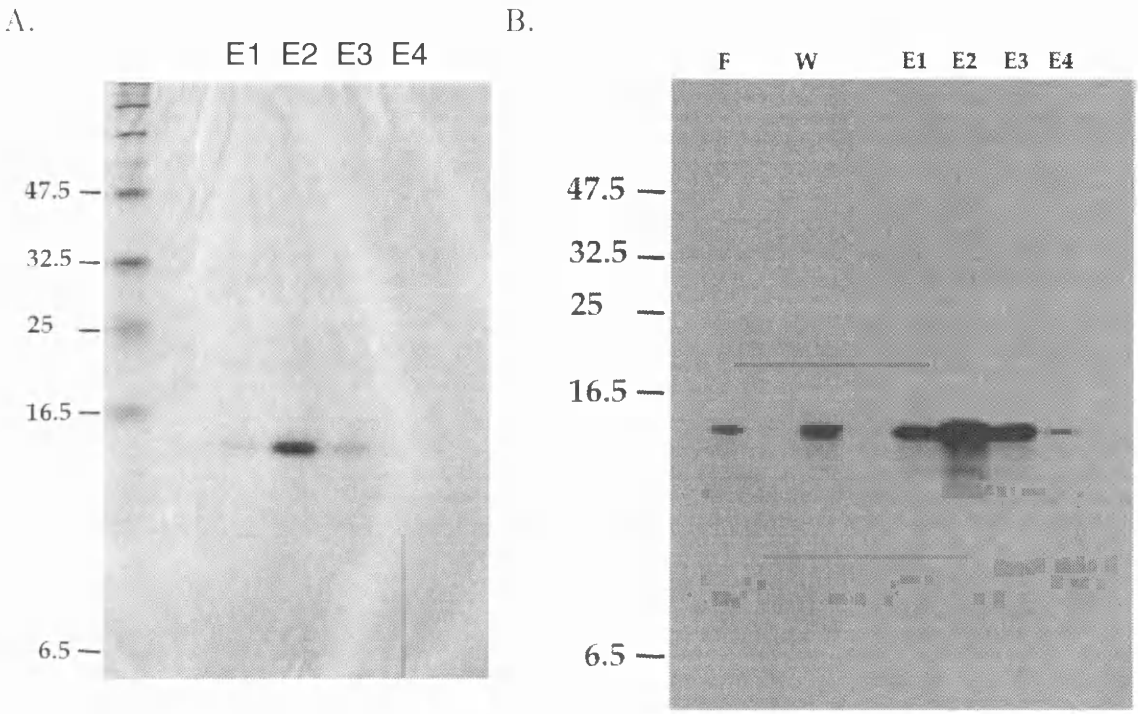


Figure 3.59: Immuno-affinity purification of FLAG-leptin. The isolated transcript of the ob-ATS plasmid was purified using immuno-affinity purification with the anti-FLAG M2 affinity gel. (A.) SDS-PAGE stained with Brilliant Blue. (B.) Western blot analysis. F, Flow through sample; W Wash sample; E1, E2, E3, E4 Elution samples. In the Western blot analysis, anti-FLAG M2 antibody (SIGMA) (10 $\mu$g/ml) was used in a combination with the HRP conjugated anti-mouse antibody (SIGMA) (1:15,000 dilution) in ECL detection.

### 3.4.5 Binding analysis

The effect of the $Q^{28}$ deletion from the leptin sequence on the leptin binding to the receptor was evaluated using BiaCore. The capturing assay, described in section 3.3.3, was used. Data were collected for both human and mouse leptin receptor chimeras (ObR-Fc). The concentration range of leptin was 0.2 - 300 nM. Data were processed as described in section 3.3.6 and fitted to a 1:1 Langmuir binding model, Fig. 3.60-3.61.

The accuracy of the fitting model was assessed by an examination of residual fits, Fig. 3.62-3.63. The difference between experimental and theoretical data for both human and mouse chimeras is smaller then 2 RU, which is the level of instrumental noise. This indicates that the 1:1 Langmuir model approximates kinetic processes on the chip surface very accurately.

Derived kinetic constants are summarised in tables 3.14, 3.15. Calculated average values of association and dissociation rate constants, and the dissociation constant for both human and mouse leptin receptor chimeras (ObR-Fc) are presented in table 3.16.

Comparison of data obtained for $\Delta$Q28 with those for the wild-type leptin, table 3.6, indicate that deletion of $Q^{28}$ resulted in a 10-fold increase in $K_D$ for both human and mouse receptor chimeras, Fig 3.64. The main contribution to this increase in $K_D$ resulted from a change in the dissociation rate constant. The association rate was very similar for leptin wild type and $\Delta$Q28 molecules.

| Experiment No. | $k_a/10^5$ $M^{-1} \cdot s^{-1}$ | $k_d/10^{-4}$ $s^{-1}$ | $\chi^2$ | Cell |
|---|---|---|---|---|
| 1. | 2.58 | 9.18 | 0.113 | Fc2 |
| 2. | 2.51 | 6.87 | 0.140 | Fc3 |
| 3. | 3.15 | 6.90 | 0.098 | Fc2 |
| 4. | 3.17 | 6.85 | 0.094 | Fc3 |
| 5. | 2.52 | 7.82 | 0.120 | Fc2 |
| 6. | 2.99 | 7.13 | 0.094 | Fc3 |

Table 3.14: Values of kinetic constants for hObR/ΔQ28 interaction determined from separate experiments; $k_a$ and $k_d$ are the association and dissociation rate constants, $\chi^2$ describes the closeness of fit and *Cell* corresponds to the chip flow cell used.

| Experiment No. | $k_a/10^5$ $M^{-1} \cdot s^{-1}$ | $k_d/10^{-3}$ $s^{-1}$ | $\chi^2$ | Cell |
|---|---|---|---|---|
| 1. | 2.73 | 1.98 | 0.118 | Fc4 |
| 2. | 3.75 | 1.54 | 0.092 | Fc4 |
| 3. | 5.09 | 2.22 | 0.110 | Fc2 |
| 4. | 5.17 | 2.24 | 0.112 | Fc4 |

Table 3.15: Values of kinetic constants for mObR/ΔQ28 interaction determined from separate experiments; $k_a$ and $k_d$ are the association and dissociation rate constants, $\chi^2$ describes the closeness of fit and *Cell* corresponds to the chip flow cell used.

| ObR | $k_a/10^5$ $M^{-1} \cdot s^{-1}$ | $k_d/10^{-4}$ $s^{-1}$ | $K_D/10^{-9}$ M |
|---|---|---|---|
| h | $2.8 \pm 0.3$ | $7.1 \pm 0.4$ | $2.5 \pm 0.4$ |
| m | $4 \pm 1$ | $20 \pm 3$ | $5 \pm 2$ |

Table 3.16: Kinetic constants for hOb-R/ΔQ28 and mOb-R/ΔQ28 interactions. Data represent the average value ± standard deviation derived from values obtained in separate experiments; $k_a$ and $k_d$ are the association and dissociation rate constants, $K_D$ is the equilibrium dissociation constant.

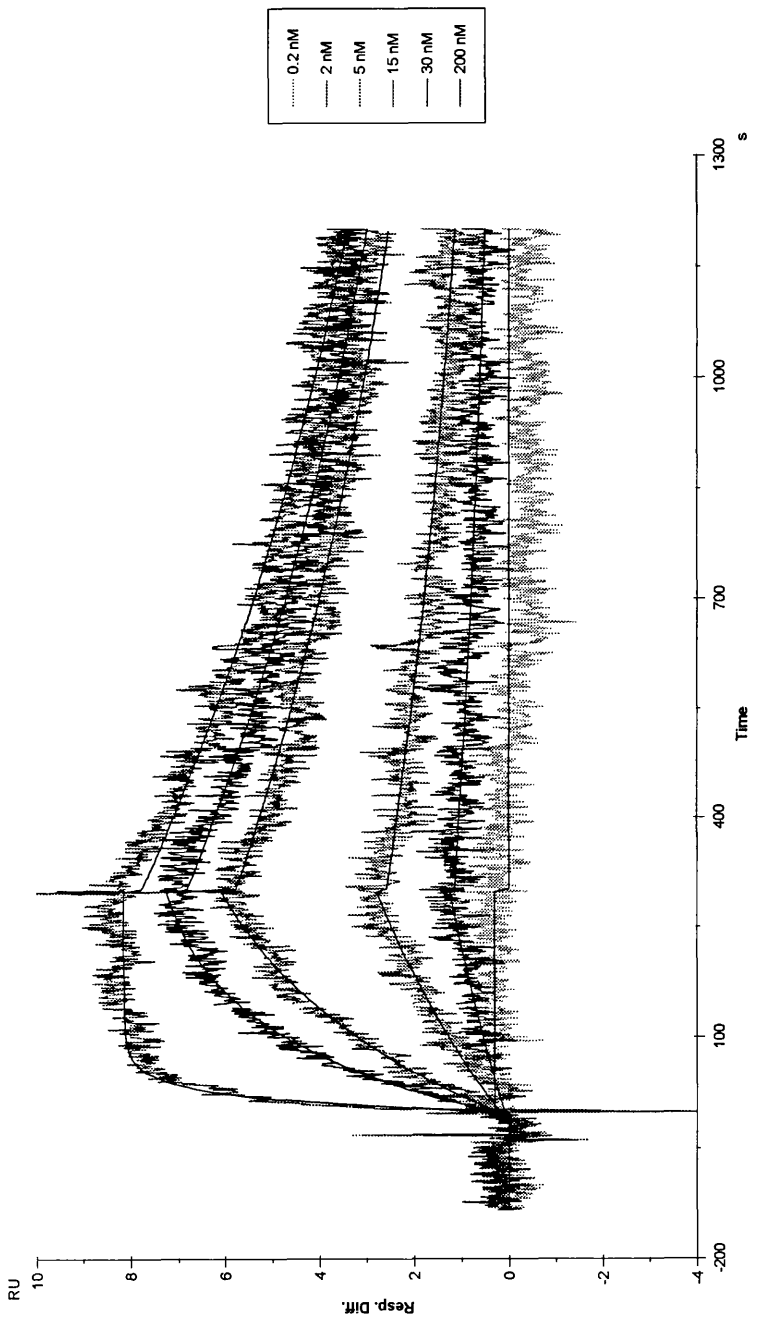


Figure 3.60: Fitting of corrected data for hOb-R/h$\Delta$Q28 interaction to a 1:1 (Langmuir) binding model.

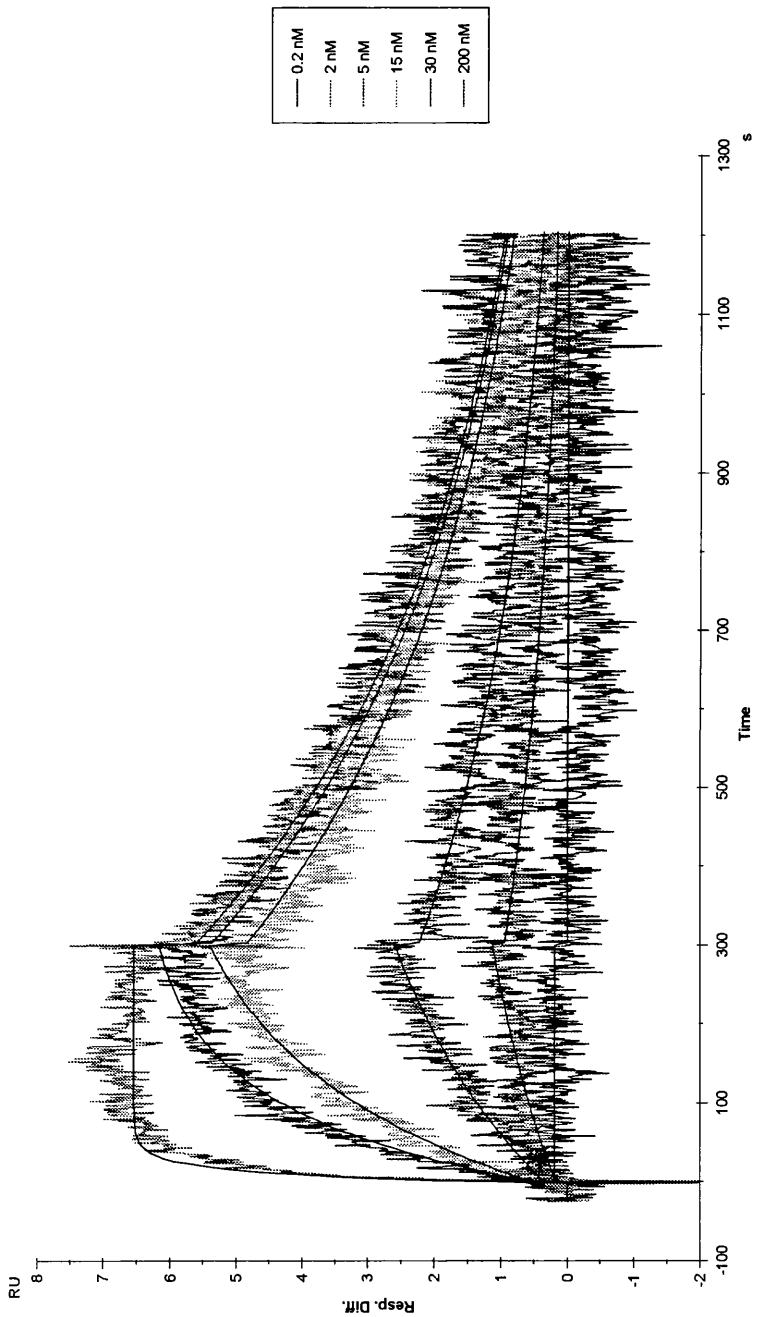


Figure 3.61: Fitting of corrected data for mOb-R/h$\Delta$Q28 interaction to a 1:1 (Langmuir) binding model.

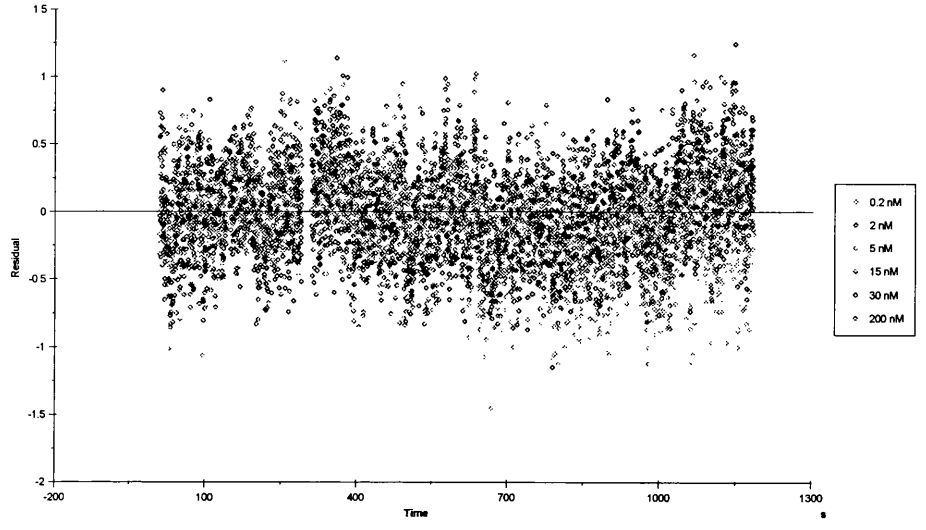


Figure 3.62: Residual plots for hOb-R/hΔQ28 interaction.

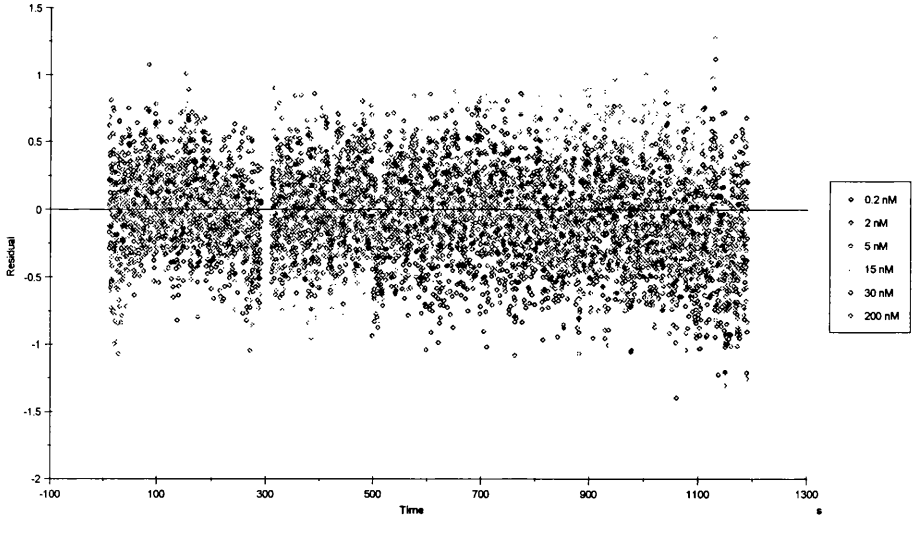


Figure 3.63: Residual plots for mOb-R/hΔQ28 interaction.

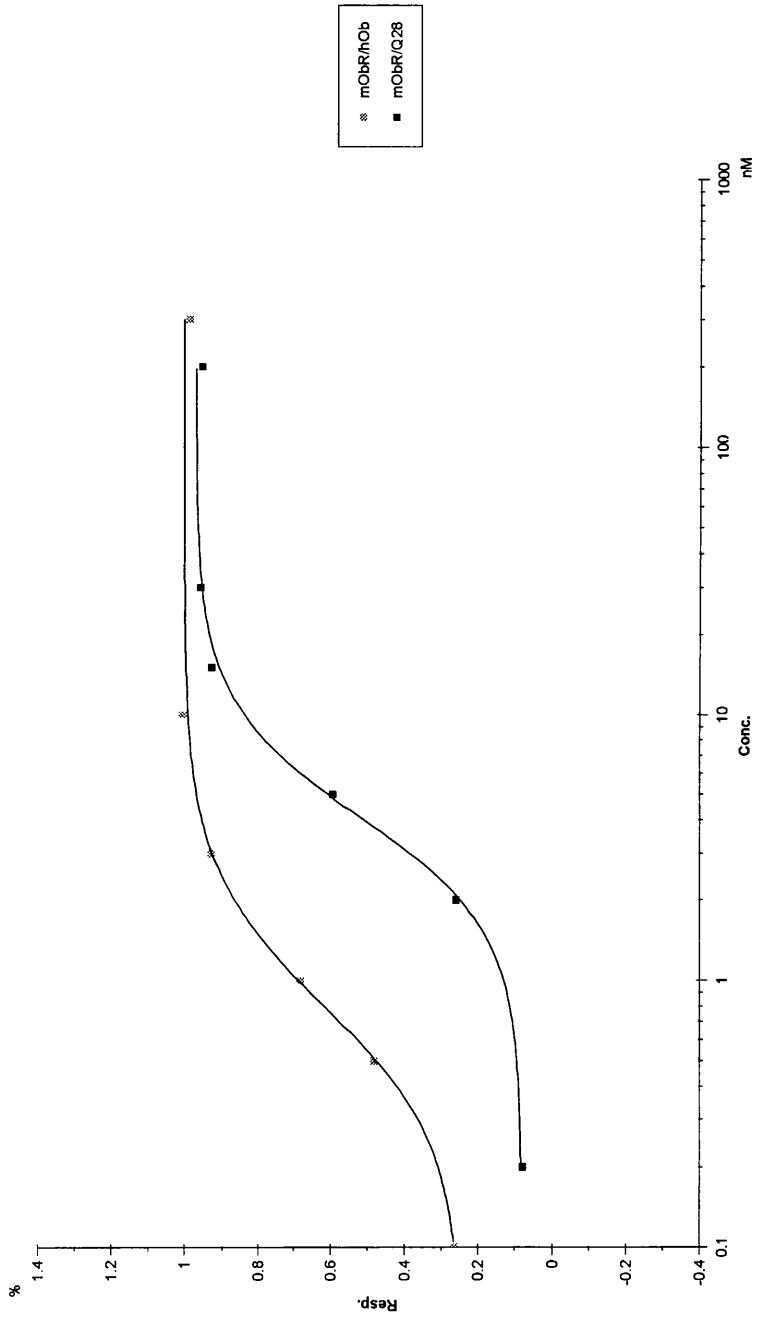


Figure 3.64: Binding of human Ob and $\Delta$Q28 to the mObR-Fc chimera. Data represent a concentration (Conc.) dependence of the normalised ligand bound (Resp.). The deletion of $Q^{28}$ resulted in about 10 fold increase in $K_D$.

# Chapter 4

# Discussion

## 4.1 BiaCore analysis of leptin - leptin receptor interaction

The BiaCore instrument was used to analyse the leptin - leptin receptor interaction, Section 3.3. A chimeric receptor consisting of two receptor extracellular domains fused together via Fc region of $IgG_1$ (ObR-Fc) was used. This is a useful experimental system for studying a recently proposed model of leptin receptor activation [71]. According to this model, leptin receptor exists as a dimer in both ligand-free and ligand-bound states. This model predicts that the receptor is activated by a conformation change introduced by leptin binding.

This model differs from a common model for activation of cytokine receptors. The leptin receptor belongs to the cytokine receptor family according to its primary sequence. The model proposed for cytokine receptors requires that ligand binding activates cytokine receptors by inducing a change in their oligomerisation state. The most common mechanism is dimerization of monomeric receptor by ligand [53, 94]. However, experimental evidence indicates that this is not the case for leptin receptor [71].

Here, the leptin - leptin receptor interaction was evaluated using the receptor chimera immobilised on to the BiaCore chip. In the capturing assay used, Protein G was covalently linked to the chip surface and employed for receptor capture and immobilisation, (Fig. 3.36) The interaction was evaluated using human, mouse and rat leptin in combination with human or mouse chimeric receptors.

Data were collected in parallel experiments from one active (ObR-Fc) and one control (Protein G) cell, (Fig. 3.40), with leptin injections usually ranging

from 0.1 to 30 nM. Nonspecific binding and a contribution of bulk refractive index were corrected for by subtracting data from the control cell from data from active one,(Fig. 3.41.)

The effect of mass transport was completely eliminated by immobilising small amounts of the receptor (100 - 200 RU). The insignificance of mass transport was confirmed by analysing the association phase of the interaction. The flow rate was changed from 15 - 100 $\mu$l/min and leptin binding was monitored,(Fig. 3.39) Because no increase in the initial binding was observed when the flow rate was raised from 15 to 75 $\mu$l/min, mass transport was treated as not limiting and was, therefore, not considered in data analysis.

The only phenomenon which complicated data analysis was a drifting baseline, (Fig. 3.42A), a consequence of the capturing assay used. Use of protein G facilitated the correct orientation of receptor molecules away from the chip surface, thereby minimising the effects of surface heterogeneity. On the other hand, the complex between the ObR-Fc and the Protein G slowly dissociated. The drifting baseline could be treated in two ways. Data corrected for nonspecific binding and bulk refractive index could be either fitted to the 1:1 binding model with exponentially drifting baseline from BIAevaluation software or the drift could be corrected by subtracting a bulk injection (0 nM) from (0.1-30 nM) binding data. We used the second option, as it also corrected for injection artifacts. An example of data corrected for drifting baseline is in Fig. 3.42B. Corrected data were fitted to the 1:1 Langmuir binding model. Fitted data are presented in Fig 3.43 - 3.48.

Association and dissociation rate constants, $k_a$, $k_d$, and the analyte maximum binding capacity, $R_{max}$, were determined as model fitting parameters. The rate constants, $k_a$ and $k_d$, were fitted globally to all six sensorgrams. $R_{max}$ was fitted locally for each sensorgram. Local fitting of $R_{max}$ was used to reflect possible minor differences due to ObR-Fc dissociation from the Protein G complex.

Values for the association and dissociation rate constants, $k_a$ and $k_d$, were determined as average values from repeated experiments, Tables 3.7 - 3.12. Small variations observed may be due to either differences in leptin samples used (pipetting error, protein degradation) or instrumental artefact.

An aspect worth consideration is the possibility of protein degradation. During an experiment the samples were kept in a rack equilibrated for $25°C$. Because experiments were very time-consuming (normally 20 hour required for completion) some degradation could have occurred. This unwanted fea-

ture could be minimised by employing a cooling system which would keep the sample rack at $4°C$. In the meantime, it is important to determine kinetic constants from several independent experiments to minimise experimental bias.

### 4.1.1 Determination of binding site

The importance of accurate data becomes obvious when areas of applications are considered. The genuine advantage of BiaCore is a direct determination of the association and dissociation rate constants, $k_a$ and $k_d$. A knowledge of $k_a$ and $k_d$ can be effectively exploited for analysis of molecular binding sites [95, 96]. These studies have demonstrated different roles for charged and bulk residues in molecular interactions. Charged residues are important in the association phase, when the electric charge appears to provide a driving force for complex formation. By contrast, bulky uncharged residues are crucial for complex stabilisation as they determine the spatial complementarity of interacting molecules. Thus, the association rate constant, $k_a$, is likely to reflect a contribution from an interaction of charged residues while the dissociation rate constant, $k_d$, probably reflects a contribution from nonpolar bulk residues.

Thus, the ability of the BiaCore to measure $k_a$ and $k_d$ can be exploited for effective analysis of suspected binding sites. The BiaCore in combination with site-specific mutagenesis can provide information about target residues involved in binding or not.

This approach could also be used to some extent in analysis of the leptin - leptin receptor interaction. Human, mouse and rat leptin molecules have very high sequence identity (84%), (Fig. 4.1). In mouse and rat amino acid sequences there are only six different residues, four of which are chemically similar. The human sequence stands apart as it bears 19 additional differences (out of 146). Of these, 11 are chemically similar. Thus, the three leptin molecules can be considered as naturally occurring mutant variants and used in BiaCore analysis to determine a binding site.

According to the leptin crystal structure, Fig. 1.2, [10], leptin has two possible receptor binding sites. The first is in the first part of the AB loop, Fig 4.1, containing the residues flanked by Thr27 and Gly38. This region is not visible in the crystal structure because of its high flexibility. This flexibility has also been observed in a similar region of growth hormone (hGH) [14], another member of the cytokine family. This region in growth hormone shows extensive conformational changes upon receptor binding, changing from a coil structure in the free-ligand structure to a helix in the receptor complex. Thus,

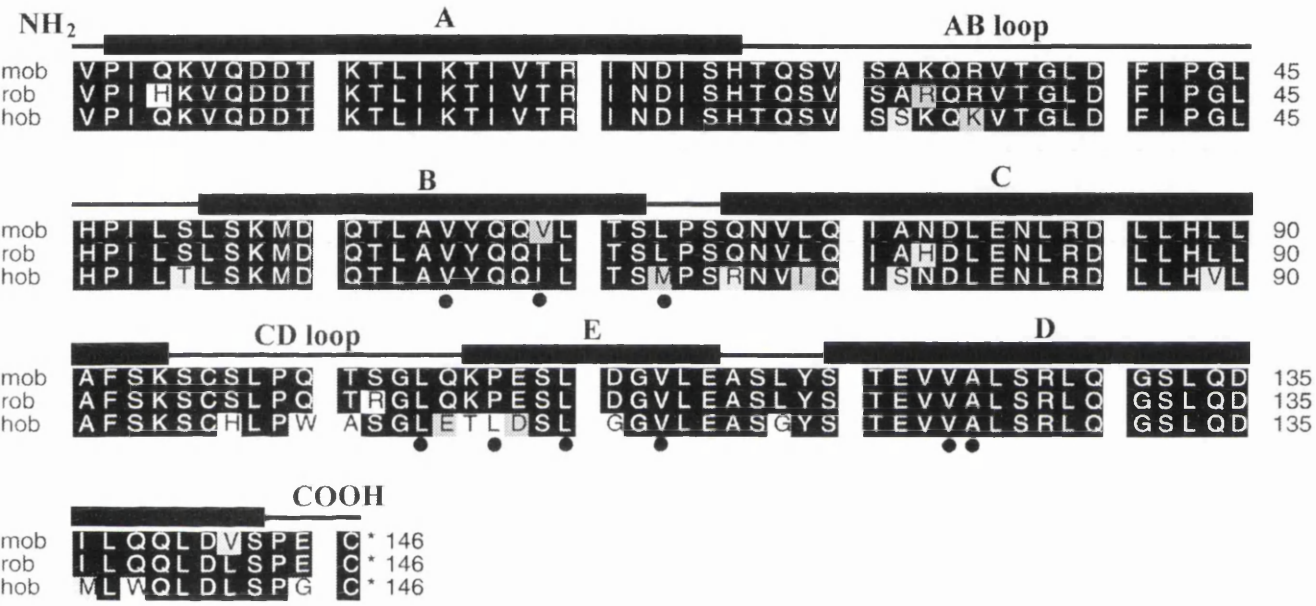


Figure 4.1: Sequence alignment of human, mouse and rat OB proteins. Helices A-E, determined by the crystal structure of leptin-E100 [10], are depicted. Residues forming the hydrophobic domain are marked with a circle. Made with the Pileup programme from GCG package.

this leptin region may also represent a coil which would assume an ordered conformation after binding the receptor.

The second possible receptor binding site is a large hydrophobic cylindrical core parallel to the helical bundle axis, Fig 1.3. It is formed by the most conserved residues of the four helices that face each other. These are residues Val 60, Ile 64 in the BD bundle, Met 68 in the C-terminal end of helix B and Val 124 and Ala 125 in the N terminus of helix D. This lipophilic surface is buried by Leu 104, Leu 107, Leu 110, Leu 114 and Val 113 of helix E in the CD loop. The E helix serves as a hydrophobic cap.

In the first possible binding site, the AB loop, there are only three conserved mutations between the rodent leptins and human leptin. The second possible binding site, the hydrophobic core, is much richer in mutations. However, these two regions are not exclusive domains of diversity between the three molecules. To associate differences in $k_a$ and $k_d$ between species, Table 3.6, with the location of binding site, it would be necessary to introduce more specific mutations in leptin.

The strategy of introducing targeted mutations was initiated by analysis of binding properties of a mutated human leptin molecule with deleted glutamine 28 ($Q^{28}$). Glutamine 28 is localised in the first part of the AB loop, residues 27 to 38, and may be important for binding. Its affinity for both human and mouse leptin receptor chimeras was analysed by BiaCore. Results showed that this mutant has a 10-fold lower affinity for both receptors, indicating that $Q^{28}$ may be important for binding. A change in affinity due to a different folding of the mutant can be ruled out because the highly flexible AB loop is unlikely to contribute to the formation of the tertiary structure.

### 4.1.2 Kinetics and stoichiometry of interaction

The kinetic data obtained indicate that human, mouse and rat Ob bind both human and mouse chimeric receptors (ObR-Fc) with high affinity ($K_D \approx 0.2$ nM). The association rate is similar for the different species of leptin to either receptor and the differences in affinity results mainly from a variance in the dissociation rates. The affinity of human leptin for its cognate receptor ($K_D = 0.22 \pm 0.1$ nM) reflects a very strong ligand binding to dimerised receptor. This value is consistently 50-fold smaller than that reported previously where the $K_D$ was found to be 9.5 nM [97], using monomeric receptor. Together, these results suggest that receptor dimerization stabilises the complex.

Because the BiaCore instrument measures the mass of molecules bound to

the sensor surface, data can be analysed to determine the stoichiometry of surface molecular complexes. For the leptin:leptin receptor interaction, our data, summarised in Table 3.13, indicate a 1:1 interaction, i.e. one monomeric ObR-Fc molecule interacts with one Ob molecule (one dimerised ObR-Fc molecule interacts with two Ob molecules). The apparent 1:2 stoichiometry (around 0.5) observed when high amounts of hObR-Fc are immobilised is likely to be due to steric restriction on the sensor surface which hinders Ob molecules from binding to all presented binding sites. The same reason leads us to interpret reactions with measured 0.8 - 1.1 stoichiometry as 1:1 interaction.

The 1:1 stoichiometry of interaction is interesting in many respects. First of all, it is in agreement with data obtained from native polyacrylamide gel electrophoresis [71]. Secondly, it suggests that leptin triggers receptor activation through a change in conformation rather than through oligomerisation of the receptor. Thirdly, because dimeric receptor acts as two independent monomers in its interaction with ligand, there should be no difference in $K_D$ between dimeric and monomeric receptor. However, $K_D$ obtained for our dimeric human receptor ($K_D = 0.2 \pm 0.1$ nM), is only about one-fiftieth of that reported for the monomeric receptor ($K_D = 9.5$ nM) [97]. This difference is not negligible. It may be due to intrinsic difference of the interaction system or may be the consequence of the oligomerisation state of the receptor. It is possible that receptor dimerisation induces a particular structural modification of the receptor, modifying its ligand recognition sites and hence improving its affinity for the ligand. Both sites would be entirely functional and independent. The improved affinity would therefore not be a consequence of ligand bivalent binding, as usually observed.

There are several other factors, which could contribute to the differences observed. Experimental systems used here and previously [97] are not entirely similar. In both cases, a Pharmacia Biosensor BIAcore™ instrument was used, but recombinant leptin receptor molecules (monomeric and dimeric) were immobilised on a sensor chip in different ways. The monomeric receptor was immobilised directly on to an NTA (nitrilo-tri-acetic acid) sensor chip via the 6×His epitope localised in its C-terminus. The dimeric receptor was anchored on to a CM5 sensor chip via Protein G. Ligand binding experiments were performed under identical experimental conditions in HEPES-buffered saline at room temperature.

It must also be considered, that human leptin receptor contains extensive glycosylation, approximately 36 % [98]. Recombinant monomeric and dimeric

receptors discussed above were expressed in Baculovirus (BV) and a mouse myeloma cell line, NSO, respectively. Level of post-translation modifications in the BV is usually lower than in mammalian cell lines. This implies that the level of glycosylation in these two proteins may be different and this could affect their function.

Another source of differences could be the dimeric receptor itself. It consists of two extracellular domains linked together via the Fc portion of $IgG_1$. This covalent link could restrict the mutual orientation of monomers, that could, in turn, affect dimer affinity for ligand. However, the hinge region in the Fc portion allows slight relative motion between the monomers, that could compensate for the restriction raised by the linkage. It is also not clear whether the covalent linkage of the receptor extracellular domains leads to a specific interaction between the two monomeric molecules, forming a dimer, or holds two monomers together but without any specific contact.

Our observation that the dimeric receptor interacts with two molecules of leptin supports the idea that the receptor, expressed on the cell surface as a dimer, interacts with its ligand in 1:1 stoichiometry, as recently proposed [71]. This opens a question on the geometry of this receptor-ligand complex, (Fig. 4.2) As was mentioned above, each leptin molecule has two possible receptor binding sites: the AB loop and the hydrophobic cylindrical core, (Fig 1.3) Each of the leptin receptor extracellular domains possesses two cytokine-binding homology regions (CHR) as predicted from the primary sequence, and each represents a possible binding site [47]. The receptor dimer could therefore be predicted to possess four ligand binding sites and the two leptin molecules could satisfy all four receptor binding sites which could in part explain the very high affinity observed for this interaction. However, only the second cytokine-binding homology region has been reported to bind the ligand [99].

An analysis of the BiaCore data provides additional evidence for this model. Two BiaCore models are available: the 1:1 simple model and the 1:1 model with a parallel binding to two different sites. The first model was found much more appropriate for analysis of the curves. This suggests that there is only one distinctive binding site on the ObR-Fc chimera.

However, the 1:1 stoichiometry does not restrict the leptin oligomerisation state. It is possible that leptin could act either as a dimer or as two independent monomers binding to the dimerised receptor. Thus, two reaction mechanisms must be considered. In the first, leptin would have to dimerise

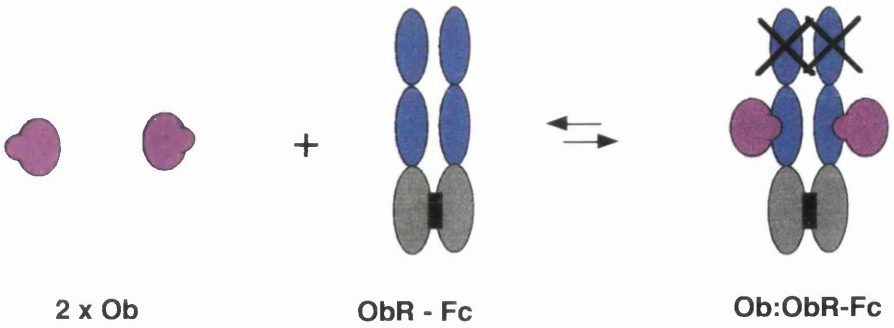


Figure 4.2: Model of leptin-leptin receptor complex. The leptin molecule has two possible receptor binding sites. Each of the leptin receptor extracellular domains possesses two predicted binding sites. However, only the second cytokine-binding homology region has been reported to bind the ligand [99].

before binding to the chimeric receptor, equations 4.1, 4.2. In the second, a monomeric leptin molecule would bind to the chimeric receptor first, followed by a binding of the second leptin molecule to the Ob:ObR-Fc complex, equations 4.3, 4.4. These two processes are intrinsically different and characterised by different rate constants ($k^1$ and $k^2$). The BiaCore analytical system is not fast enough to clearly distinguish between them. However, the 1:1 Langmuir model used suggests that the dimerisation of leptin does not occur before interaction with chimeric receptor.

$$Ob + Ob \underset{k^1_{d1}}{\overset{k^1_{a1}}{\rightleftharpoons}} Ob_2 \tag{4.1}$$

$$Ob_2 + ObR - Fc \underset{k^1_{d2}}{\overset{k^1_{a2}}{\rightleftharpoons}} Ob : ObR - Fc : Ob \tag{4.2}$$

$$or$$

$$Ob + ObR - Fc \underset{k^2_{d1}}{\overset{k^2_{a1}}{\rightleftharpoons}} Ob : ObR - Fc \tag{4.3}$$

$$Ob + Ob : ObR - Fc \underset{k^2_{d2}}{\overset{k^2_{a2}}{\rightleftharpoons}} Ob : ObR - Fc : Ob \tag{4.4}$$

Furthermore, a new role for leptin, which could interfere with its receptor binding, has recently been proposed. Leptin has been suggested to act as a transporter of free fatty acids (FFA) [100]. We used BiaCore to investigate this possibility. The small size of FFA, about 300 daltons, means that the

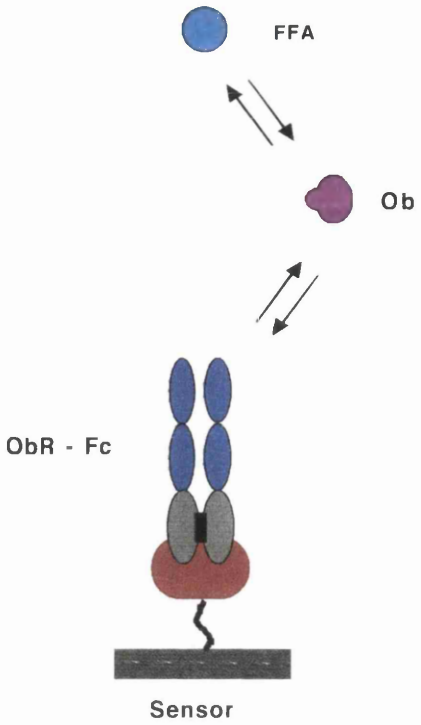


Figure 4.3: Leptin interaction with free fatty acids. A competitive approach, when the free fatty acid (FFA) competes with the immobilised leptin receptor (ObR-Fc) for binding to leptin (Ob), was used to investigate a possible role of leptin as a FFA transporter.

interaction between leptin and FFA can not be measured directly, because the instrument BiaCore™ 2000 used can not detect molecules smaller than 10,000 daltons. Therefore, it was decided to use an alternative competitive approach, in which the FFA competes with the immobilised leptin receptor for binding to leptin, Fig 4.3.

Arachidonic and oleic acids were used in this experiment. Arachidonic acid was found previously to bind leptin [100], while oleic acid did not and was used as negative control. The results demonstrated that arachidonic acid does not compete with leptin receptor for binding to leptin as arachidonic acid at concentrations as high as 30 $\mu$M did not have any effect on 30 nM leptin binding to leptin receptor (data not shown).

This observation rules out the possibility that FFA binds to the receptor binding site on the leptin molecule. However, it is possible that leptin bears an independent binding site for FFA. An ideal candidate would be the leptin hydrophobic cylindrical core, Fig. 1.3, as FFA has been found previously to bind to the hydrophobic cavity of several proteins like adipocyte lipid-binding protein (ALBP) and intestinal fatty acid-binding protein (I-FABP) [101, 102].

### 4.1.3 Molecular complexity

A situation depicted above, when leptin may interact simultaneously with several molecules (leptin receptor, free fatty acids, sugar molecules) indicates a potentially complex nature of leptin action in its authentic physiological environment. It must be admitted that the inherent enigmatic nature of biological systems makes them very difficult to study, because simultaneous experimental evaluation of their inner regularities is impossible due to high multiplicity of such systems. Thus, it is important to search for new ways to measure and analyse the emerging complexity of biological systems. This task will be very valuable in our post-genomic era. Employment of BiaCore in this field is likely to prove extremely beneficial as BiaCore data is exactly the sort of information needed. An accumulation of accurate kinetic data can provide an information pool which could be highly valuable for overcoming experimental difficulties associated with complex systems. Simultaneous interactions can be successfully modelled using powerful computer systems. Software designed for analysis of complex biological interactions is a rapidly expanding business. However, "Silicon Biology" is in acute need of input data: values of kinetic constants, cellular localisation of interacting components etc., which can only be provided by experimentalists. The BiaCore together with other analytical techniques, such as microcalorimetry and analytical centrifugation, will probably be the most valid supply of experimental data for metamorphosis of integral cellular mechanisms into the virtual reality of superpowerful computers.

## 4.2 Leptin action

### 4.2.1 Active body

As described in Chapter 1, extensive investigations of the molecular control of the appetite revealed that leptin, one of the key molecules, is involved in a very complex framework of molecular interactions. Leptin is engaged in the control of food intake, stimulates energy expenditure, acts as a signal to the reproductive system, influences insulin secretion, lipolysis and sugar transport, possesses immuno-modulatory and anti-inflammatory effects and also inhibits bone formation, to mention its functions so far experimentally demonstrated.

In a classical description of human physiology, these functions are attributed to different systems, which exert a high degree of autonomy. These are the immune, reproductive and digestive systems. Leptin ability to regulate and coordinate the activity of such diverse systems implies that leptin belongs

to an arsenal of the endocrine or nervous systems, which coordinate the action of different organs. However, this leptin aspiration is difficult to accommodate within the current physiological concept.

Leptin is not a classical hormone, because it is not secreted by any of well defined endocrine glands, such as the thyroid or pituitary gland. Instead, leptin is produced in adipose tissue, which serves us as our energy storage compartment and no ability to coordinate the action of distinct organs is attributed to it.

A localisation of the leptin source, recently extended to the placenta and stomach, also disqualified leptin from being engaged by the central nervous system (CNS). The CNS in its postulated superiority, is not concerned with protein molecules produced outside its own domain. However, leptin cancels out the autonomy of CNS, as it is able to get across the blood-brain barrier and to activate specific centres in the hypothalamus.

Leptin emerges from these considerations as a very mysterious cytokine molecule, which possesses the regulatory roles previously attributed only to the molecules of the endocrine and nervous systems. However, leptin is neither hormone nor neurotransmitter. This implies that the privileged control position in the hierarchy of the physiological systems is not occupied exclusively by the endocrine and nervous systems. Furthermore, it indicates that our bodies are not passive participants in the control of physiological processes, but that they exercise very active interaction with both endocrine and nervous systems. Therefore, it may be said that rather than the brain controls the body, the body uses the brain to arrange tasks it finds appropriate.

Leptin seems to use several means of body regulation simultaneously. It acts through the endocrine and nervous modes of action, as well as through auto- or paracrine pathways, Section 1.4. Leptin action through the nervous system has a very interesting inner structure, characterised by a high degree of redundancy, Fig. 4.4. Leptin acts directly on the hypothalamus, Sections 1.4.2 and 1.5, through which it regulates several physiological functions including the sympathetic nerve activity and, therefore, the activity of peripheral organs. At the same time, the leptin receptor expression in the autonomic ganglia, localised outside the CNS, Section 1.4.3, implies a possibility that the hypothalamus is by-passed in the control of an innervation of peripheral organs. In some cases, the nervous system is left aside completely, as leptin has been shown to act through auto-pathways, as demonstrated for the adipose tissue, Section 1.4.3. This again indicates a very vital regulation role of

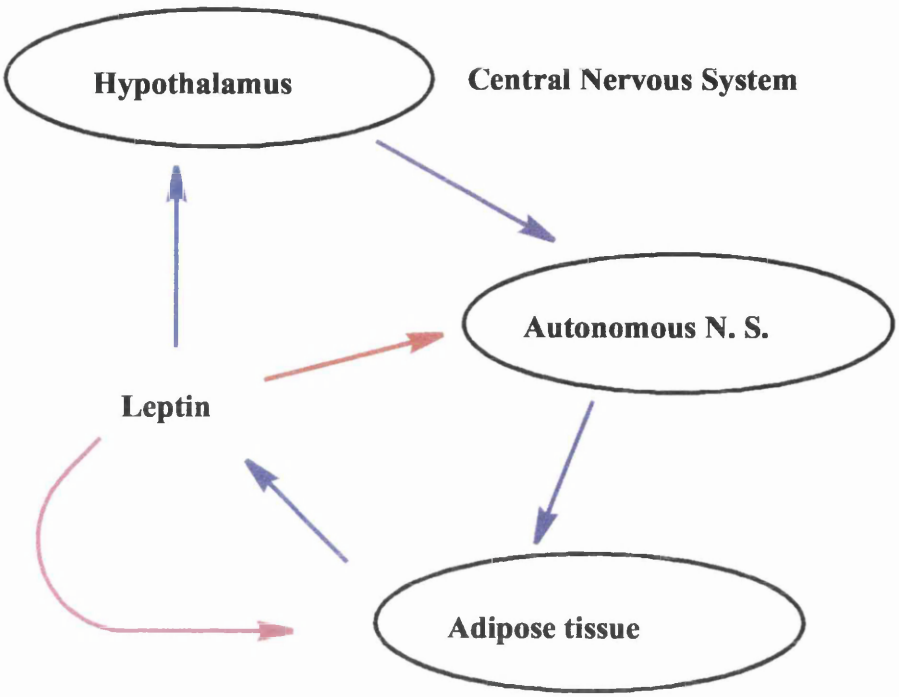


Figure 4.4: Leptin action through the nervous system. Leptin acts directly on the hypothalamus, through which it regulates several physiological functions including the sympathetic nerve activity and, therefore, the activity of peripheral organs. At the same time, the leptin receptor expression in the autonomic ganglia, localised outside the CNS, implies a possibility that the hypothalamus is by-passed in the control of an innervation of peripheral organs. In some cases, the nervous system is left aside completely, as leptin has been shown to act through auto-pathway, as demonstrated for the adipose tissue.

leptin, supporting an idea that our bodies actively participate in the control of physiological processes.

### 4.2.2 Rodent models of leptin action

There is one limitation concerning our knowledge of the action of leptin. Most of the investigations have been done in rodents. This fact raises the question of the adequacy of rodent models for studying human physiology. With respect to leptin, several factors must be considered.

First is the role of leptin as a molecular signal terminating food consumption, if any such signal exists. Leptin circulation is regulated in a fundamentally different way in humans and rodents, Section 1.3. Levels of human leptin increase only after chronic increase in caloric intake. On the contrary, in rodents leptin levels change acutely following every meal. This may indicate

that leptin in humans does not act as a satiety signal as it does in rodents.

Another controversial area is the effect of leptin on energy metabolism, Section 1.4.3. Leptin does not have any direct effect on human adrenal catecholamine production, which diminishes its potential direct effect in energy metabolism through *epinephrine* regulation. This is in contrast to rodents where the adrenal medulla expresses abundant leptin receptor, and a direct effect of leptin on energy metabolism is likely to occur.

There is also the question of a cold-induced thermogenesis which protects us from stress following exposure to environmental temperatures. Humans, as opposed to rodents, have a broad thermo-neutral zone with relatively small changes in metabolic rate occurring over relatively wide temperature changes.

Finally, there is a morphological difference between human and rodents, which underlies the above discussed variations. In rodents, a major site of adaptive thermogenesis, brown adipose tissue, exists. The role of brown adipose tissue in man is controversial. We do not have large, distinct depots of brown adipose tissue and therefore, humans may not by able to convert superfluous energy to heat by the adaptive thermogenesis.

### 4.2.3 Leptin and obesity

An interesting consequence of using a rodent model for studying leptin action is the confusion over genetic predisposition for obesity. There is a striking difference between humans and rodents, because several genetic disorders have been identified for rodents, but none for humans.

At present, three rodent "obese" strains are known. These are the *ob/ob* and *db/db* mouse and *fa/fa* rat. The *ob/ob* mouse lacks leptin itself [1]. The *db/db* mouse has a single mutation in the leptin receptor, Section 1.5.1, resulting in a change of a functional receptor Ob-Rb to its nonfunctional splicing variant Ob-Ra. In the *fa/fa* rat [103], another single point mutation ($Gly^{269} \rightarrow$ Pro) inactivate the receptor.

In humans, no such mutation has been so far identified. An exception is a family of Kabilian origin with a homozygous mutation in the leptin receptor gene which result in their profound obesity [104]. However, it is quite difficult to establish a link between this Turkish family and millions of obese people in the developed world. Thus, it is most likely that the human obesity is not associated with any particular genetic disorder. More likely, it results simply from a sedentary lifestyle and a high-fat diet.

### 4.2.4 Body-brain concept

Experimental data available on the physiological role of leptin, Sections 1.2-1.4, indicate that the molecular basis of the hypothalamus mode of leptin action is at present much better understood than leptin signalling in peripheral organs. This reflects the fact that the hypothalamus is in general considered to be a supreme coordinator of all physiological processes and, therefore, the primary target in studying their control.

However, the analysis of the intrinsic structure of leptin engagement in energy balance suggests, Section 4.2.1, that the role of the hypothalamus in the control of our energy-storage compartment (adipose tissue) is not that dominant. Apart from the hypothalamus, leptin uses several other modes of action, including even the auto-regulatory pathway. Thus, we should asked ourselves, where is the dominant role of the hypothalamus in the control of the adipose tissue derived from. It is tempting to speculate that this idea is not deduced from experimental data but from a current "philosophical" concept of human beings.

According to this concept, the brain and spinal cord form an independent logical unit (Central Nervous System, CNS) which controls the body. The body itself does not possess any ability to participate in this control. Within this tradition human beings are reduced to robots, whose bodily activities are explained in mechanical terms and fully controlled by a computer, positioned in the robot's "skull".

This concept has its origin in Descartes's meditations at the beginning of the 17th century. Descartes describes human beings and, in fact, the whole Universe as the three-dimensional world of physics, *res extensa*, which is explicable entirely in terms of interacting elementary particles, attributed only with quantitative properties such as size, shape, velocity etc. This physical world is perceived by *res cogitas*, thinking substance, which is independent of any material substance and which is capable of analysing all the physical phenomena in mathematical language.

Formulating his theory, Descartes led the shift from the traditional 'scholastic' explanation of things described by their qualities noted by our five senses such as colours, tastes, smells, textures and sounds towards a quantitative analysis of the interactions between microscopic particles, of which our ordinary world is composed. This shift in thinking catalysed profound changes in the way we understand the Universe and formed the ground base for modern science.

On the other hand, the concept of human being, which he has left for us, is rather awkward. Human beings are for Descartes dualistic entities composed of mind, *res cogitas*, and body, *res extensa*, bearing the attributes defined previously. Thus, our body is a three-dimensional sum of inanimate particles, mechanical interaction of which is reflected by the mind. This concept is obviously an archetype of our current description of our nature. The only feature changed is the corporealisation of our mind, which has been associated with the brain.

Descartes himself never managed to explain how mind, the thinking substance with no contact with physical world, would control our physical body. This puzzle has not been solved by any of his followers either. Furthermore, Descartes has eventually been shown to have made a logical mistake in deriving the core of his theory, probably still best known in the quotation: I am thinking, therefore I exist (*Cogito ergo sum*).

These antagonisms urge us to think about a better scientific description of human beings based more strictly on experimental observations rather than on disproved concepts from the 17th century. Stimulation for this intellectual activity can be derived from the discoveries achieved in expanding interdisciplinary research addressing complex biological phenomena. The notion of a high degree of cooperation emerging from these studies indicates that physiological processes in every living creature, including human individuals, can be fully described only within the global context these creatures themselves represent. Understanding the brain is simply not enough for knowing ourselves. This new body of information can be used to redraw a scientific description of human beings and cast away a schizophrenic concept of a mechanistic individual suffering from its intrinsic division between body and brain. Instead, human beings can be described as integral individuals, manifesting a deep inner organisation, with democratic rather then hierarchic structure.

The satisfaction for a strenuous effort to reveal the molecular interactions, leptin is engaged in, does not need to be sought only in lurid economical profit. This experimentation itself is an inexhaustible wellspring of profound rumination on our own nature without which we would probably be those mechanistic robots from the dawning of the Enlightenment.

# Appendices

# Appendix A

# Solutions

## A.1 General solutions

**KCl** 4M in distilled water; sterilised by autoclave

**NaCl** 5M in distilled water; sterilised by autoclave

**TE buffer** 10mM Tris, 1mM EDTA, pH 7.4

**LB Medium** Bacto-Tryptone: Yeast extract: NaCl 2:1:1

**IPTG** 0.1M stock in distilled water; filter sterilised; stored at -20°C

**X-Gal** 2% stock in N',N'-dimethyl formamide; stored at -20°C

**Ampicillin** 100 mg/ml stock in distilled water; filter-sterilised; stored at -20°C

**10x PBS**

- 3 M NaCl
- 2.7 mM KCl
- 8.3 mM $Na_2HPO_4$
- 1.5 mM $KH_2PO_4$, pH 7.0

**Tfb1**

- 30 mM KOAc
- 250 mM $MnCl_2$

- 100mM KCl
- 10mM $CaCl_2$
- 0.2mM EDTA
- 15% Glycerol

**Tfb2**

- 10 mM Na-MOPS, pH 7.0
- 275 mM $CaCl_2$
- 10mM KCl
- 15% Glycerol

## A.2 Solutions for DNA work

**Buffer P1 (QIAGEN)**

- 50 mM Tris-HCl, pH 8.0
- 10 mM EDTA
- 100 mg/ml RNase A

**Buffer P2 (QIAGEN)** 0.2 M NaOH, 1% SDS

**Buffer P3 (QIAGEN)** 3.0 M potassium acetate, pH 5.5

**Buffer QBT (QIAGEN)**

- 750 mM NaCl
- 50 mM MOPS, pH 7.0
- 15% isopropanol
- 0.15% Triton® X-100

**Buffer QC (QIAGEN)**

- 1.0 mM NaCl

- 50 mM MOPS, pH 7.0
- 15% isopropanol

**Buffer QF (QIAGEN)**

- 1.25 mM NaCl
- 50 mM Tris-Cl, pH 8.5
- 15% isopropanol

**10x T4 DNA Ligase Buffer** 100 mM Tris-HCl, pH 7.5, 100 mM $MgCl_2$

**50 x TAE, 1 l** 242 g Tris base, 57.1 ml glacial acid, 100 ml 0.5 M EDTA

**Ethidium Bromide Stock** 10 mg/ml in TE; stored away from light

**10 x RNA Electrophoresis Buffer** 0.2 M MOPS, 10 mM EDTA pH 7.0

## A.3 Solutions for Deae-Dextran transfection

**DEAE-DEXTRAN** 10 mg/ml in 1×PBS

**Chloroquine** 100 mM in 1×PBS

**DMEN** 10% NU serum + additions according to the cell line used

**DMSO** 10% DMSO in 1×PBS

## A.4 Solutions for *E. coli* expression work

**Buffer for osmotic shock**

- 500 mM Sucrose
- 30 mM Tris-HCl
- 1 mM EDTA

**Extraction Buffer A**

- 50 mM Tris-HCl, pH 8.0
- 5 mM EDTA

- 50 $\mu$g/ml sodium azide

**Extraction Buffer B**

- 1.5 M NaCl
- 0.1 M $CaCl_2$
- 0.1 M $MgCl_2$
- 0.02 mg/ml DNAse I
- 0.05 mg/ml ovomucoid protease inhibitor

## A.5 Solutions for protein work

### A.5.1 Solutions required for Western Blotting

**Tris buffered saline (TBS), pH 7.6**

- 0.695 (3.475) g Trizma base
- 3.03 (15.15) g Trizma HCl
- 8.0 (40) g Sodium Chloride
- Dilute to 1000 (5000) ml with distilled water. Store at $2-8°C$

**Phosphate buffered saline (PBS), pH 7.5**

- 11.5 g Di-sodium hydrogen orthophosphate, anhydrous
- 2.96 g Sodium di-hydrogen orthophosphate
- 5.84 g Sodium chloride
- Dilute to 1000 ml with distilled water. Adjust pH to 7.5 with hydrochloric acid. Store at $2-8°C$

**PBS-Tween (PBS-T), TBS-Tween (TBS-T)** Dilute required volume of Tween-20 in PBS (TBS) to give a 0.1% (v/v) solution. Store at $2-8°C$

## A.5.2 Solutions required for SDS-PAGE

Table A.1: Solutions for resolving gel

| Solution components | Volumes (ml) per mold volume of 15 ml | 30 ml | 60 ml |
|---|---|---|---|
| 6% | | | |
| $H_2O$ | 7.975 | 16.050 | 32.100 |
| 30 % acrylamide mix | 3.000 | 6.000 | 12.000 |
| 1.5M Tris (pH 8.8) | 3.800 | 7.500 | 15.000 |
| 20 % SDS | 0.075 | 0.150 | 0.300 |
| 10 % ammonium persulfate | 0.150 | 0.300 | 0.600 |
| TEMED | 0.012 | 0.024 | 0.048 |
| 8% | | | |
| $H_2O$ | 6.975 | 14.050 | 28.100 |
| 30 % acrylamide mix | 4.000 | 8.000 | 16.000 |
| 1.5M Tris (pH 8.8) | 3.800 | 7.500 | 15.000 |
| 20 % SDS | 0.075 | 0.150 | 0.300 |
| 10 % ammonium persulfate | 0.150 | 0.300 | 0.600 |
| TEMED | 0.009 | 0.018 | 0.036 |

Table A.2: Solutions for preparing 5% stacking gel

| Solution components | Volumes (ml) per mold volume of 4 ml | 10 ml | 20 ml |
|---|---|---|---|
| $H_2O$ | 2.720 | 6.850 | 13.700 |
| 30 % acrylamide mix | 0.670 | 1.700 | 3.400 |
| 1.0 M Tris (pH 6.8) | 0.500 | 1.250 | 2.500 |
| 20 % SDS | 0.020 | 0.050 | 0.100 |
| 10 % ammonium persulfate | 0.040 | 0.100 | 0.200 |
| TEMED | 0.004 | 0.010 | 0.020 |

Table A.3: Solutions for 10× running buffer and transfer buffer

| Components | **10×Running Buffer ( 1 $\ell$ )** **Amount ( g )** | **Transfer Buffer ( 5 $\ell$ )** **Amount ( g )** |
|---|---|---|
| Tris-base | 30.3 | 15.0 |
| Glycine | 144.2 | 72.0 |
| SDS | 10.0 | - |
| Methanol | - | 1 $\ell$ |

Table A.4: Fixing solution for drying gels

| **Components** | **Volume** |
|---|---|
| 50% methanol | 125 ml |
| 10% glacial acetic acid | 25 ml |
| $H_2O$ | 100 ml |

Table A.5: Soaking solution for drying gels

| **Components** | **Volume** |
|---|---|
| 7% methanol | 17.5 ml |
| 1% glycerol | 2.5 ml |
| 10% glacial acetic acid | 17.5 ml |
| $H_2O$ | 228.5 ml |

# Appendix B

# Kinetic theory

## B.1 Association kinetics

The formation of a surface-bound complex in the BIA flow cell between analyte A and surface-bound ligand B can be described by a simple scheme

$$A + B \underset{k_d}{\overset{k_a}{\rightleftharpoons}} AB$$

The rate of association $d[AB]/dt$ is directly proportional to concentrations of free analyte [A] and ligand [B] while that for dissociation $d[AB]/dt$ is directly proportional to the concentration of the complex formed [AB]:

$$\frac{d[AB]}{dt} = k_a[A][B] \tag{B.1}$$

$$-\frac{d[AB]}{dt} = k_d[AB] \tag{B.2}$$

where $k_a$ and $k_d$ are association and dissociation rate constants, respectively. During the association phase of the BIA experiment when analyte is passing over the surface-bound ligand, association and dissociation processes happen simultaneously and the rate of association $d[AB]/dt$ is

$$\frac{d[AB]}{dt} = k_a[A][B] - k_d[AB] \tag{B.3}$$

The equation B.3 implies that the association of molecular complex depends on both $k_a$ and $k_d$.

The rate equation B.3 can be rewritten to a more useful form. Considering that the concentration of unoccupied ligand [B] is the difference between the total amount of ligand on the surface $[B]_0$ and the amount of complex [AB]:

$$[B] = [B]_0 - [AB]$$

Substituting in the rate equation B.3 for formation of AB:

$$\frac{d[AB]}{dt} = k_a[A]([B]_0 - [AB]) - k_d[AB]$$

If the total amount of ligand $[B]_0$ is expressed in terms of the maximum analyte binding capacity of the surface, all concentration terms can be expressed as SPR response in RU, eliminating the need to convert from mass to molar concentration:

$$\frac{dR}{dt} = k_a C(R_{max} - R) - k_d R \tag{B.4}$$

where $dR/dt$ is the rate of change of the SPR signal, C is the concentration of analyte, $R_{max}$ is the maximum analyte binding capacity in RU and R is the SPR signal in RU at time t.

Equation B.4 can be solved analytically if C is assumed to be constant, which is a valid approximation in real-time BIA experiments. Separating variables and integrating, equation B.4 gives:

$$R = \frac{k_a C R_{max}}{k_a C + k_d}(1 - e^{-(k_a C + k_d)t}) \tag{B.5}$$

This equation gives the response at any time during the association and can be used for non-linear regression analysis of single sensorgrams.

## B.2 Dissociation kinetics

After the pulse of analyte has passed over the sensor chip surface, the surface-bound complex dissociates in a zero-order reaction. Assuming that re-association of released analyte is negligible, the equation B.3 is reduced to

$$\frac{d[AB]}{dt} = -k_d[AB]$$

Using SPR response R expressed in Resonance Units (RU) rather than molar concentration, we get

$$\frac{dR}{dt} = -k_d R$$

Thus, the dissociation rate depends only on $k_d$. Separating variables and integrating gives

$$R_t = R_0 \cdot e^{-k_d(t-t_0)} \tag{B.6}$$

*or*

$$ln\frac{R_0}{R_t} = k_d(t-t_0) \tag{B.7}$$

where $R_t$ is the response at time t and $R_0$ is the response at an arbitrary starting time $t_0$. Equation B.7 can be used for non-linear regression analysis of the dissociation phase of a single sensorgram. Equations B.7 give

$$\frac{dR}{dt} = -k_d R_0 \cdot e^{-k_d(t-t_0)}$$

or

$$ln\frac{dR}{dt} = ln(-k_d R_0) - k_d(t-t_0)$$

Plotting $ln(R_0/R_t)$ or ln(dR/dt) against $t - t_0$ gives a straight line with slope $k_d$ or $-k_d$ and can be used for calculating $k_d$ .

## B.3 Equilibrium constants

Important characteristics of a molecular interaction are equilibrium constants $K_A$ and $K_D$. They are linked with the rate constants $k_a$ and $k_d$ by equation

$$k_a[A][B] = k_d[AB] \tag{B.8}$$

derived from B.2 for an equilibrium state when association and dissociation rates are equal. Equation B.8 can be rearranged to give

$$\frac{k_d}{k_a} = \frac{[A][B]}{[AB]} = K_D \tag{B.9}$$

*or*

$$\frac{k_a}{k_d} = \frac{[AB]}{[A][B]} = K_A \tag{B.10}$$

where $K_D$ $[M]$ and $K_A$ $[M^{-1}]$ are the dissociation and association equilibrium constants. An important advantage of BiaCore over other techniques is that it determines both $k_a$ and $k_d$ directly while other techniques provide only $K_D$ $(K_A)$. Thus, BiaCore provides more detailed information about the kinetics of the interaction, separating the association and dissociation phases.

# Appendix C

# BiaCore Macro

A macro designed to obtain binding data for all possible combinations of human and mouse ObR-Fc and human, mouse and rat Ob.

```
! hOBR immobilized on Fc3, mObR on Fc2,4; nothing on Fc1,
! h(m,r)Ob injection on Fc1,2,3,4; Detection 2-1, 3-1, 4-1
! Software: BIACORE 3000 Control Software
! Version: 3.1
! Configuration: IFC6
! Remarque : r2f2 = Glycine pH 2.0 as regeneration buffer
! Remarque : r2f3 = HBS-EP
DEFINE APROG algorithm
PARAM %position %concentration
CAPTION macro PM000510
!Regeneration
FLOW 5
FLOWPATH 1,2,3,4
QUICKINJECT R2f2 5
QUICKINJECT R2f2 5
!Immobilization of mObR on Fc2
FLOW 3
FLOWPATH 2
* QUICKINJECT R2A2 5
```

-3 RPOINT -b mObR-0.5ug/ml

120 RPOINT Level-mObR

!Immobilization of hOBR on Fc3

FLOW 3

FLOWPATH 3

* QUICKINJECT R2A1 12

-3 RPOINT -b hOBR-0.5ug/mL

260 RPOINT Level-hOBR

!Immobilization of mOBR on Fc4

FLOW 3

FLOWPATH 4

* QUICKINJECT R2A3 10

-3 RPOINT -b mOBR-1ug/mL

260 RPOINT Level-mOBR

!Leptin injection on Fc 1,2,3,4

FLOWPATH 1,2,3,4

WAIT 1500

FLOW 20

WAIT 300

* KINJECT %position 100 900

-3 RPOINT -b %concentration

310 RPOINT Leptin-level

END

DEFINE LOOP Ob-Injection-h

LPARAM %position %concentration

r2f3 hLeptin=0nM

r2b1 hLeptin=0.1nM

r2b2 hLeptin=1nM

r2b3 hLeptin=3nM

r2b4 hLeptin=5nM

r2b5 hLeptin=10nM

r2b6 hLeptin=30nM END

DEFINE LOOP Ob-Injection-m

LPARAM %position %concentration

r2f3 hLeptin=0nM

r2c1 mLeptin=0.1nM

r2c2 mLeptin=1nM

r2c3 mLeptin=3nM

r2c4 mLeptin=5nM

r2c5 mLeptin=10nM

r2c6 hLeptin=30nM END

DEFINE LOOP Ob-Injection-r

LPARAM %position %concentration

r2f3 hLeptin=0nM

r2d1 rLeptin=0.1nM

r2d2 rLeptin=1nM

r2d3 rLeptin=3nM

r2d4 rLeptin=5nM

r2d5 rLeptin=10nM

r2d6 hLeptin=30nM END

MAIN

RACK 2 THERMO-A

DETECTION 2-1,3-1,4-1

LOOP Ob-Injection-h STEP

APROG algorithm %position %concentration

ENDLOOP

LOOP Ob-Injection-m STEP

APROG algorithm %position %concentration

ENDLOOP

LOOP Ob-Injection-r STEP

```
APROG algorithm %position %concentration
ENDLOOP
APPEND Standby
END
```

# Bibliography


[1] Zhang Y., Proenca R., Maffei M., Barone M., Leopold L., and Friedman J. M. Positional cloning of the mouse obese gene and its human homologue. *Nature*, 372:425–432, 1994.

[2] Xavier P. and Sunyer F. Obesity research and clinical management. Lean times ahead. *Odyssey*, 3:26–33, 1997.

[3] Kennedy G. R. The role of depot fat in the hypothalamic control of food intake in the rat. *Proc. Royal Soc. B*, 140:578–592, 1953.

[4] Rosenbaum M., Nicolson M., Hirsch J., Heymsfield S. B., Gallagher D., Chu F., and Leibel R. L. Effects of gender, body composition, and menopause on plasma concentrations of leptin. *J. Clin. Endocrinol. Metab.*, 81:3424–3427, 1996.

[5] Hickey M. S., Israel R. G., Gardiner S. N., Considine R. V., McCammon M. R., Tyndall G. L., Houmard J. A., Marks R. H. L., and Caro J. F. Gender differences in serum leptin levels in humans. *Biochem. Mol. Med.*, 59:1–6, 1996.

[6] Stephens T. W., Basinski M., Bristow P. K., Bue-Valleskey J. M., Burgett S. G., Craft L., Hale J., Hoffmann J., Hsiung H. M., Kriauciunas A., MacKellar W., Rosteck Jr P. R., Schoner B., Smith D., Tinsley F.C., Zhang X-Y., and Heiman M. The role of neuropeptide Y in the antiobesity action of the obese gene product. *Nature*, 377:530–532, 1995.

[7] Bado A., Levasseur S., Attoub S., Kermogant S., Laigneau J-P., Bortoluzzi M-N., Moizo L., Lehy T., Guerre-Millo M., Le Marchand-Brustel Y., and Lewin M.J.M. The stomach is a source of leptin. *Nature*, 394:790–793, 1998.

[8] Masuzaki H., Ogawa Y., Sagawa N., Hosoda K., Matsumoto T., Mise H., Nishimura H., Yoshimasa Y., Tanaka I., Mori T., and Nakao K. Nonadi-

pose tissue production of leptin: Leptin as a novel placenta-derived hormone in humans. *Nat. Med.*, 3:1029–1033, 1997.

[9] Guex N. and Peitsch M.C. SWISS-MODEL and the Swiss-PdbViewer: An environment for comparative protein modeling. *Electrophoresis*, 18:2714–2723, 1997.

[10] Zhang F., Basinski M. B., Beals J. M., Briggs S. L., Churgay L.M., Clawson D. K., DiMarchi R. D., Furman T. C., Hale J. E., Hsiung H. M., Schoner B. E., Smith D. P. Zhang X. Y., Wery J-P., and Schevitz R. W. Crystal structure of the obese protein leptin-E100. *Nature*, 387:206–209, 1994.

[11] Hill C. P., Osslund T. D., and Eisenberg D. The structure of granulocyte-colony-stimulating factor and its relationship to other growth factors. *Proc. Natl. Acad. Sci. USA.*, 90:5167–5171, 1993.

[12] Robinson R. C., Grey L. M., Staunton D., Vankelecom H., Vernallis A. B., Moreau J-F., Stuart D. I., Heath J. K., and Jones E. Y. The crystal structure and biological function of leukemia inhibitory factor: Implications for receptor binding. *Cell*, 77:1101–1116, 1994.

[13] McDonald N. Q., Panayotatos N., and Hendrickson W. A. Crystal structure of dimeric human ciliary neurotrophic factor determined by MAD phasing. *EMBO J.*, 14:2689–2699, 1995.

[14] De Vos A. M., Ultsch M., and Kossiakoff A. A. Human growth hormone and extracellular domain of its receptor: Crystal structure of the complex. *Science*, 255:306–312, 1992.

[15] Watowich S. S., Wu H., Socolovsky M., Klingmuller U., Constantinescu S. N., and Lodish H.F. Cytokine receptor signal transduction and the control of hematopoietic cell development. *Ann. Rev. Cell Dev. Biol.*, 12:91–128, 1996.

[16] Takahashi N., Waelput W., and Guisez Y. Leptin is an endogenous protective protein against the toxicity exerted by tumor necrosis factor. *J. Exp. Med.*, 189:207–212, 1999.

[17] Sarraf P., Frederich R. C., Turner E. M., Ma G., Jaskowiak N. T., Rivet III D.J., Flier J. S., Lowell B. B., Fraker D. L., and Alexander H.

R. Multiple cytokines and acute inflammation raise mouse leptin levels: Potential role in inflammatory anorexia. *J. Exp. Med.*, 185:171–175, 1997.

[18] Grunfeld C., Zhao C., Fuller J., Pollock A., Moser A., Friedman J., and Feingold KR. Endotoxin and cytokines induce expression of leptin, the ob gene product, in hamsters: A role for leptin in the anorexia of infection. *J. Clin. Invest.*, 97:2152–2157, 1997.

[19] Tsuchiya T., Shimizu H., Horie T., and Mori M. Expression of leptin receptor in lung: Leptin as a growth factor. *Eur. J. Pharmacol.*, 365:273–279.

[20] Considine V. C. and Caro J. F. Leptin and the regulation of body weight. *Int. J. Biochem. Cell Biol.*, 29:1255–1272, 1997.

[21] Bradford B. L. and Bruce M. S. Towards a molecular understanding of adaptive thermogenesis. *Nature*, 404:652–660, 2000.

[22] Stellar E. The physiology of motivation. *Psychol. Rev.*, 61:5, 1954.

[23] Schwartz M. W., Woods S. C., Porte D. J., Seeley R. J., and Baskin D. G. Central nervous system control of food intake. *Nature*, 404:601–671, 2000.

[24] Erickson J. C., Hollopeter G., and Palmiter R. D. Attenuation of the obesity syndrome of ob/ob mice by the loss of neuropeptide Y. *Science*, 274:1704–1707, 1996.

[25] De Lecea L., Kilduff T. S., Peyron C., Gao X-B., Foye P. E., Danielson P. E., Fukuhara C., Battenberg E. L. F., Gautvik V. T., Bartlett F. S., Frankel W. N., Van Den Pol A. N., Bloom F. E., Gautvik K. M., and Sutcliffe J. G. The hypocretins: Hypothalamus-specific peptides with neuroexcitatory activity. *Proc. Natl. Acad. Sci. USA.*, 95:322–327, 1998.

[26] Sakurai T., Amemiya A., Ishii M., Matsuzaki I., Chemelli R. M., Tanaka H., Williams S. C., Richardson J. A., Kozlowski G. P., Wilson S., Arch J. R. S. Buckingham R. E., Haynes A. C., Carr S. A., Annan R. S., McNulty D. E., Liu W-S., Terrett J. A., Elshourbagy N. A., Bergsma D. J., and Yanagisawa M. Orexins and orexin receptors: A family of hypothalamic neuropeptides and G protein-coupled receptors that regulate feeding behavior. *Cell*, 92:572–585, 1998.

[27] Spanswick D., Smith M.A., Groppi V.E., Logan S.D., and Ashford M.L.J. Leptin inhibits hypothalamic neurons by activation of ATP-sensitive potassium channels. *Nature*, 390:521–525, 1997.

[28] Cohen B., Novick D., and Rubinstein M. Modulation of insulin activities by leptin. *Science*, 724:1185–1188, 1996.

[29] Kieffer T.J., Heller R.S., and Habener J.F. Leptin receptors expressed on pancreatic $\beta$-cells. *Biochem. Biophys. Res. Commun.*, 224:522–527, 1996.

[30] Path G., Bornstein S.R., Ehrhart-Bornstein M., and Scherbaum W.A. Interleukin-6 and the interleukin-6 receptor in the human adrenal gland: Expression and effects on steroidogenesis. *J. Clin. Endocrinol. Metab.*, 82:2343–2349, 1997.

[31] Wang Y., Kuropatwinski K.K., White D.W., Hawley T.S., Hawley R.G., Tartaglia L.A., and Baumann H. Leptin receptor action in hepatic cells. *J. Biol. Chem.*, 272:16216–16223, 1997.

[32] Zachow R. J. and Magoffin D. A. Direct intraovarian effects of leptin: Impairment of the synergistic action of insulin-like growth factor-I on follicle-stimulating hormone- dependent estradiol-17$\beta$ production by rat ovarian granulosa cells. *Endocrinology*, 138:847–850, 1997.

[33] Haynes W.G., Morgan D.A., Walsh S.A., Mark A.L., and Sivitz W.I. Receptor-mediated regional sympathetic nerve activation by leptin. *J. Clin. Invest.*, 100:270–278, 1997.

[34] Miller SM., Schmalz PF., Benarroch EE., and Szurszewski JH. Leptin receptor immunoreactivity in sympathetic prevertebral ganglion neurons of mouse and rat. *Neurosci. Lett.*, 265:75–78, 1999.

[35] Ghilardi N., Ziegler S., Wiestner A., Stoffel R., Heim M. H., and Skoda R. C. Defective STAT signaling by the leptin receptor in diabetic mice. *Proc. Natl. Acad. Sci. USA*, 93:6231–6235, 1996.

[36] Siegrist-Kaiser C. A., Pauli V., Juge-Aubry C. E., Boss O., Pernin A., Chin W. W., Cusin I., Rohner-Jeanrenaud F., Burger A. G., Zapf J., and Meier C. A. Direct effects of leptin on brown and white adipose tissue. *J. Clin. Invest.*, 100:2858–2864, 1997.

[37] Glasow A., Haidan A., Hilbers U., Breidert M., Gillespie J., Scherbaum W. A., Chrousos G. P., and Bornstein S. R. Expression of Ob receptor in normal human adrenals: Differential regulation of adrenocortical and adrenomedullary function by leptin. *J Clin. Endocr. Metab.*, 83:4459–4466, 1998.

[38] Tartaglia L. A., Dembski M., Weng X., Deng N., Culpepper J., Devos R., Richards G. J.and Deeds J., Muir C., Anker S., Moriaty A., Moore K. J., Smutko J. S., Mays G. G., Woolf E. A., Monroe C. A., and Tepper R. I. The Cloning of the Leptin receptor. *Cell*, 83:1263–1271, 1995.

[39] Chen H., Charlat O., Tartaglia L. A., Woolf E. A., Weng X., Ellis S. J., Lakey N. D., Culpepper J., Moore K. J., Breitbart R. E., Duyk G. M., Tepper R. I., and Morgenstern J. P. Evidence that the diabetes gene encodes the leptin receptor: Identification of a mutation in the leptin receptor gene in db/db mice. *Cell*, 84:491–495, 1996.

[40] Fei H., Okano H. J., Li C., Lee G-H., Zhao C., Darnell R., and Friedman J. M. Anatomic localization of alternatively spliced leptin receptors (Ob-R) in mouse brain and other tissues. *Proc. Natl. Acad. Sci. USA.*, 94:7001–7005, 1997.

[41] Lee H. G., Proenca R., Montez J. M., Carroll K. M., Darvishzadeh J. G., Lee J. I., and Friedman J. M. Abnormal splicing of the leptin receptor in diabetic mice. *Nature*, 379:632–635, 1996.

[42] Mercer J. G., Hoggard N., Williams L.M., Lawrence C.B., Hannah L.T., and Trayhurn P. Localization of leptin receptor mRNA and the long form splice variant (Ob-Rb) in mouse hypothalamus and adjacent brain regions by in situ hybridization. *FEBS Lett.*, 387:113–116, 1996.

[43] Narazaki M., Witthuhn BA., Yoshida K., Silvennoinen O., Yasukawa K., Ihle JN., Kishimoto T., and Taga T. Activation of JAK2 kinase mediated by the interleukin 6 signal transducer gp130. *Proc. Natl. Acad. Sci. USA.*, 91:2285–2289, 1994.

[44] Baumann H., Symes A. J., Comeau M. R., Morella K. K., Wang Y., Friend D., Ziegler S. F., Fink J. S., and Gearing D.P. Multiple regions within the cytoplasmic domains of the leukemia inhibitory factor receptor and gp130 cooperate in signal transduction in hepatic and neuronal cells. *Mol. Cell Biol.*, 14:138–146, 1994.

[45] Stahl N., Farruggella T. J., Boulton T. G., Zhong Z., Darnell Jr J. E., and Yancopoulos G. D. Choice of STATs and other substrates specified by modular tyrosine-based motifs in cytokine receptors. *Science*, 267:1349–1353, 1995.

[46] Murakami M., Narazaki M., Hili M., Yawata H., Yasukawa K., Hamaguchi M., Taga T., and Kishimoto T. Critical cytoplasmic region of the interleukin 6 signal transducer gp130 is conserved in the cytokine receptor family. *Proc. Natl. Acad. Sci. U.S.A.*, 88:11349–11353, 1991.

[47] Bazan J.F. Structural design and molecular evolution of a cytokine receptor superfamily. *Mol. Cell Biol.*, 87:6934–6938, 1990.

[48] Somers W., Ultsch M., De Vos A. M., and Kossiakoff A. A. The X-ray structure of growth hormone-prolactin receptor complex. *Nature*, 372:478 - 481, 1994.

[49] Livnah O., Stura E. A., Johnson D. L., Middleton S. A., Mulcahy L. S., Wrighton N. C., Dower W. J.and Jolliffe L. K., and Wilson I. A. Functional mimicry of a protein hormone by a peptide agonist: The EPO receptor complex at 2.8A. *Science*, 273:464–471, 1996.

[50] Walter M. R., Windsor W. T., Nagabhushan T. L., Lundell D. J., Lunn C. A., Zavodny P. J, and Narula S. K. Crystal structure of a complex between interferon-$\gamma$ and its soluble high-affinity receptor. *Nature*, 376:230–235, 1995.

[51] Gurney A.L. and Wong S.C.and Henzel W.J.and De Sauvage F.J. Distinct regions of c-Mpl cytoplasmic domain are coupled to the JAK-STAT signal transduction pathway and Shc phosphorylation. *Proc. Natl. Acad. Sci. USA*, 92:5292–5296, 1995.

[52] Nicholson S. E., Novak U., Ziegler S. F., and Layton J. E. Distinct regions of the granulocyte colony-stimulating factor receptor are required for tyrosine phosphorylation of the signaling molecules JAK2, STAT3, and p42, p44(MAPK). *Blood*, 86:3698–3704, 1995.

[53] Kishimoto T., Taga T., and Akira S. Cytokine signal transduction. *Cell*, 76:253–262, 1994.

[54] Murakami M., Hibi M., Nakagawa N., Nakawaga T., Yasukawa K., Yamanishi K., Taga T., and Kishimoto T. IL-6-induced homodimerization of gp130 and associated activation of a tyrosine kinase. *Science*, 260:1808–1810, 1993.

[55] Shuai K., Horvath C. M., Huang L. H. T., Qureshi S. A., Cowburn D., and Damell J. E. Interferon activation of the transcription factor STAT91 involves dimerization through SH2-phosphotyrosyl peptide interactions. *Cell*, 76:821828, 1994.

[56] Sekimoto T., Imamoto N., Nakajima K., Hirano T., and Yoneda Y. Extracellular signal-dependent nuclear import of STAT1 is mediated by nuclear pore-targeting complex formation with NPI-1, but not Rch1. *EMBO J.*, 16:7067–7077, 1997.

[57] Tartaglia L. A. The Leptin Receptor. *J. Biol. Chem.*, 272:6093–6096, 1997.

[58] Liu K. D., Gaffen S. L., and Goldsmith M. A. JAK/STAT signaling by cytokine receptors. *Curr. Opin. Immunol.*, 10:271–278, 1998.

[59] Baumann H., Morella K. M., White D.W., Dembski M., Bailon P. S., Kim H., Lai C., and Tartaglia L.A. The full-length leptin receptor has signaling capabilities of interleukin 6-type cytokine receptors. *Proc. Natl. Acad. Sci. USA*, 93:8374–8378, 1996.

[60] Durbin J. E., Hackenmiller R., Simon M. C., and Levy D. E. Targeted disruption of the mouse STAT1 gene results in compromised innate immunity to viral disease. *Cell*, 84:443–450, 1996.

[61] Meraz M. A., White J. M., Sheehan K. C. F., Bach E. A., Rodig S. J., Dighe A. S., Kaplan D. H., Riley J. K., Greenlund A. C., Campbell D., Carver-Moore K., DuBois R. N., Clark R., Aguet M., and Schreiber R. D. Targeted disruption of the STAT1 gene in mice reveals unexpected physiologic specificity in the JAK-STAT signaling pathway. *Cell*, 84:431–442, 1996.

[62] Takeda K., Noguchi K., Shi W., Tanaka T., Matsumoto M., Yoshida N., Kishimoto T., and Akira S. Targeted disruption of the mouse STAT3 gene leads to early embryonic lethality. *Proc. Natl. Acad. Sci. USA.*, 94:3801–3804, 1997.

[63] Hakansson M. L. and Meister B. Transcription factor STAT3 in leptin target neurons of the rat hypothalamus. *Neuroendocrinology*, 68:420–427, 1998.

[64] McCowen K. C. Chow J. C. Smith R. J. Leptin signaling in the hypothalamus of normal rats in vivo. *Endocrinology*, 139:4442–4447, 1998.

[65] Wang Y., Morella K.K., Ripperger J., Lai C.-F., Gearing D. P., Fey G. H., Campos S. P., and Baumann H. Receptors for interleukin-3 (IL-3) and growth hormone mediate an IL-6-type transcriptional induction in the presence of JAK2 or STAT3. *Blood*, 86:1671–1679, 1995.

[66] White D.W., Kuropatwinski K., Devos R., Baumann H., and Tartaglia L.A. Leptin receptor (OB-R) signaling. Cytoplasmic domain mutational analysis and evidence for receptor homooligomerization. *J. Biol. Chem.*, 272:4065–4071, 1997.

[67] Ishezaka Ikeda E., Fukunaga R., Wood W. J., Goedell D.V., and Nagata S. Signal transduction mediated by growth hormone receptor and its chimeric molecules with the granulocyte colony-stimulating factor receptor. *Proc. Natl. Acad. Sci. U.S.A.*, 90:123–127, 1993.

[68] Paulson J. C. and Colley K. J. Glycosyltransferases. Structure, localization, and control of cell type-specific glycosylation. *J. Biol. Chem.*, 264:17615–17618, 1989.

[69] Svensson E. C., Conley P. B., and Paulson J. C. Regulated expression of $\alpha$2,6-sialyltransferase by the liver-enriched transcription factors HNF-1, DBP, and L. *J. Biol. Chem.*, 265:20836–20868, 1990.

[70] Tan J. C., Braun S., Rong H., DiGiacomo R., Dolphin E., Baldwin S., Narula S. K., Zavodny P. J., and C Chou-C. Characterization of recombinant extracellular domain of human interleukin-10 receptor. *J. Biol. Chem.*, 270:12906–12911, 1995.

[71] Devos R., Guisez Y., Van der Heyden J., White D. W., Kalai M., Fountoulakis M., and Plaetinck G. Ligand-independent dimerization of the extracellular domain of the leptin receptor and determination of the stoichiometry of leptin binding. *J. Biol. Chem*, 272:18304–18310, 1997.

[72] Blumberg D. D. General precautions for working in a molecular biology laboratory. *Methods Enzymol.*, 152, 1987.

[73] Gluzman Y. SV40-transformed simian cells support the replication of early SV40 mutants. *Cell*, 23:175–182, 1981.

[74] Graham F. L. *Virology*, 77:319–329, 1977.

[75] Chomczynski P. and Sacchi N. Single-step method of RNA isolation by acid guanidinium thiocyanate-phenol-chloroform extraction. *Anal. Biochem.*, 162:156–159, 1987.

[76] Sambrook J., Fritsch E.F., and Maniatis T. *Molecular Cloning.* Cold Spring Harbor Laboratory Press, 1989.

[77] Weiss B., Jacquemin-Sablon A., Live T. R., Fareed G. C., and Richardson C.C. Enzymatic breakage and joining of deoxyribonucleic acid. VI. Further purification and properties of polynucleotide ligase from Escherichia coli infected with bacteriophage T4. *J. Biol. Chem.*, 243:4543–4555, 1986.

[78] Myers T. W. and Gelfand D. H. Reverse transcription and DNA amplification by a Thermus thermophilus DNA polymerase. *Biochemistry*, 30:7661–7666, 1991.

[79] Bradford M. A rapid and sensitive method for the quantitation of microgram quantities of protein utilizing the principle of protein-dye binding. *Anal. Biochem.*, 72:248–252, 1976.

[80] Johnsson B., Lofas S., and Lindquist G. Immobilization of proteins to a carboxymethyldextran-modified gold surface for biospecific interaction analysis in surface plasmon resonance sensors. *Anal. Biochem.*, 198:268–277, 1991.

[81] Deng W. P. and Nickoloff J. A. Site-directed mutagenesis of virtually any plasmid by eliminating a unique site. *Anal. Biochem.*, 200:81–88, 1992.

[82] Harrison P.T., Campbell I.W., and Allen J.M. Use of GPI-anchored proteins to study biomolecular interactions by surface plasmon resonance. *FEBS Lett.*, 442:301–306, 1998.

[83] Kozak M. An analysis of 5'-noncoding sequences for 699 vertebrate messenger RNAs. *Nucleic Acids Res.*, 15:8125–8148, 1987.

[84] Luoh S-M., Di Marco F., Levin N., Armanini M., Xie M-H., Nelson C., Bennett G.L., Williams M., Spencer S.A., Gurney A., and De Sauvage FJ. Cloning and characterization of a human leptin receptor using a biologically active leptin immunoadhesin. *J. Mol. Endocrinol.*, 18:77–85, 1997.

[85] Bjorbaek C., Uotani S., Da Silva B., and Flier J. S. Divergent signaling capacities of the long and short isoforms of the leptin receptor. *J. Biol. Chem.*, 51:32686–32695, 1997.

[86] Tessier D. C., Thomas D. Y., Khouri H. E., Laliberte F., and Vernet T. Enhanced secretion from insect cells of a foreign protein fused to honeybee melittin signal peptide. *Gene*, 98:177–183, 1991.

[87] *Invitrogen catalogue.* 2000.

[88] *BIAtechnology Handbook.* Biacore AB, 1998.

[89] Doupnik C.A., Dessauer C.W., Slepak V.Z., Gilman A.G., Davidson N., and Lester H.A. Time resolved kinetics of direct $G_{\beta 1\gamma 2}$ interactions with the carboxyl terminus of kir3.4 inward rectifier $K^+$ channel subunits. *Neuropharmacology*, 35:923–931, 1996.

[90] Nieba L., Nieba-Axmann S. E., Persson A., Hamalainen M., Edebratt F., Hansson A., Lidholm J., Magnusson K., Karlsson A. F., and Pluckthun A. BIACORE analysis of histidine-tagged proteins using a chelating NTA sensor chip. *Anal. Biochem.*, 252:217–228, 1997.

[91] Gershon P.D. and Khilko S. Stable chelating linkage for reversible immobilization of oligohistidine tagged proteins in the BIAcore surface plasmon resonance detector. *J. Immunol. Methods*, 183:65–76, 1995.

[92] Joss L., Morton T.A., Doyle M. L., and Myszka D. G. Interpreting kinetic rate constants from optical biosensor data recorded on a decaying surface. *Anal. Biochem.*, 261:203–210, 1998.

[93] Isse N., Ogawa Y., Tamura N., Masuzaki H., Mori K., Okazaki T., Satoh N., Shigemoto M., Yoshimasa Y., Nishi S., Hosoda K., Inazawa J., and Nakao K. Structural organization and chromosomal assignment of the human obese gene. *J. Biol. Chem.*, 270:27728–27733, 1995.

[94] Heldin C.H. Dimerization of cell surface receptors in signal transduction. *Cell*, 80:213–223, 1994.

[95] Cunningham B. C. and Wells J. A. Comparison of a structural and a functional epitope. *J. Mol. Biol.*, 234:554–563, 1993.

[96] Rajotte D., Cadieux C., Haman A., Wilkes B. C., Clark S. C., Hercus T., Woodcock J. A., Lopez A., and Hoang T. Crucial role of the residue R280 at the F'-G' loop of the human granulocyte/macrophage colony-stimulating factor receptor $\alpha$ chain for ligand recognition. *J. Exp. Med.*, 185:1939–1950, 1997.

[97] Rock F. L., Peterson D., Weig B. C., Kastelein R. A., and Bazan J. F. Binding of leptin to the soluble ectodomain of recombinant leptin receptor. *Horm. Metab. Res.*, 28:748–750, 1996.

[98] Haniu M., Arakawa T., Bures E. J., Young Y., Hui J. O., Rohde M. F., Welcher A. A., and Horan T. Human Leptin Receptor. Determination of disulfide structure and N-glycosylation sites of the extracellular domain. *J. Biol. Chem.*, 273:28691–28699, 1998.

[99] Fong T. M., Huang R-R. C., Tota M. R., Mao C., Smith T., Varnerin J., Kaprinskiy V. V., Krause J.E., and Van der Ploeg L. H. T. Localization of leptin binding domain in the leptin receptor. *Mol. Pharmacol.*, 53:234–240, 1998.

[100] Campbell F.M., Gordon M.J., Hoggard N., and Dutta-Roy A.K. Interaction of free fatty acids with human leptin. *Biochem. Biophys. Res. Commun.*, 247:654–658, 1998.

[101] LaLonde J. M., Levenson M. A., Roe J. J., Bernlohr D. A., and Banaszak L. J. Adipocyte lipid-binding protein complexed with arachidonic acid. Titration calorimetry and X-ray crystallographic studies. *J. Biol. Chem.*, 269:25339–25347, 1994.

[102] Cistola D. P., Kim K., Rogl H., and Frieden C. Fatty acid interactions with a helix-less variant of intestinal fatty acid-binding protein. *Biochemistry*, 35:7559–7565, 1996.

[103] Iida M., Murakami T., Ishida K., Mizuno A., Kuwajima M., and Shima K. Substitution at codon 269 (glutamine $\rightarrow$ proline) of the leptin recep-

tor (OB-R) cDNA is the only mutation found in the Zucker fatty (fa/fa) rat. *Biochem. Biophys. Res. Commun.*, 224:597–604, 1996.

[104] Clement K., Valsse C., Lahlou N., Cabrol S., Pelloux V., Cassuto D., Gourmelen M., Dina C., Chambaz J., Lacorte J-M., Basdevant A., Bougneres P., Lebouc Y., Froguel P., and Guy-Grand B. A mutation in the human leptin receptor gene causes obesity and pituitary dysfunction. *Nature*, 392:398–401, 1998.